THE UNIVERSITY OF MICHIGAN

INDUSTRY PROGRAM OF THE COLLEGE OF ENGINEERING

AN INVESTIGATION OF THE CORRELATION OF THE ACOUSTIC EMISSION PHENOMENON WITH THE SCATTER IN FATIGUE DATA

Larry D. Mitchell

A dissertation submitted in partial fulfillment
of the requirements for the degree of
Doctor of Philosophy in the
University of Michigan
Department of Mechanical Engineering
1965

October, 1965

IP-719

ACKNOWLEDGMENTS

The author gratefully acknowledges all those who aided in this investigation, in particular the following:

Professor Julian R. Frederick, Chairman of the Doctoral Committee, for his encouragement, counsel, and enlightening discussions of dislocation mechanisms.

Professor Hugh E. Bradley, member of the Doctoral Committee, for his valuable advice and counsel regarding the statistics involved in this work.

Professors D. Felbeck, R. Juvinall, and L. Quackenbush, Doctoral Committee members, for their advice and assistance.

The National Science Foundation for support of this study and for providing the author financial support.

E. I. du Pont de Nemours & Co., Inc. for a predoctoral fellowship.

Mr. B. Schofield and Mr. J. Kerawalla for their candid discussions of acoustic emission and of dislocation mechanisms for generation of acoustic emissions.

Professors H. Alvord and F. Fisher for their cooperation in the supply of needed electronic equipment.

Professor L. Colwell for his interest and assistance in the use of the numerically controlled LeBlond lathe.

Messrs. R. Crandall and D. Seigle for their assistance with the statistical computer programs.

The Research Incorporated Division of Materials Testing Systems for their excellent cooperation and for their supplying experimental components which made it possible to obtain the necessary fatigue data.

The Mechanical Engineering Department and Office of the Dean of the Engineering School for their cooperation and for supplying the audiometric room.

The Staff of the Mechanical Engineering Machine Tool and Electronics Laboratory for their cooperation in the fabrication of the loading frame and special equipment.

Mr. D. Danford and all the staff of the University of Michigan Industry Program for their assistance in the preparation of this manuscript.

TABLE OF CONTENTS

TABLE OF CONTENTS (CONT'D)

LIST OF TABLES

LIST OF FIGURES

LIST OF FIGURES (CONT'D)

LIST OF APPENDICIES

1.1 INTRODUCTION: GENERAL

Fatigue failures have plagued the public for years. As a result the engineer has had the continuing task of trying to design parts to prevent fatigue failure. To accomplish this, researchers have taken three distinct approaches to solve the problem: (a) the determination of design parameters in the fatigue problem; (b) the determination of strength values for specific material and material heat treatments (1,* pp. 31-47) (2) (3) (4, pp. 273-388); and (c) the determination of possible dislocation mechanisms that bring about fatigue failure (5) (6, pp. 335-336) (7).

The results of approaches (a) and (b) have produced design techniques to prevent fatigue. Faires (1, pp. 94-127), Faupel (8, pp. 627-652), Lipson and Juvinall (9), and others have systematically presented these techniques, but none has been able to develop a design technique where the fatigue life of each specimen can be predicted even approximately. Scatter prevails even when all known parameters are controlled. The fatigue lives of "identical" specimens under "identical" loading have been reported (2, pp. 17-25) (3, pp. 90-92) (10, pp. 365-392) to have maximum to minimum life ratios ranging from 2:1 to 10:1. An acknowledgment of this scatter in fatigue life has resulted in a new discipline called Mechanical Reliability (10). The objective in this descipline is to design for the existent scatter. This essentially requires a lowering of the design stress. As a result the applied

---

* Numbers in parenthesis refer to references listed at the end of this thesis.

stresses are below those that will cause early failure. This is essentially an educated increase in safety factor which results in an overdesigned part in the majority of applications. The necessity for an increase in part size is due to only a few weak parts. This is an inefficient, but at least a workable, technique for preventing "infant" mortalities.

Recognizing that a more sophisticated and long range approach was necessary, electron microscopic (5) and dislocation theory work (6, pp. 335-362) (7) relative to fatigue has been undertaken. This is the third type of approach. The primary aim in this work has been to provide an understanding of the basic dislocation mechanism operating during fatigue. Progress has been slow and of only infrequent practical value. It appears that it will be several years until dislocation theory in fatigue will reach a stage of development where one could use it to develop new materials with less scatter or to determine specific controllable causes of scatter.

1.2 THE PROBLEM: FATIGUE SCATTER

At this time one finds oneself in a dilemma. Should one overdesign in a time when the most efficient, most economical, and lightest design is expected? The aircraft industry faces this problem in its severest form. Their objective is lowest weight at maximum reliability. One finds that, considering the state of the fatigue art, to increase reliability one must strengthen by judiciously oversizing or by specially treating areas of a part. In all these cases either the cost increases or the weight increases.

One possible technique that is being looked into with more vigor is the use of a single or a series of nondestructive testing (NDT) techniques to sort out the low life specimens (11) (12). Applications of such techniques will allow one to design for a given reliability at a lighter weight and a lower manufacturing cost. An effective nondestructive testing technique would eliminate, by inspection, the low life parts. This is a truncation of the life distribution at the low end. One must realize, however, that one can expect a resultant weight reduction, but not necessarily a cost reduction. Manufacturing cost reductions caused by the elimination of special part processing and overdesigning could easily be offset by inspection costs and increases scrapage rates. Regardless of this fact, the search must continue for an effective nondestructive testing technique to be used by aircraft companies and others where catastrophic failure is a problem or where potential economic benefit exists.

1.3 LITERATURE REVIEW

A discussion of the order of the topics in the literature review is appropriate at this time. In the field of material failures there are a number of unanswered problems. Hence, a nondestructive testing technique could be used in a number of these problem areas. It was the initial aim of this research to find a nondestructive testing use for the phenomenon observed and reported as "acoustic emission" or "electro-acoustic phenomenon". Acoustic emissionsare detectable elastic waves excited within a piece of material while some changing load is being applied. From the first part of the literature review one finds that acoustic emissions exist and that physical models have been hpothesized to explain their existence. Hence, the next step is to determine what material properties might be explained by the observed emission phenomena. Thus, the materials' literature was reviewed to find possible applications of these phenomena.

1.3.1 Acoustic Emission: History

In 1950 Dr. Ing. Joseph Kaiser published his doctoral thesis (13) which concerned itself with the first observations of acoustic emission phenomena in tin, lead, duraluminum, copper, brass, steel, and tool steel. As a result of his work, Kaiser concluded that sound pulses could be detected at a stress as low as 71 psi (his lowest determinable stress level). Most important, he indicated that sound pulses observed on the first load were irreversible. If one were to reload the same specimen to the same stress no emission should be expected. However, Kaiser reported that upon exceeding the previous load the emissions would reappear. This has since been referred to as the "Kaiser effect" in the literature. In addition, Kaiser has reported to have shown by his work that the actual stress-strain curve has a stepwise progression rather than a continuous progression as indicated by the conventional stress-strain curves. No subsequent investigators have been able to show this, especially since Figure 2 in his thesis (13, p. 8) indicated this stepwise effect in the "elastic" and low plastic region. This stepwise action was not shown in the gross plastic region of the stress-strain curve. Mr. B. Schofield (14) of Lessells and Associates, who hired Kaiser as a consultant before Kaiser's death, indicates that strain transducers with sensitivities of about 10^{-8} are required to associate stepwise strain characteristics with emission characteristics. He has not been able to show the stepwise progression of the stress-strain curve.

Subsequently, Kaiser published a condensed version of this work in 1953 (15).

In late 1953 Dr. W. Späth hypothesized (16) that the regularly spaced slip lines observed on previously loaded specimens are caused by a set of very high frequency mechanical surface vibrations inherent to the deformation process. These ultrasonic vibrations are reflected off internal surfaces and flaws thus producing standing waves and a secondary stress field that add to the primary static field. The regions of maximum slip are associated with regions of maximum local stress; and the regions of minimum slip, with minimum stress. Dr. Späth cites Kaiser's work in acoustic emission as examples of this mechanism in operation.

Intrigued by Kaiser's 1953 report and a copy of Kaiser's original thesis, Lessells and Associates entered the acoustic emission field on December 15, 1954. A series of progress reports (17) (18) (19) (20) (21) (22) (23) (24) (25) and final reports (26) (27) (28) have been produced under the direction of Mr. B. Schofield. A chronological discussion of these reports is not included here because the last two reports (27) (28) have summarized all the information Lessells has published relative to acoustic emission. These two reports will be discussed in their chronological sequence.

Prior to the publication of these last Lessells' reports, Kaiser in 1957 (29) published his work using the acoustic emission technique to determine transformation temperatures in melting and solidifying metals. In 1958 Borchers and Kaiser (30) published similar work on the transition temperatures in the lead-tin system.

Also, in 1958 J. Plateau, C. Buchet, and C. Crussard (31) reported that when a stress is applied to a .05% carbon steel, large acoustic emissions immediately preceed the upper yield point, S_{yu}. This was attributed to very rapid growth of a deformation band coming from a nucleus of Piobert-Lüder bands.

In 1960 (32) and 1962 (33) Borchers and Tensi reported research that attributed the emissions during the "elastic limit extension" (upper-lower yield point) directly to the elastic limit extension. They also showed that acoustic emission rate is proportional to the deformation rate during elastic limit extension.

In the above work the emphasis has been upon the emission phenomenon at or very near the upper-lower yield point. The general conclusion is that this emission to due to the rapid deformation process that forms Piobert-Lüders bands.

Tatro in 1959 (34) and in an undated report (35) as well as Tatro and Liptai in 1962 (36) and 1963 (37) have made several contributions to the current theories regarding the sources of acoustic emissions. In the beginning Tatro considered the emission as a detection of crystal slip. Slowly evidence accumulated that the emission phenomenon was a surface related rather than a volume related phenomenon (35). Experiments were carried out in an effort to show that the emissions were due to surface or surface oxide cracking; however, final conclusions are that the acoustic emission phenomenon is surface related and is attributable to dislocation breakthrough to, or dislocation avalanche at the specimen surface (37). This releases localized strain energy which results in emissions.

This provided the first hopeful sign that acoustic emission might be correlated with fatigue. One knows that fatigue is usually a surface initiated failure phenomenon while acoustic emission is a surface related phenomenon. In fact, Tatro and Liptai have in several places (36)(37) indicated its possible use in fatigue studies.

Schofield in 1963 (27) and 1964 (28) provides his latest information concerning acoustic emission. Up to these two reports Schofield had reported two types of emission. One is termed burst and the other is termed "high frequency." Figure 1.1 shows a typical load burst emission from AISI E4340 steel. Figure 1.2 shows a typical "high frequency" emission from the same steel. In his early investigations Schofield has demonstrated that acoustic emissions are fundamentally related to the deformation process. However, pinpointing specific dislocation and slip

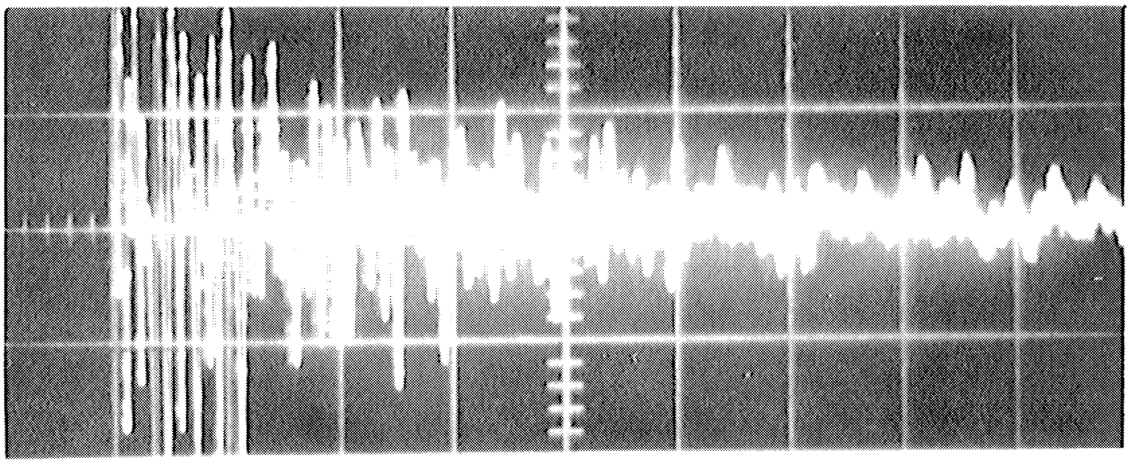

Figure 1.1. Burst Type Emission from AISI E4340 Steel.

Specimen (167-325-0-212)
Ordinate: 0.2 volts/cm
Abscissa: 1.0 msec/cm

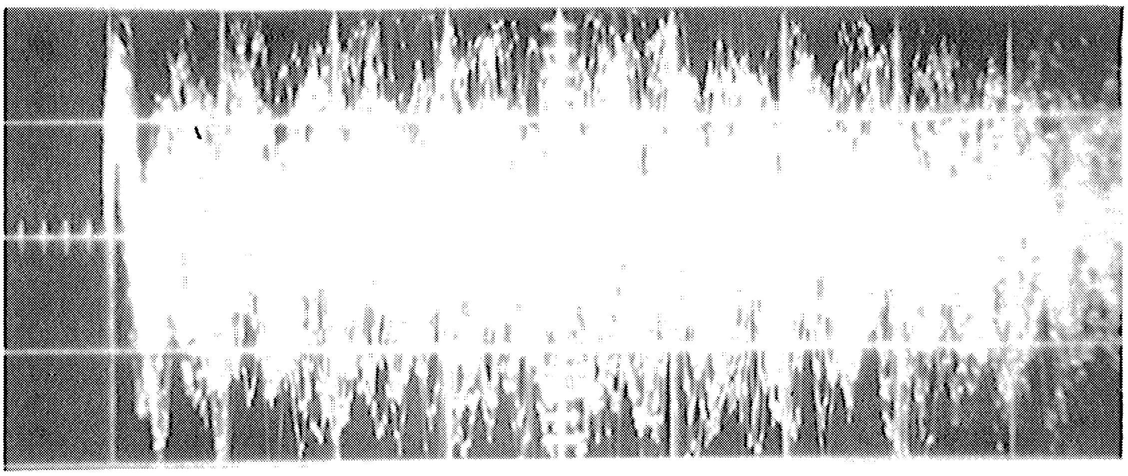

Figure 1.2. "High Frequency" Emission from AISI E4340 Steel.

Specimen (168-522-4-330)
Ordinate: 0.2 volts/cm
Abscissa: 2.0 msec/cm

mechanisms has been difficult. While considering Tatro's work and his own, Schofield decided that the surface contribution to emission was not clear. Upon reviewing the literature he found that the surface condition measurably affects the critical shear stress, creep, stress-strain curves, and the strain hardening slope. As a result a series of experiments was conducted with and without oxide, and with and without electropolishing of the surface. From these tests Schofield has concluded that oxide cracking is not a source of emission (27). In fact, oxides play a secondary role in that they affect the emission character only by affecting the deformation characteristic of the material (28). He concludes that the "high frequency" type emission is most probably due to dislocation pinning following slip deformation and to activation of the cross slip mechanism (27, p. 11). In addition, the burst type emission is attributed to the rapid deformation mechanism acting during stacking fault formation and/or mechanical twin formation (28, p. 12).

It is advantageous to point out that the act of pinning a dislocation after slip deformation is the end of localized plastic deformation. If the pinning can be measured by acoustic techniques, then the amount of permanent dislocation motion associated with each stress cycle can be measured. Accumulation of such motion can cause fatigue failures. Moreover, it also appears that activation of cross slip can be measured by acoustic emission. It is important to remember these two observations.

They will be used in section 1.4 to bring the literature surveys in sections 1.3.1 and 1.3.2 together.

1.3.2 Fatigue: Macro- and Micro-

A presentation scheme has been chosen that divides the fatigue literature review into the macroscopic approach or gross design parameter techniques and into the microscopic approach or dislocation theory view of fatigue. In both cases the review will be kept as concise as possible and will dwell only on those items that bear an apparent relation to the acoustic emission information obtainable from metals during deformation processes.

1.3.2.1 Macroscopic Approach

Fatigue has been studied since about 1860. In the process various parameters have been found that seem to affect the fatigue response. Summaries of these parameters, such as type of load and surface effect, have been published many places (1, pp. 96-121) (9, pp. 99-120)(7, pp. 30-47, 78-89, and 123-153) (4, pp. 63-156) (38, pp. 72-75). It is generally recognized that fatigue is usually a result of surface or near surface nucleation of microscopic cracks. The fact that fatigue is normally a surface bound phenomenon during crack initiation has resulted in much investigation of variables that might affect the surface or the stress at the surface. The following have been thought to be important in fatigue: mode of loading (bending, torsion, etc.), stress concentration factors, notch sensitivity, size effect, surface condition, surface treatment, inclusion concentrations and sizes, humidity and/or corrosive atmosphere, radiation, and other environmental factors.

It is most important that one recognizes all these factors when planning a fatigue experiment. With this insight into the macroscopic aspects of fatigue we turn to the microscopic fatigue models proposed for fatigue to see if they coincide with the acoustic emission models.

1.3.2.2 Microscopic Approach

Several dislocation mechanisms have been proposed for fatigue but all agree that fatigue cracks are started by slip at the surface (6, pp. 357-361). For example, copper whiskers do not fail in fatigue even at very high stresses (equivalent to $\pm$ 3% strain) so long as they are not yielded plastically (6, p. 357). Subsequent to yielding and during sufficiently large cyclic loading of the part, the plastic strain is accumulated in the yielded zone with a resultant fatigue failure. Also, note that fatigue is not primarily due to developing a large internal stress, since failures occur below static ultimate strength and in those places where the range of stress is greatest (6, p. 357) (8, p. 630). This may indicate that both the load and the unload process have mechanisms operating that cause fatigue.

In the study of dislocation theory two major mechanisms have been proposed to explain fatigue failure, the Cottrell-Hull model (6, Figure 10.13) and the Mott model (6, Figure 10.14). Each attempts to explain the intrusions and extrusions (6, Figures 10.11 and 10.12) (7) seen on close examination of fatigue specimens. Figure 1.3 shows the Cottrell-Hull model in sequential operation. Two sources of dislocation Q_1 and Q_2 are shown (Figure 1.3a). Q_1 is such that its resolved shear stress allows slip, which uses it as a source, to occur first along the dotted line through Q_1 (Figure 1.3b). With increased stress the resolved shear stress at Q_2 increases to the critical state for slip to occur with Q_2 as a source. This is shown in Figure 1.3c. In Figures 1.3d and 1.3e the load is subsequently reversed and both an intrusion and extrusion are produced. It should be noted that this first model depends on plastic dislocation motion and dislocation movements toward the material surface.

The Mott model for fatigue is depicted in Figure 1.4. It is assumed that a void (ABCDA'B'C'D') exists below the surface or two opposed edge dislocations generate a void below the surface. A screw dislocation, PQ, moves around the cavity until the particle CDD'C'EFF'E' is extruded. This leaves an initial fatigue crack and also produces an extrusion. In this mechanism the screw dislocation with suitably applied stresses must cross slip from one plane to another. An increased cross slip phenomenon is then considered a detriment in fatigue.

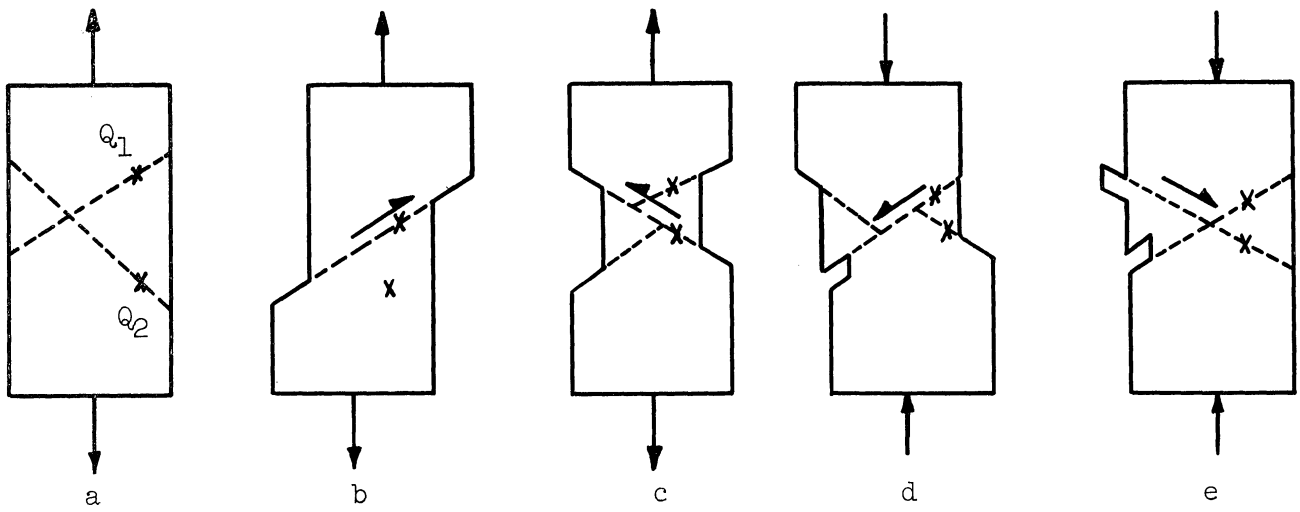

Figure 1.3. Cottrell-Hull Fatigue Model.
[After Mc Lean (6, Fig. 10.13), Modified For Use Here].

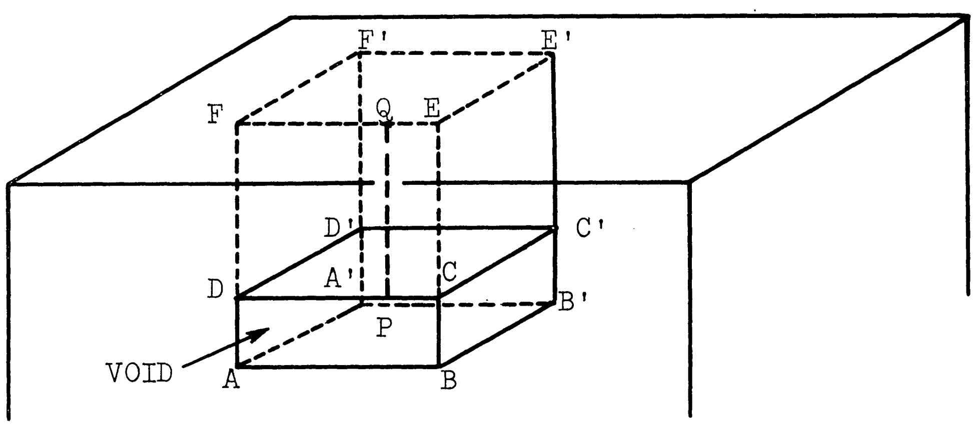

Figure 1.4. Mott Extrusion Model.
[After McLean (6, Fig. 10.14), Modified For Use Here].

1.4 OBJECTIVES OF THE RESEARCH

In the process of reviewing the above discussions of the literature in acoustic emission and in fatigue one notices similarities relative to each being a surface effect and to the mechanisms proposed to explain their existence. Both acoustic emission and fatigue are thought to be surface related phenomena, both are directly associated with plastic deformations in materials, and both appear to be affected by the extent of the cross slip mechanism. Then, if one is able to measure plastic deformation by means of listening to dislocations repinning after such plastic deformation has occurred and if one can determine the activity of the cross slip mechanism be listening to its activation, one finds a justification for expecting a correlation between fatigue life and acoustic emission. Fatigue life is simply a measure of the cumulative effect of many cycles of plastic deformation and cross slip.

It is, then, expected that an increased emission at a given stress will be indicative of large plastic deformation caused at that stress and, therefore, a lower fatigue life. Also, an increased emission could be a result of an increased cross slip activity but an increased cross slip activity results in a lower life. Expecting early fatigue failures to be caused by increased plastic deformation and cross slip, one must conclude that the local stresses are abnormally high relative to the local strengths. This could be caused by localized stress concentrations such as voids, inclusions, surface markings, etc. (39). Moreover, localized weak areas which experience premature yielding could be due to the inhomogeneities within the material. It appears that the emissions might measure the ability of a specific specimen to withstand a specific stress in fatigue.

The objectives are twofold. The first and most important is to determine whether or not acoustic emission is correlated with fatigue life and the second is to provide knowledge about acoustic emissions in commercially available material in both the load and unload modes.

In setting up the first objective one realizes that if the correlation is high and positive the conclusion drawn by Schofield as to mechanisms for emission generation are reinforced; however, if the correlation is low, this will indicate that at least in AISI E4340 aircraft quality steel other effects are overshadowing Schofield's proposed mechanisms.

In setting the second objective one sees that additional emission data in a commercial material may suggest other possible sources for emission than those already hypothesized. Obtaining the emission character itself in commercial materials, where physical properties and characteristics are well known, may give a more fruitful insight into the cause of certain emissions than obtaining emission characteristics from single crystals such as used by Schofield (27) (28). This is so because one may be able to associate an emission with an easily recognizable physical characteristic of the commercial material.

2.1 DESCRIPTION OF THE EXPERIMENT

In designing an experiment to determine the correlation between two variables one must first physically justify the reason for believing that a correlation might exist. If this were not done one could correlate two completely unrelated phenomena just because the data points "happened" to be highly correlated to a third variable such as time. The physical justification for expecting a correlation such as that sought here has been presented in section 1.3 and 1.4.

In accordance with an outline proposed by Hicks (40) for planning an experiment one finds that there are a number of preliminary steps that should be taken.

A choice of response variables is the first necessary step. In this case the response variable is fatigue life, N. Here both N and log N will be used as the response variable. This difference will essentially denote the assumption of an additive or of a multiplicative model, respectively.

Next a list of independent variables must be developed along with the values of each. An indication of whether they were selected as fixed or random variables is desirable. Table 2.1 is a summary of these selections.

It is important to understand that in Table 2.1 as many variables are held fixed as possible while still generating a test specimen that is similar in variation to a manufactured part. Since a meaningful non-destructive testing technique is sought for industrial use, it was felt

TABLE 2.1

VARIABLES IN THE EXPERIMENTAL DESIGN

Variable	Levels	Type	Remark
Life, N	---	Dependent	---
Material	AISI E4340	Fixed	---
Manufacturer	Republic Steel	Fixed	---
Steel Heat	#3321345	Fixed	---
Supplier	J.T. Ryerson, Detroit, Mich.	Fixed	---
Specimen Manuf.	Tape controlled lathe	Fixed	---
Applied Stress	75,80,85,90,95,100ksi	Fixed	Dual stress level, 75-90 & 90-75ksi.
Total Indicator Reading, TIR	---	Random	Measured. Result of the manufacturing process.
Surface Finish, RMS	---	Random	Measured. Result of the manufacturing process.
Room Remperature, T	---	Random	Measured. Result of daily air temperature fluctuations.
Room Humidity, H	0	Fixed	Room Humidity was measured but its effect was set to zero by maintaining a mineral oil coating on the specimens.
Bar Number, B	0,1,2,3,4,5,6	Fixed	Recorded. Equivalent to heat treatment position effect.
Position Number, P	0-29	Fixed	Recorded. Equivalent to Longitudinal heat treatment effect.
Stress Beyond the Yield Point, Sp	---	Random	Recorded
Emission Character	---	Random	Major independent variables of interest, recorded.
Acoustic Tensile Testing Machine	---	Fixed	One machine used.
Fatigue Machine	Research Incorporated	Fixed	One machine used.
Fatigue Rate	30cps	Fixed	---
Acoustic Load Rate	20,000psi/min.	Fixed	---

that the specimen must not be idealized, that the stress on the specimens must be applied at different levels to see if the correlation holds at different stress levels, and that the levels of all uncontrollable variables must be recorded. The experiment was designed with five groups of thirty specimens fatigued at a single stress level but it also was designed to include two groups of thirty specimens which were each fatigued at two different stress levels. The dual stress level work was planned into the experiment so that the ability of the emission characteristic to predict fatigue lives in cumulative damage could be checked if success were obtained in the single stress level predictions.

2.1.1. Material

The first consideration was to select a material for the work. The primary factor in this selection was the fact the aircraft companies would probably be the first to use the nondestructive testing technique that is being searched for here. This would simply be a case of economics. Therefore, a readily available aircraft quality AISI E4340 cold drawn and annealed steel was selected. Eight round bars, 1 1/8" x 12 ft , were purchased. Complete manufacturing and processing information (41), a hardenability certification, and a certified test report (42) are presented in Appendix I. Table 2.2 shows the material properties as tabulated by the supplier (43). Table 2.3 gives the material properties as determined by experiment on this heat of material. The data were taken on a Baldwin-Southwark 60,000-lb. tensile machine using a Templin type recorder and an O.S. Peters Type 6134A2, electro-mechanical, 2 inch gage length extensometer.

TABLE 2.2

TABULATED PROPERTIES OF AISI E4340
COLD DRAWN AND ANNEALED STEEL (43)

S_u	=	111.0	ksi
S_y	=	99.0	ksi*
ϵ	=	16	%
A_r	=	42	%
R_C	=	19	
BHN	=	223	
Machinability 55% of AISI B1112			

* This was obtained by the divides method (43, p. 237). It is suggested that this data is for AISI E4340 in the cold drawn state. The supplier has not been able to verify that this data is for an AISI E4340 cold drawn and annealed steel, although they have published it as such.

TABLE 2.3

EXPERIMENTALLY DETERMINED PROPERTIES OF REPUBLIC STEEL'S HEAT #3321345 OF AISI E4340 STEEL

Spec. Number	S_u(ksi)	S_{yu}(ksi)	S_f(ksi)*	S_f[True](ksi)*	%ϵ	% A_r	R_C	Range R_C
0-42-3	115.0	73.0	87.5	173	23.0	49.4	22.4	19.5-23.5
1-21-5	116.0	75.0	95.0	171	20.5	44.5	22.9	19.0-23.0
2-22-1	112.5	71.5	95.5	169	22.0	43.5	21.9	20.0-24.0
3-50-6	108.5	70.0	90.0	170	22.0	47.0	20.2	18.0-21.6
4-40-2	107.3	74.5	83.0	177	25.0	53.2	23.7	21.5-24.5
5-52-0	111.5	74.0	91.0	169	21.5	46.3	23.2	19.5-27.5
6-51-4	107.0	73.0	88.0	163	22.5	46.0	21.4	18.0-24.0
Average	111.1	73.0	90.0	170	22.4	47.2	22.2	---------

* S_f = Load @ Fracture/A_o and S_f[True] = Load @ Fracture/A_f. A_o = Original area. A_f = Final area at fracture.

S_{yu} = upper yield stress.

R_C = Hardness, Rockwell C.

One of the eight bars was used for lathe setup and to make check and trial specimens. Figure 2.1 shows how the seven remaining bars were cut up into three sections. A part of each section was reserved for making one tensile specimen. The remainder of each section was used to make ten fatigue specimens. The parts of the bars set aside for tensile specimens were coded as follows. The first digit of a two digit code number is the bar number; the second digit, the section number. It was decided that of the twenty-one parts available for making tensile specimens only seven would be used. A random selection procedure, similar to the one explained later for the fatigue work, was employed to select which parts were to be made into tensile specimens. The randomization code was of the form X-XX-X which, respectively, are test sequence number, part coding, and manufacturing sequence number. This plan resulted in a test where the specimens were selected at random from the batch of twenty-one possible specimens. Also, these specimens were randomized relative to the test sequence and to the manufacturing sequence.

Engineering stress-strain curves are not presented since they are conventional medium carbon steel curves. The difference between the upper and lower yield stresses is small and ranges from 200 to 1,500 psi. Representative data are shown in Table 2.3.

2.1.2 Design of the Experiment

First, one considers the number of observations to be taken. In this case a single variable, stress, S, is set and all other variables are held as nearly constant as possible and recorded. At each stress level it was decided to test thirty specimens. This should provide adequate

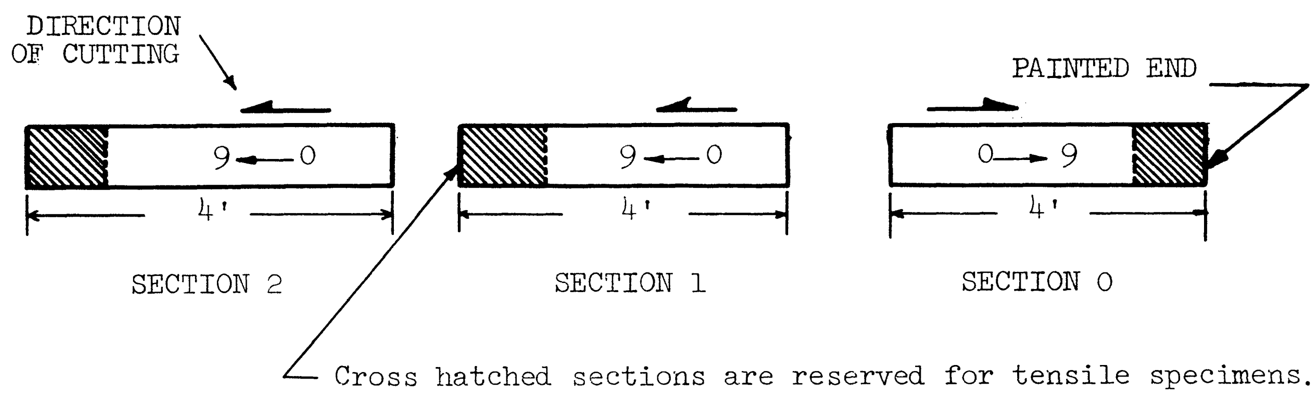

Figure 2.1. Section and Position Numbering Scheme for Specimens as Cut from Bar.

estimates of the expected effect that each stress has on life, as well as providing sufficient scatter at each stress level so as to allow the emission to predict fatigue life at each stress level.

The major question in the design of an experiment is whether to use a completely randomized design, a randomized block design, or other types of designs (40, pp. 21-74). In this case the completely randomized design (40, pp. 21-41) was selected so that when the order of experimentation is carried out the several stress level applications would occur completely random in time. This is done so that any effects caused by uncontrolled variables, unknown variables, or time dependent test equipment trends would tend to be spread out among all the stress levels. In this way the overall error term is increased, but there is little chance of obliteration of the emission-life correlation which is sought. The randomization plan used here has randomized the testing sequence on both the acoustic test machine and the fatigue machine relative to bar number, position number, and stress level. Also, bar number, position number, and stress level are randomized relative to one another. This provides the maximum amount of insurance against the confounding of data owing to unknown variables or trends.

The model for this type of experiment then becomes

$$N_{ijkl...} = \mu + EMISSION_i + STRESS_j + TIR_k + RMS_l + ... + e_{ijkl...}$$

or

$$LOG\ N_{ijkl...} = \mu + EMISSION_i + STRESS_j + TIR_k + RMS_l + ... + e_{ijkl...}$$

where $EMISSION_i$ is the effect of the ith category of the emission characteristic and $e_{ijkl\ldots}$ is the portion of the life not predicted by the independent variables, the error term. In the former case the model is one of additivity whereas the latter indicates a model of multiplicity. In reviewing the fatigue literature one finds a predominant use of the multiplicative techniques in fatigue design procedure (1, p. 99) (9, Chapter 11) (10, pp. 377-387). It is interesting to note that the computerized statistical analysis also found the multiplicative model to be applicable.

2.1.2.1 Bar Coding

In preparation to complete the randomization of the experiment it is necessary to assign position numbers to parts as they are machined. Figure 2.1 shows the assignment scheme. A two digit position number is used. The first digit is the section number; the second, the position number within the section. Postion numbers in any one bar go from zero to twenty-nine. These numbers are the last two digits of a three digit term. The first digit of the three digit term indicates the bar origin of the specimen. For example, a code such as 321 means the specimen comes from bar number three, the left most section in Figure 2.1, and the second specimen from the right. This is true because the coding starts from the right in this section and 1 is the second number in the coding sequence.

The first assumption that was necessary so that the completely randomized model could be used was that the bars received from the single heat of steel were, in fact, a random selection or that there was no appreciable "bar" effect. The assumption of a random selection could not be justified. However, the assumption of neglectible bar effect was justified by the fact that the final annealing was done in a continuous furnace where the bars travel for thirty feet with the bar length perpendicular to the direction of travel. This type of anneal would eliminate much of the bar differences that would be expected from a batch type anneal. Bar effects might be expected in bars coming from a batch anneal process owing to positional temperature differences. These differences may result in appreciable changes in properties. In the continuous annealing process such temperature differences are minimized. However, to minimize any effect that might exist it was decided to randomize both bar number and position relative to one another, relative to time, and relative to stress level.

The second assumption concerned the orientation of the bar before the positions were assigned as in Figure 2.1. Since no clear-cut distinction was observable relative to the orientation except the color coded end markings, it was assumed that the coded end indicated an end which was uniformly on one side of the annealing furnace. The validity of the assumption was verified by the supplier. This was necessary if one were to try to relate any general fatigue strength trends to position along the bar.

The complete coding system used in the randomization was of the form XXX-XXX-X-XXXX. Group one indicated the testing sequence number;

group two, the bar and position number; group three, the stress level; and group four, the roughing tool bit number, bit side number, and the number of previous cuts with that bit and side plus one. The random generation of the first three groups is described in the next section but the tooling information was only recorded to provide tool life information relative to that material and lathe program for the laboratory technician. The latter data are not important to this study. Figure 2.2 shows such coding applied to a specimen.

2.1.2.2 Randomization

The generation of the randomization was done by hand using the Rand Corporation's random number table (44). Because of the extensive time required to complete a randomization between time, bar number, position, and stress in a single pass the randomization was done in two passes. Pass one randomized the time sequence relative to bar number and position. Pass two randomized the time sequence relative to stress. Then the total code was formed by associating time sequences in each pass with one another.

The following procedure was followed in completing the randomization.

1. Select a page, column, and line from the random number table.
2. Use the number entered to indicate the starting line and column for the randomization.
3. For the first pass select a three number set starting as indicated in step 2.

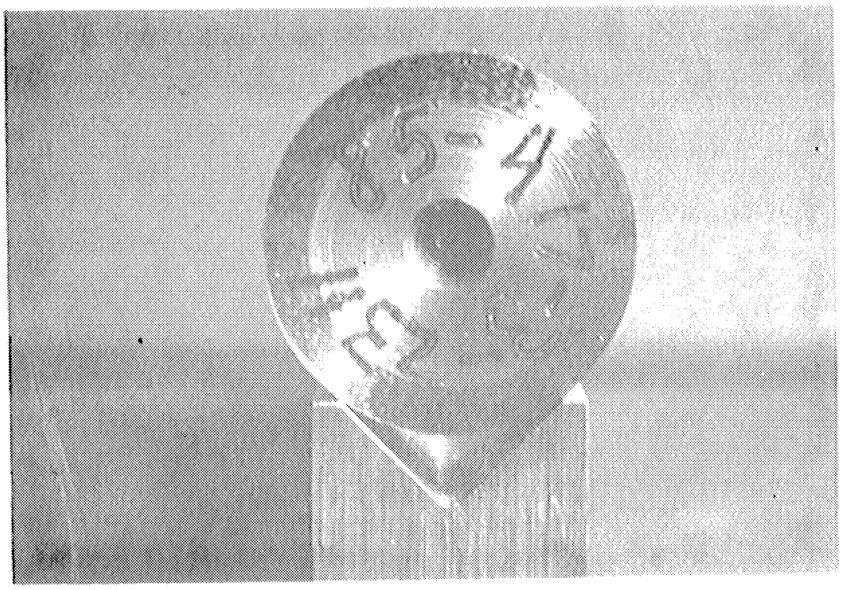

Figure 2.2 Specimen Coding Sample.

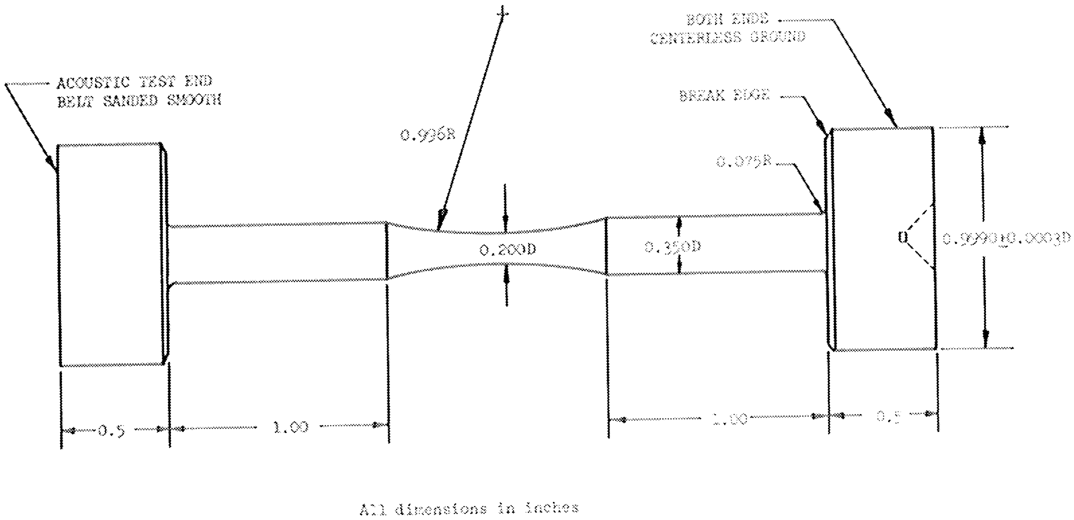

Figure 2.3 Fatigue Specimen used in the Study.

4. Associate each three digit number with a consecutive time sequence number, such as 1, 2, 3, etc.
5. Continue step 4 until all specimens are assigned a time sequence number.
6. Repeat steps 1 and 2 for pass two.
7. Use a one number column for stress selection.
8. Associate each stress selection with a time sequence.
9. Generate the total code by merging the randomized codes obtained in steps 4 and 8.

After the completion of the completely randomized coding the manufacturing process was started.

2.1.3 Manufacturing of the Specimens

Because of the high cost of having two hundred and thirty specimens manufactured outside of the University facilities and because of the difficulty of learning the detailed processing history of individual specimens manufactured in an outside shop, the recently acquired LeBlond 2013 tape turn lathe (numerically controlled lathe) was used to manufacture the specimens.

The specimen design shown in Figure 2.3 was used for this correlative study. After the specimens were machined using the tape lathe they were marked by means of an electrical etching pen with the randomized code. They were then cleaned in acetone and stored in mineral oil as suggested in the ASTM fatigue manual (45, p. 37). If recleaning of a specimen was necessary, chloroform was used to remove the mineral oil. This was followed by a cleaning in acetone and a thorough drying before restorage. In general, once the specimen was stored in mineral oil the oil was not removed. The fatigue tests were run with the oil in place. This was done to eliminate, as much as possible, the effects of atmospheric moisture on the fatigue results. Effective coverage was verified by noting the fatigue fractures after failure. The fracture showed a uniform dark ring encircling the plan view of the fracture. The wetting action of the mineral oil resulted in the coat of mineral oil moving into the fractured area. After longer waiting periods the full plan view of the fracture became dark because of mineral oil wetting.

Following the machining of the ten trial specimens, of the two hundred and ten single and dual stress level specimens, and of the ten check specimens (to be used if emission correlation were good), the entire batch was centerless ground to 0.9990 $\pm$ 0.0003 in. in diameter. This was done to provide accurate specimen seating. Following the grinding the inside edges of each specimen head were broken to prevent seizure during the seating process.

It is calculated that with the clearances and tolerances used the induced bending stress owing to eccentric seating will have an expected value of zero and a maximum value of 2.6% of the axial stress, if the grip seats are square. For a further discussion of the system bending see sections 2.1.5 and 2.1.6.

2.1.4 Specimen Inspection

In the process of completing the data charts the following data were required: total indicator reading (TIR) of the test section relative to the seating heads, RMS(Root Mean Square) surface finish, and the diameter of the test section.

2.1.4.1 Total Indicator Reading (TIR)

The TIR was obtained by inserting each specimen in a precision vee block, rotating the specimen, and reading the swing of a dial indicator whose smallest division was 0.0001 in.

2.1.4.2 Surface Finish

the RMS surface finish was determined by averaging the readings of the two sides of the circular notch in each specimen. The readings were taken away from the section of minimum area so that no additional surface markings would be applied at the expected failure section. All the readingswere taken using the automatic tracing system called the Physicists Research Motortrace, Type V. This held the Micrometrical Head MA 42257 using a DA type skid. The head output is fed into the Physicists Research Corporation's Profilometer Amplimeter, Model 1, Type C. Calibration procedures indicated the readings to be 0.5 μ in. RMS high. This was deemed small and no correction of data was made.

2.1.4.3 Test Section Diameter

The test section was measured using a Gaertner Scientific Corporation's tool maker's microscope, serial number 538. The smallest gradation on this instrument was 0.0001 in. Here, the average of two readings was taken unless great divergence was found. If so, the measurements were repeated. This measurement will not appear in any data since the applied load was adjusted to account for the area differences so as to maintain the fixed stress levels.

2.1.5 Acoustic Equipment and Tests

When one considers running acoustic tests he immediately asks whether the environment is quiet enough to complete the tests. To answer this, one should know how loud the phenomena are that he wishes to measure. Tatro and Liptai (36, p. 1) (37, part I) indicate that the levels of acoustic emission are very low. Schofield (26, p. iii) indicates the same but personal conversation with him (14) indicated that no determination of level was ever made. As a result it was decided to construct the detection system and determine its minimum electronic peak trigger level. The objective would be to get the detected ambient acoustic and structure-borne noise below the inherent amplifier noise.

2.1.5.1 Electronic Equipment

Figure 2.4 shows the block diagram of the detection system. Figures 2.5 and 2.6 show the physical arrangement of the electronic equipment. The PZT-5 pickup, retainer cap, and hushed amplifier are maintained inside the audiometric room.

Details of the retainer cap pictured in Figure 2.7 are as follows. The photograph shows a copper retainer holding the PZT-5 ceramic

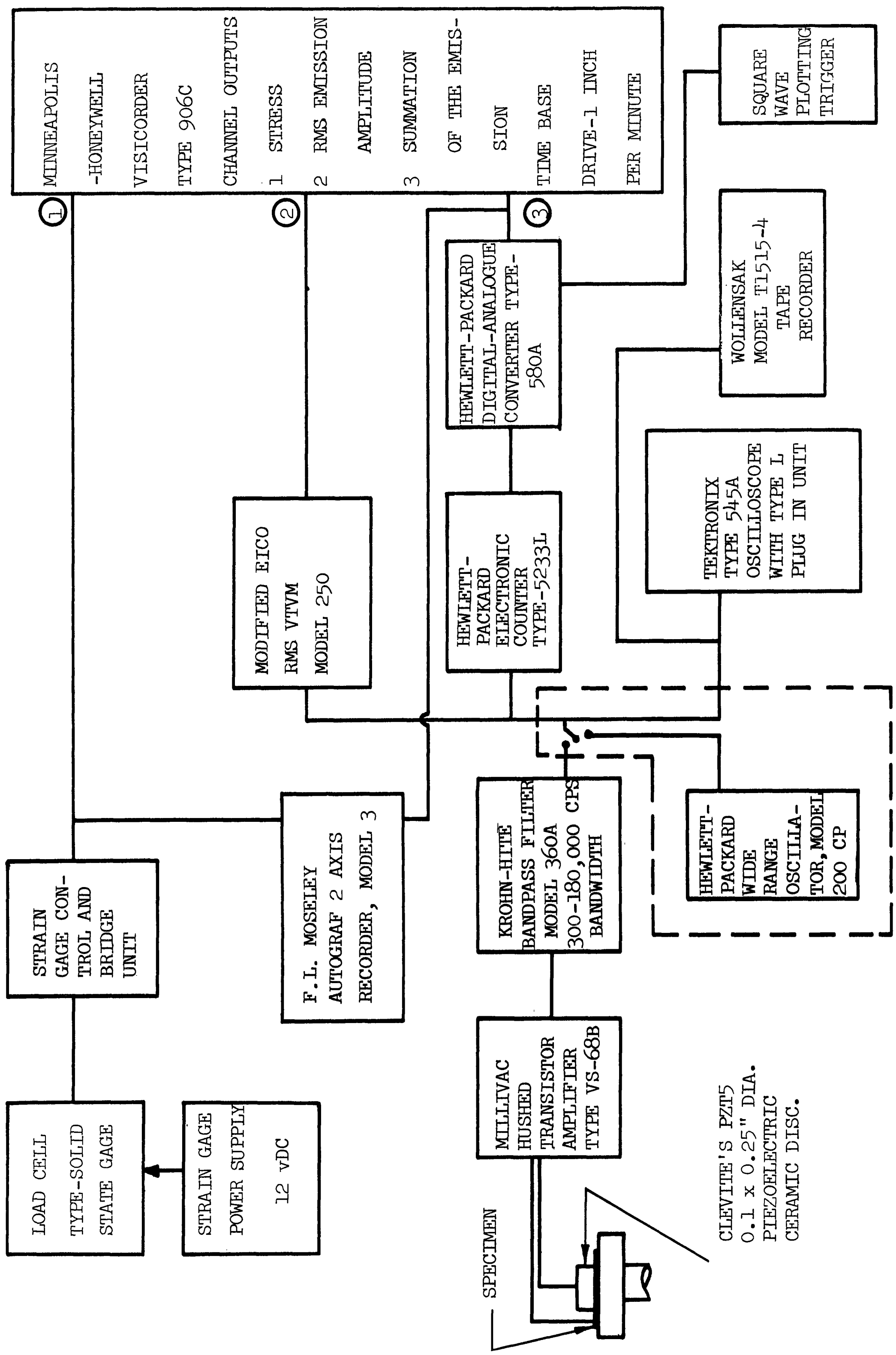

Figure 2.4. Block Diagram of Acoustic Detection System.

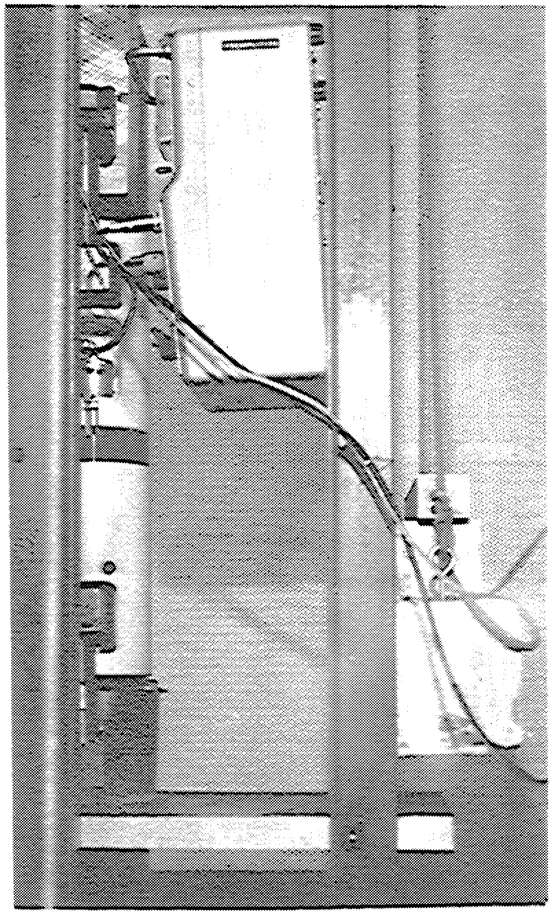

Figure 2.5. Electronic Equipment in Industrial Acoustics Company's 402A Audiometric Room.

Figure 2.6. Electronic Equipment Outside of Audiometric Room.

(center). The retainer is spring loaded so that the insertion of a specimen causes a constant crystal contacting force from specimen to specimen. This helps assure a constant acoustic contact between the specimen and the PZT-5. The small screws holding the copper retaining disc in place are there to provide a shorted input to the amplifier should the cap inadvertently come off while connected to the operative amplifier. This is necessary because transient high input voltages can burn out the first unprotected transitor in the hushed amplifier. In Figure 2.8 the retainer cap is assembled on a specimen. The set screws in Figures 2.7 and 2.8 are used to retain the transducer assembly. The major natural frequencies of the piezoelectric ceramic discs are approximately 700, 330, 230, and 150 kc. Here, only 150 kc appears in the response region of the system. The 150 kc resonance is the circumferential mode. It is not expected that this frequency is easily excited. No 150 kc frequency was seen.

The high level electrical signal from the amplifier is carried via a special electrical panel in the audiometric room wall to the Krohn-Hite filter where a bandwidth of 300-180,000 cps is set. A discussion of this width will be given in section 2.1.5.2. This filtered signal is sent to a scope for viewing, to a recorder for listening, to a counter for accumulating a permanent record of the totalized emission,and to a modified vacuum tube voltmeter for recording the RMS voltage output of the PZT-5 ceramic disc.

The counting system totalizes any wave peak within the ring-down, the damped oscillations shown in Figure 1.1, or any wave peak in

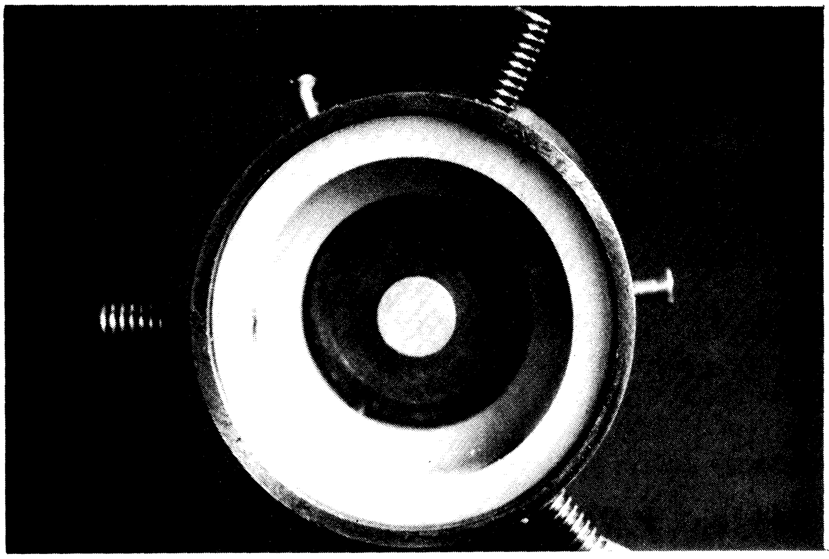

Figure 2.7. Retainer Cap for PZT-5 Ceramic Disc.

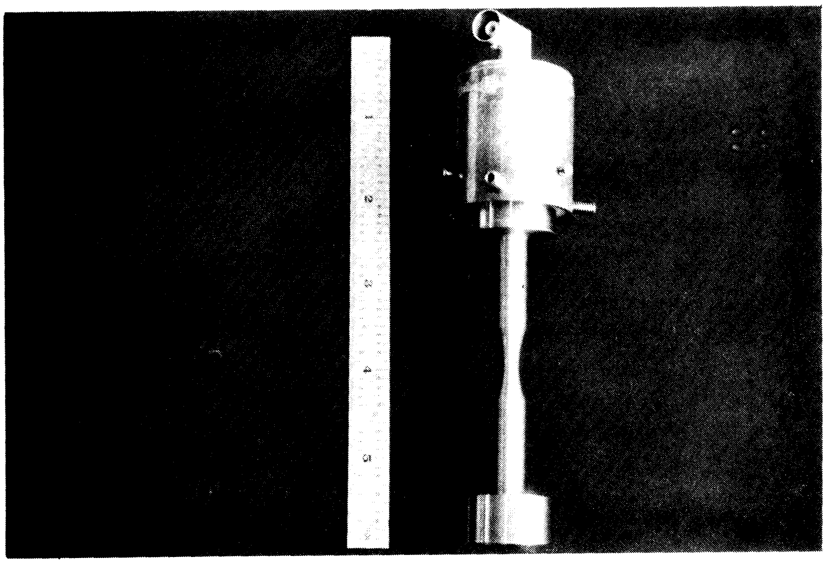

Figure 2.8. Assembled Acoustic Transducer.

a "high frequency" waveform, if the amplitude of the wave is above the trigger level of the counter. Thus a high amplitude burst may be counted as fifteen peaks but a lower amplitude burst, as ten peaks. The reason for this is that not only is the actual number of bursts or number of "high frequency" emission periods important but, also, the magnitude of each is important. Some local deformations may be larger than others. These might result in larger acoustic emissions. This system, therefore, does a crude integration, so to speak, on the acoustic output. It generates a count which is proportional to the plastic deformation and cross slip if the models proposed of Schofield are assumed to be correct (28, pp. 8-12).

Referring again to Figure 2.4 one sees that the output of the Visicorder gives a simultaneous record of the stress, cumulative total emissions, and RMS voltage output as functions of time. In additon, a load-cumulative emission plot is produced on an X-Y recorder.

2.1.5.2 Acoustic Isolation

The actual detection equipment to be used in the research was used to investigate the acoustic isolation necessary to bring the external noise output of the PZT-5 below the electronic noise level of the amplifier. The results of the tests are shown in Figure 2.9. Note that the ordinate is in terms of decibels, where zero dB is referenced to the electronic noise level of the amplifier with a 20-180,000 cps bandwidth.

Studies of various isolation systems indicated that the most

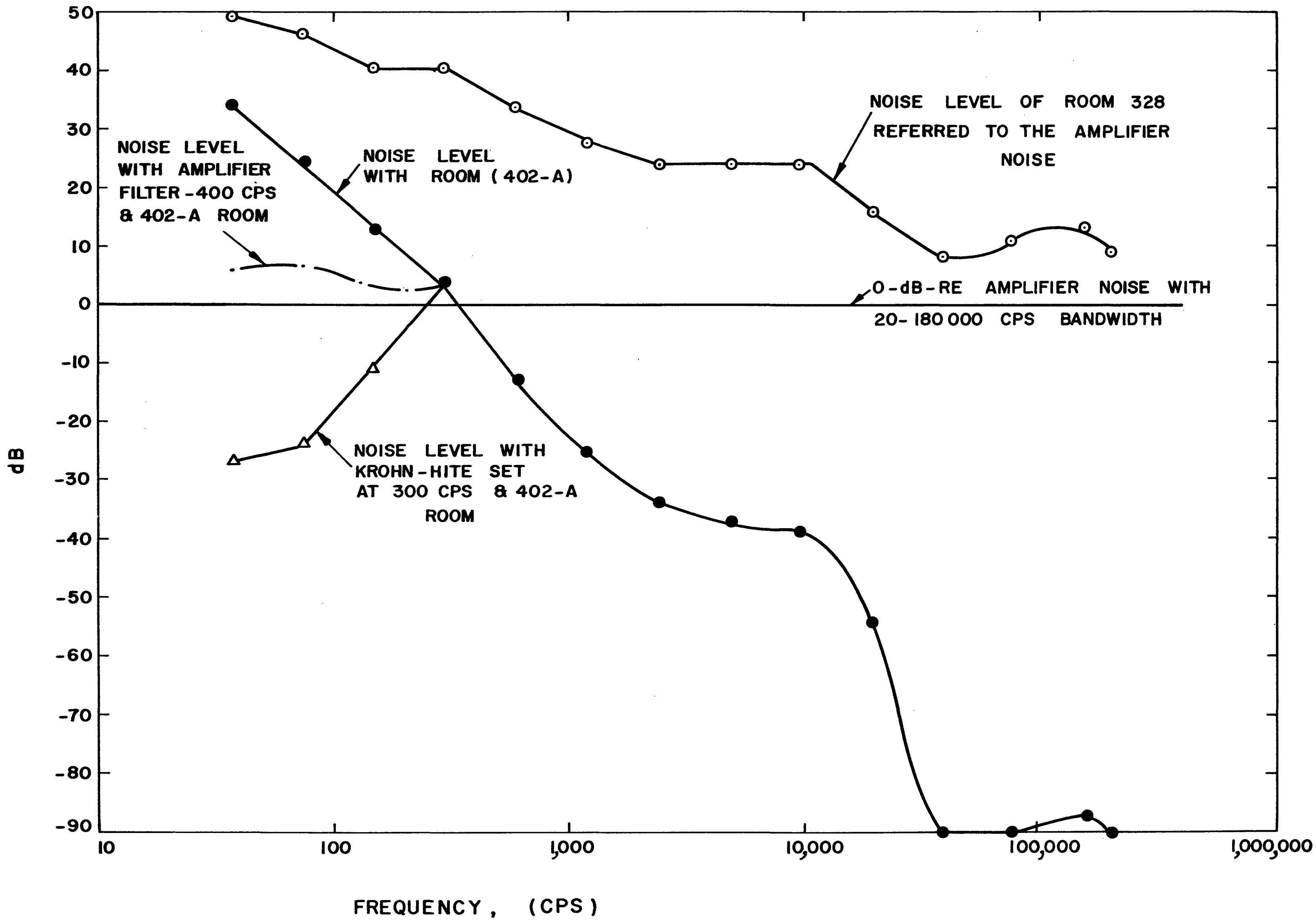

Figure 2.9. dB History of the Environment.

efficient solution from the standpoint of time and money was the use of an Industrial Acoustics Company's, model 402A Audiometric room and a Krohn-Hite bandpass filter set for a lower cutoff of 300 cps. The upper cutoff was 180,000 cps, since this was the upper limit of the hushed amplifier which seemed to generate some objectionable noise above this frequency.

As a result of the above installation it was found that the RMS noise level referred to the input of the amplifier is 3.6 μv with an approximate input impedance of 4×10^{11} ohms at the 50 megohm, 50 picofarad (μμf) input setting. This figure is very deceiving since the actual peak voltage level is the voltage that triggers the counter. In order to control this trigger level a sine wave calibration circuit was provided to allow accurate resetting of the trigger. No ambient noise was registered on the counter when its trigger level was set using a 17.5 μv RMS sine wave voltage. This is equivalent to a 24.8 μv peak trigger voltage. This calibration circuit is shown in Figure 2.4.

The high ratio of ambient peak voltage to RMS ambient voltage is due to the fact that most of the noise is from high frequency, spiked waveforms. The effective voltage (RMS) is low relative to the peak voltage. However, by lowering the bandwidth to 300-20,000 cps one finds a peak trigger voltage of 7.6 μv while the RMS voltage is 1.74 μv. This again points to the high frequency amplifier noise as the source of the high trigger level, since actual acoustic noise reduction at high frequencies is 30 to 90 dB below the amplifier noise level. It is concluded that the sound isolation is adequate and is performing its planned function.

2.1.5.3 Acoustic Tensile Testing Machine

This machine was designed to test specimens to maximum loads of 10,000 pounds while detecting low-level acoustic emissions. It was designed so that the specimen could be cycled through load-unload fluctuations such as would be applied in fatigue. Figure 2.10 shows schematically this machine. Figure 2.5 shows the chain-type self-aligning tension grips. The grips in this machine were made of Zytel (molded nylon polymer). This was done because conversations with B. H. Schofield (14) indicated that Zytel is more silent than other commonly available materials that otherwise met the design requirements.

The operation of the acoustic tensile machine is as follows. To apply a load to the specimen one lowers tank # 1 by means of a synchronous motor driven pulley system. This allows the water in tank # 2 to drain out and reduce the buoyant force on the sand ballast tank. The increasing load is transmitted and multiplied through the 20:1 lever system. The load is then carried throught the chain-type self-aligning grips to the specimen. The calibrated load cell which is mounted on top of a crossbar in one of the chain links reads the load. When the maximum desired load is reached, the motor drive is used to raise tank # 1 to allow the water to refloat the sand ballast tank. The load on the specimen then reduces to zero. The rate of loading is essentially controlled by the

* indicates that acoustic isolation or mismatch material is used.

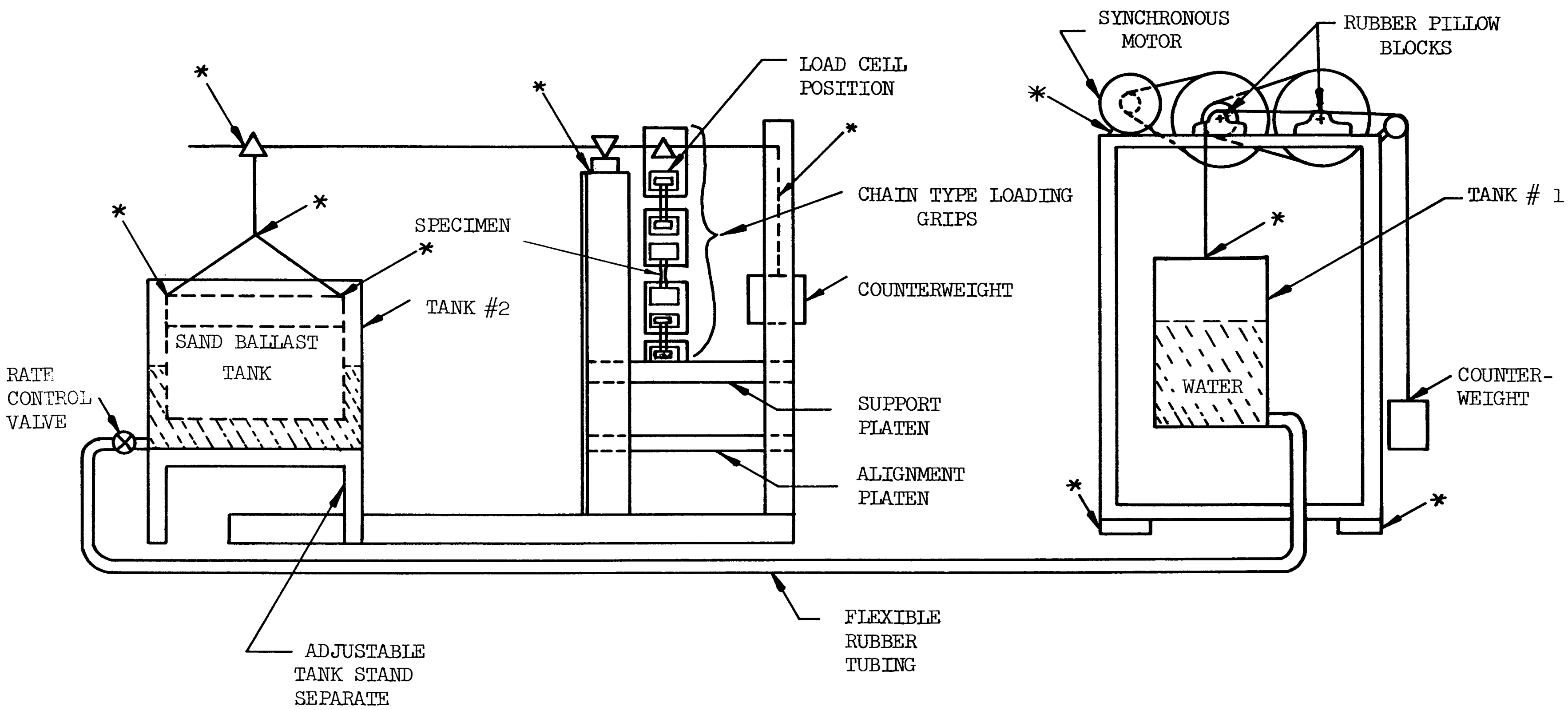

Figure 2.10. Schematic of the Acoustic Tensile Testing Machine.

water flow rate. This rate is adjusted by means of the control valve at the inlet of tank # 2. In this experiment a loading rate of about 20,000 psi per minute was maintained.

2.1.5.4 The Acoustic Experiments

With the acoustic equipment completed the acoustic test series was started. First, ten sample specimens were tested to provide familiarization and debugging time on the acoustic apparatus as well as to provide the acoustic characteristics for the trial specimens. These specimens were used for the determination of an approximate stress-life curve for the material. This was used to select the stress levels for the main body of the tests. Several suspicious characteristics were observed during these preliminary tests. First, the acoustic information had no "high frequency" component, which was expected, and second , the fatigue limit seemed to be between 56,000-65,000 psi or lower. Estimates using the Little line (46, pp. 104-105) indicate that the tension-tension fatigue limit is approximately 69,000 psi.

These facts suggested that some bending was present in addition to the axial load. So, before the major work was started, a solid state load cell and power supply were constructed. The cell shape was similar to a standard fatigue specimen except that a flat was milled on one side instead of generating a circular notch. The gages were mounted on this flat. Successive polar positioning of the gage provided an ability to check bending. This check revealed that a 39.5% bending stress relative to the axial stress was induced by the acoustic grips. Removal and inspection of the grips showed a machining burr which was subsequently removed. The bending stress after this corrective measure was taken was reduced to 5.2% of the axial stress. Bending checks were carried out on the chain-type self-aligning grips on the Research Incorporated fatigue machine. These grips are duplicates of the acoustic grips with the exception that they are made from AISI 1020 and carburized AISI 6150 steel. Bending here was again recorded in a polar manner giving a maximum value of 5.45%.

In order to minimize the difference in stress patterns in the acoustic test machine and the fatigue machine the polar diagrams were compared and each specimen in the test was oriented so that the maximum stress in the acoustic machine occurred at the same point in the specimen while undergoing fatigue testing. This technique resulted in a maximum stress pattern difference of 1.5%.

Two specimens were lost because of poor seating of a specimen in the Zytel grip, thus bending and damaging both the specimens and grips. The grips were reprocessed and checked for bending. In this case the bending reached a maximum of 3.5%. This resulted in a maximum bending stress pattern difference of 2.0% relative to the fatigue grips.

The large bending stress components in the acoustic tests had probably induced large permanent bending deflections in the trial specimens. These deflections would induce large bending stresses upon fatiguing and, therefore, early failure of the specimen. This is equivalent to a lowering of stress-life curve for this material. Thus the stress levels were selected slightly high to help account for this effect. As a result coded stress levels 0 through 6 were assigned, respectively, as fatigue loads of 0-95, 0-90, 0-85, 0-80, and 0-75 ksi to failure; 0-90 ksi for 10^4 cycles then 0-75 ksi to failure; and finally 0-75 ksi for $2x10^5$ cycles followed by 0-90 ksi to failure. After starting the fatigue tests it was found that about half of the 75 ksi (code 4) were running past $5x10^6$ cycles. Since this study was proposed to study life in the finite, not infinite, life region of the fatigue diagram it was decided to reassign and test all the remaining twenty-six code 4 specimens at 100 ksi. The effect that this reassignment had on the statistical analysis is discussed later.

With the debugging completed the standard test series was started. The procedure was to install the PZT-5 crystal retainer cap, mount the assembly into the grips, turn on the amplifier, seal the audiometric room, calibrate the load cell, calibrate the analogue-cumulative emission output, calibrate the counter trigger to 17.5 μv RMS sine wave voltage referred to the amplifier input, check the ambient transducer voltage output, lower tank # 1 (Figure 2.10) in order to load the specimen, then when the maximum load is reached unload the specimen by raising tank # 1, record the final emission values, and lastly remove and store the Visicorder and X-Y recorder outputs. The specimen is then removed and returned to the mineral oil until tested in fatigue at the same level as it was stressed in the acoustic work. Dual stress level fatigue specimens, which were to be fatigue tested sequentially at one stress level for an assigned number of cycles and then at another stress level to failure, were stressed in the acoustic tensile machine two times - once at each of the two stress levels and in the order of the stress level applications in the fatigue experiments.

2.1.6 The Fatigue Machine and Tests

Following the acoustic tests a series of fatigue tests were performed lasting about six weeks. These tests were completed on a Research Incorporated Materials Testing System which is discussed below.

2.1.6.1 The Fatigue Machine

The physical arrangement of the fatigue equipment is shown in Figure 2.11. This shows the control console to the left, the load frame to the right, and the power supply to the rear. The equipment is modular in nature and consists of a 50,000 pound loading frame equipped with a 20,000 pound hydraulic loader. The machine was used in its load controlled state so that the acoustic load would not be exceeded in fatigue. This load control is supplied by the closed loop electro-hydraulic control system shown in Figure 2.12.

Essentially, the operation is as follows: an input command is entered into the summing junction. The command is amplified and converted to a current signal which drives a 15 gpm servovalve. The valve controls the oil supply to the hydraulic cylinder which in turn loads the specimen. The load cell senses the load and sends a signal to the summing junction. At the summing junction an error signal is generated and the electronic controller modifies its previous command to the servovalve. This error signal correction is done every 0.0001 sec. In this way the system provides

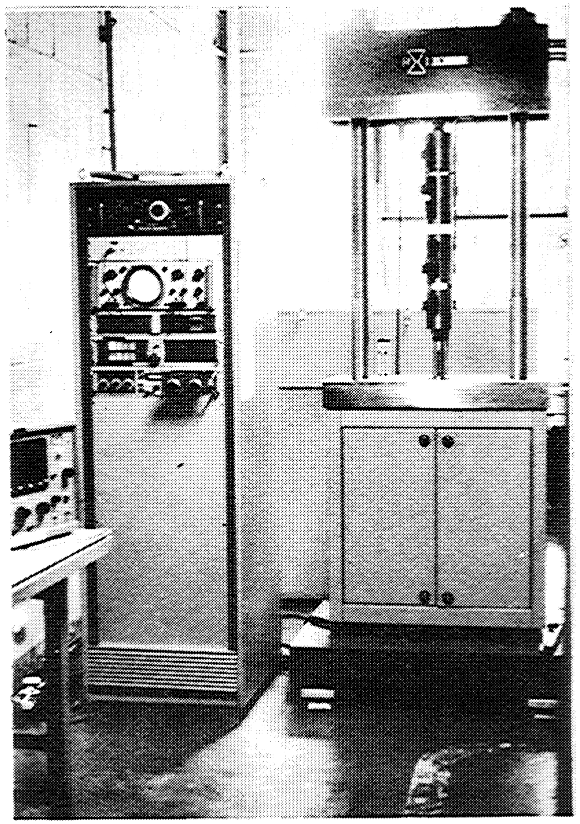

Figure 2.11. Research Incorporated Fatigue Machine.

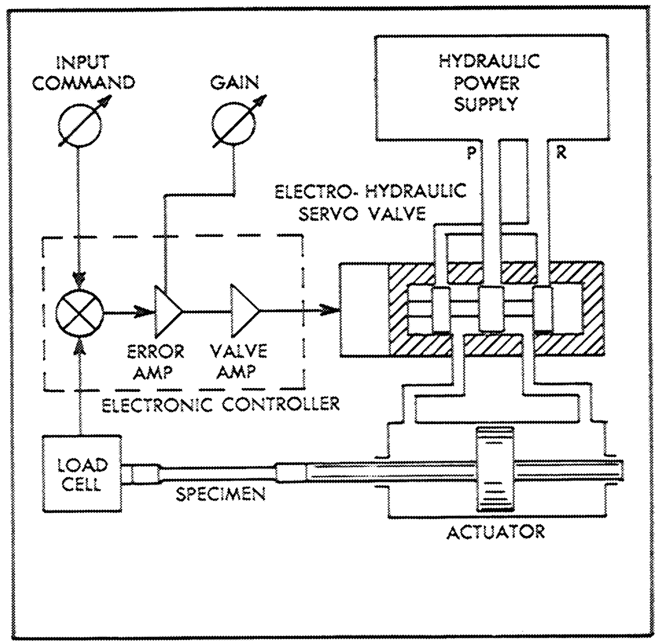

Figure 2.12. Closed Loop Load Control System.
[After Research Incorporated (47)]

rapid load control for fatigue studies. The system using a 10 gpm hydraulic supply, a 15 gpm servovalve, a Model 401.01 Servac, and a 401.10 series Input Module with a special experimental transformer could operate at cycling rates in excess of 30 cps at 100,000 psi on the specimens used in this research. It was decided to maintain a constant driving frequency of 30 cps so as to avoid any life changes (8, pp. 632-633) owing to changes in this frequency.

Figure 2.13 shows the Taylor wet bulb-dry bulb recorder, serial number 77JM216-995, used to record the wet and dry bulb temperatures in the testing room. Barometric pressure readings were supplied by the University of Michigan Meterology and Oceanography Department. Calculations using these three terms resulted in an absolute humidity in grains of water per pound of dry air. The counter in the left-hand corner of Figure 2.13 was used to check the driving frequency of the fatigue machine and to indicate the accumulated time, in seconds, for specimen failure to occur. This provides a check on the mechanical counter supplied with the machine (upper limit of 35 cps).

Figure 2.14 shows the tension-tension chain-type fatigue grips used on the fatigue machine. These are constructed using bearings where a lead-teflon mixture is impregnated into a porous bronze carrier that is mounted on a steel backing (48) (49).

3.1 ACOUSTIC EMISSION: ITS CHARACTER

In the process of performing acoustic tests it became necessary

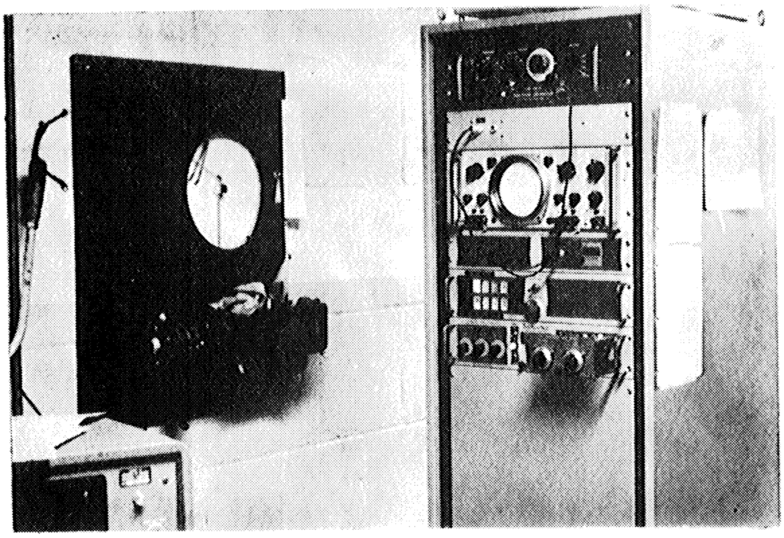

Figure 2.13. Humidity Recorder and Electronic Counter.

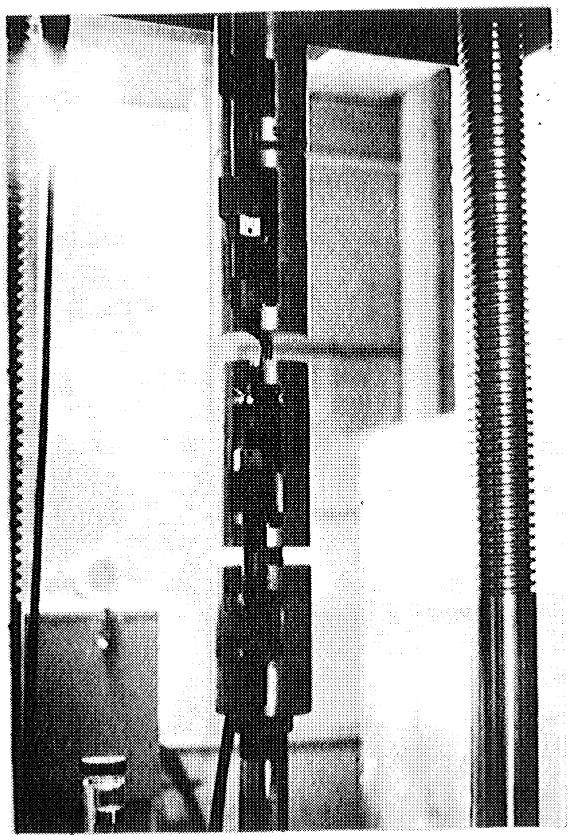

Figure 2.14. Tension-Tension Self-Aligning Fatigue Grips.

to characterize the emission information by defining a number of terms relating to it.

3.1.1 Emission Character

The physical appearances of the two major types of emission are shown in Figures 1.1 and 1.2. Figure 3.1 shows the typical ambient noise level of the amplifier operating with ambient acoustical environment sensed by the PZT-5 transducer. The oscilloscope sensitivity is identical in Figures 1.1, 1.2, and 3.1, namely 0.2 volts per centimeter. In comparing Figures 1.1 and 3.1 the peak signal to peak noise ratio, S/N, was 11:1. Other waveforms observed had a S/N ratio of 15:1. The full input amplifier gain could not be used since some signals were sufficient to saturate the amplifier if the maximum 80 dB gain were used. This would cause total blanking out of the signal. It was necessary instead to use the amplifier at a gain of 70 dB (3160X). This indicated that the levels of the emissions were not as low as had previously been reported.

A calculation was made of the detection capabilities of the piezoelectric crystal that was used in this work. Perfect coupling of the crystal to the specimen is assumed. The pressure found using this assumption will be lower than the actual pressure. This calculated pressure will be referenced to the threshold of hearing, .0002 μ bar, 0.1 newton/m^2, or 1.0 dyne/cm^2 (50, p. 50). This calculated pressure is the average pressure exciting the crystal from within the specimen. It is not the airborne acoustic emission level in the vicinity of the specimen. A compression

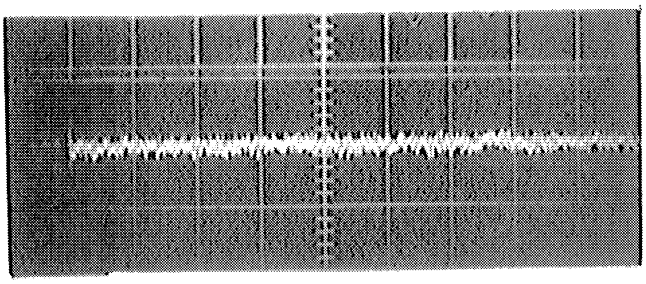

Figure 3.1. Ambient Noise Level.
Ordinate: 0.2 volts/cm
Abscissa: 0.2 msec/cm

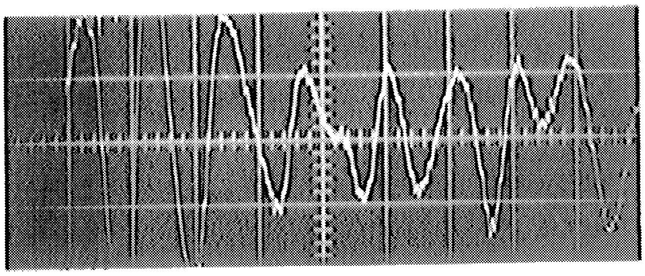

Figure 3.2. Burst Type Ringdown.
Ordinate: 0.2 volts/cm
Abscissa: 0.1 msec/cm

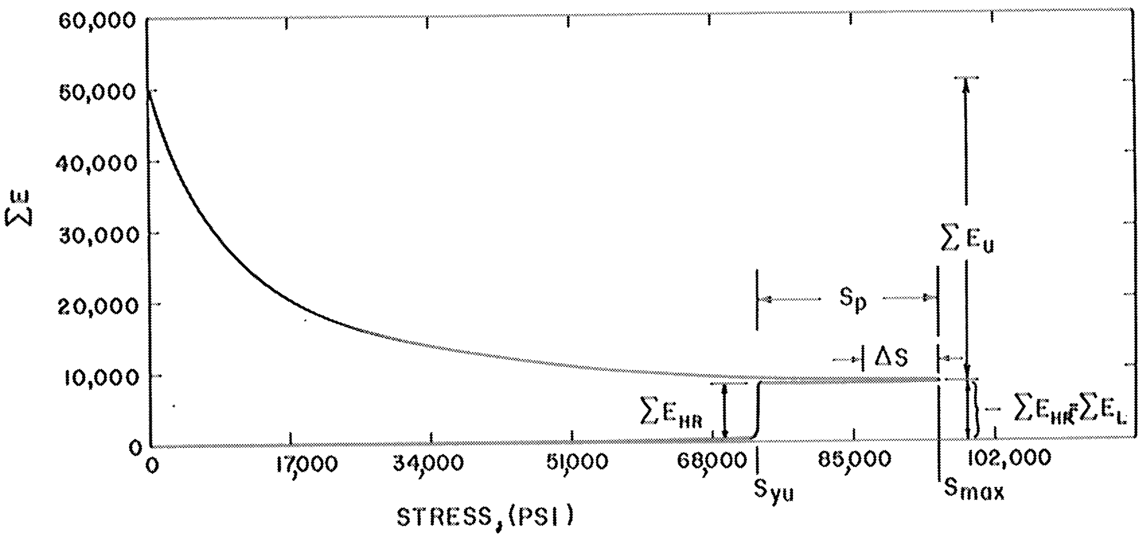

Figure 3.3. Typical X-Y Record of Acoustic Emission Data.
(Specimen 88-118-0-035)

wave reflected internally from end to end within the specimen is an extremely inefficient means of producing airborne sound. The energy that is radiated out into the air is well below a pressure that will be detected.

If only those pulses are counted that produce a voltage peak signal level of 24.8 μv at the input of the amplifying system, the pressure level of these pulses can be determined by the use of the piezoelectric stress constant, g_{33} , for the PZT-5 crystal which is used as the detector. This calculation is as follows.

$$g_{33} = \frac{\text{volt}}{\text{meter}} \times \frac{\text{meter}^2}{\text{newton}}$$

$$g_{33}\ (\text{PZT-5}) = 24.4\text{x}10^{-3}\ \frac{\text{volt meter}}{\text{newton}}. \qquad (51)$$

$$\text{volts}_{\text{minimum}} = 17.5\text{x}10^{-6} \times \sqrt{2} = 24.8\text{x}10^{-6} \text{ volts.}$$

The crystal length is 0.1 inch or $25.4\text{x}10^{-4}$ meters,

$$\text{hence } 24.4\text{x}10^{-3} = \frac{v}{l} \times \frac{1}{\text{stress}} = \frac{24.8\text{x}10^{-6}}{25.4\text{x}10^{-4}} \times \frac{1}{\text{stress}}$$

or the minimum detectable stress = 0.4 $^{\text{newton}}/_{\text{meter}^2}$.

In decibel notation this is $\text{dB} = 20 \log \frac{\text{stress}}{0.1\ \frac{\text{newton}}{\text{meter}^2}} =$

$$12 \text{ dB re } 0.1\ \frac{\text{newton}}{\text{meter}^2}\ .$$

Actual photographed outputs show levels which are as high as 15 times this level and, therefore, are 35.6 dB re 0.1 $\frac{\text{newton}}{\text{meter}^2}$ or 23.6 dB above the counting threshold, 0.4 $\frac{\text{newton}}{\text{meter}^2}$.

Another point to be clarified is that concerning the output frequency. Figure 3.2 shows an expanded burst ringdown similar to that shown in Figure 1.1. Calculations show that the frequency of the ringdown shown in this photograph is about 8,500 cps. Similar calculations for waves shown in other photographs give values from 8,500 to 10,500 cps with most frequencies being close to 10,000 cps.

Similar calculations were carried out using the waveforms shown in Figure 1.2 and other results. It was found that the frequencies of these "high frequency" emissions ranged from 8,000 to 10,000 cps. This is evidence that the term "high frequency" emission is a misnomer. The burst and "high frequency" types of emission both have the same frequency. However, it is not too difficult to imagine that a higher frequency component exists when the oscilloscope screen becomes filled with waveforms. In this work the "high frequency" emission will be termed high rate emission. Experiments show that 10,000 cps is approximately the mechanical ringing frequency of the specimen when externally excited. The ringing frequency of the electronic circuitry was found to be about 125,000 cps.

3.1.1.1 Terminology

Referring to Figures 3.3 and 3.4 one can define a number of terms necessary for a discussion of the emission results. The curves in Figures 3.3 and 3.4 are the actual output from specimens stressed to

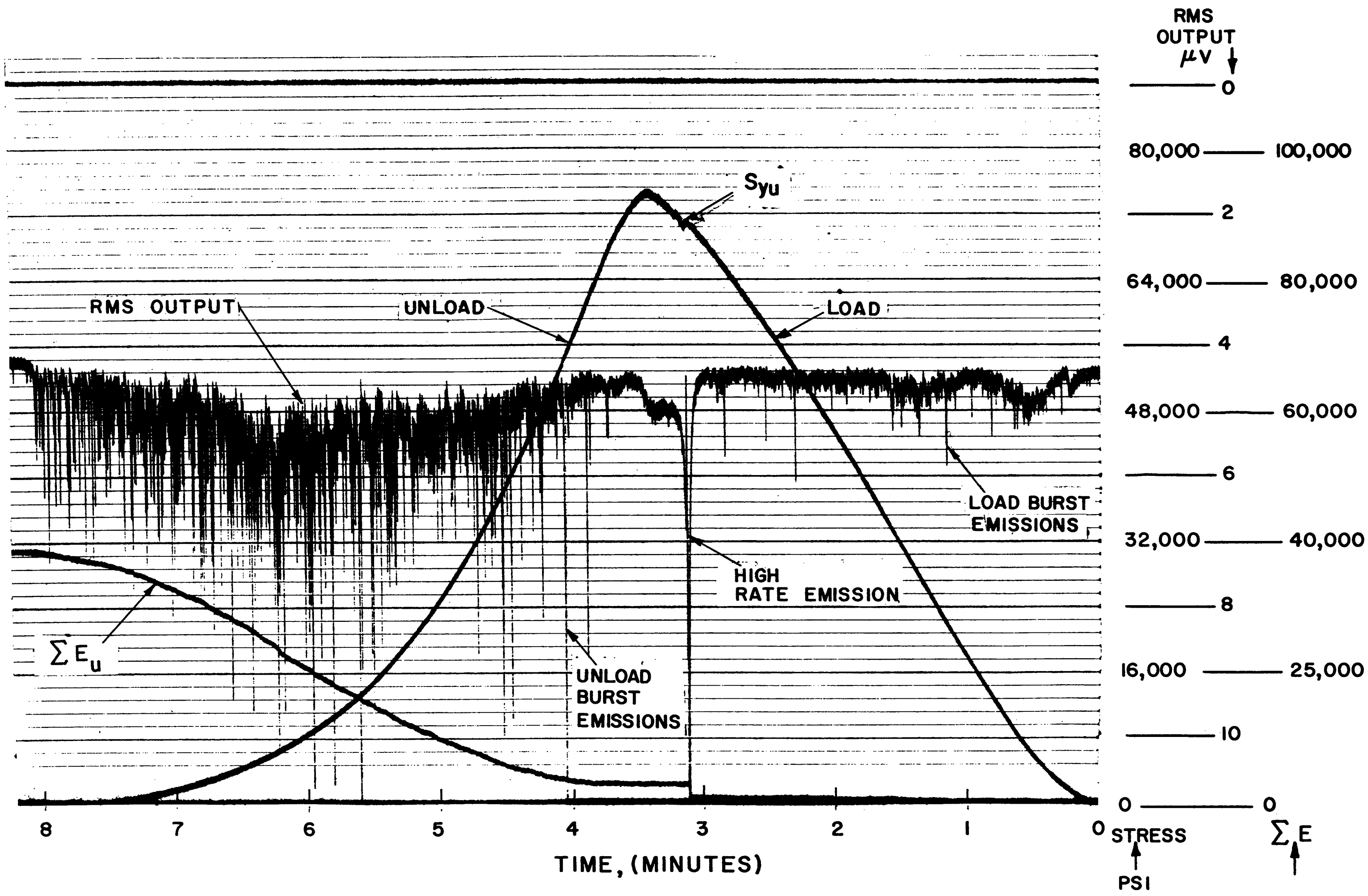

Figure 3.4. Typical Visicorder Trace of Emission Data.
(Specimen 174-407-4-231)

95,000 and 75,000 psi, respectively. The ordinate of Figure 3.3 is instantaneous cumulated emission. The abscissa is the applied stress. In Figure 3.4 the abscissa is time with ordinates shown as stress, cumulated emission, and RMS output voltage of the detection system. (Note the directions). As the specimen is loaded a small number of burst type emissions are seen up to the upper yield stress, S_{yu}. At this point the high rate emission appears. This point is coincident with the upper-lower yield point phenomenon in each specimen. This confirms the observation of previous investigators (32) (33). The emission in this region is termed ΣE_{HR}. Continued loading results in subsidence of the high rate emission and a recurrence of burst type emission. This is seen up to the maximum applied stress, S_{max}. The total of the burst type emission that occurs during the application of the load is termed ΣE_L . This does not include the ΣE_{HR}.

In the process of unloading there is a period of silence where no activity is observed. This period is measured in terms of stress and is called the "stress delay," ΔS. At the end of the ΔS one sees again the occurrence of burst emissions. The bursts on unload appear to be of exactly the same form as those seen on the load except their rate of occurrence is much higher and changes with load. This does not say that the actual waveform frequency has increased. This emission during the unload is termed the unload emission, ΣE_U . The emission during unload has not been seen or considered previously to this time except for one observation by Schofield (28, Figures 12, 13, and 14). The unload character found in the present study is remarkably consistent in shape and repeatable within a given specimen. Use of another specimen results in the same characteristic unload emission curve except its total could reach ΣE_U values ranging from 8,000 to 70,000. It is convenient to define the total emission as $\Sigma E_T = \Sigma E_L + \Sigma E_U$. The last term to be defined is the stress into the plastic range, S_P . This is the engineering stress applied beyond S_{yu} or $S_P = S_{max} - S_{yu}$.

4.1 STATISTICAL ANALYSIS OF THE DATA

After obtaining all of the experimental data (see Appendix II) it was decided to use two statistical computer programs to analyze them. These programs are the MCA (Multiple Classification Analysis) and SRWSL (Stepwise Regression with Simple Learning). The latter will be termed the regression program for brevity.

4.1.1 The MCA Program

The MCA program was used in order to provide some knowledge as to the function that might be expected if a regression analysis were attempted on the data. The problem with most regression programs is that they have only a limited number of available functions from which to find the least squares fit. If the problem being solved has a functional relationship that is not available to the computer, the computer will either have no success with the solution of the problem or it will approximate the function by a truncated infinte series. The latter usually is not possible owing to the large amounts of computer time necessary to generate a sufficiently good approximation of the function.

Therefore, for this work the shortcomings of the regression program were circumvented and more insight into the problem was obtained by using the MCA program first.

4.1.1.1 Details of the MCA Program

The MCA program is used to investigate the effect of each of the several independent variables on a dependent variable, in this case N or log N. Two methods (52, p. 2) (53, pp. 3-4) are used to determine the effects of a given independent variable. First, all the independent variables are categorized. For example, the RMS surface finish in μ in., which varies from 90 to 350 μ in. RMS, is broken down into classes 0 to 5 which are not necessarily uniform in range of RMS. Once this is done the program analyzes the data by determining the deviation of the dependent variable from the dependent variable grand mean for each class of the independent variable. This is the unadjusted deviation method.

However, the second treatment, the adjusted deviation technique, is most important. In a real experiment it is generally impossible to investigate a dependent variable while holding all but one independent variable constant. To give insight into problems of this kind, the MCA program examined the relationship of each of the several independent variables to a single dependent variable while holding all other variables constant (53, p. 4) (54, p. 3). The program gives a set of adjusted deviations which represent the effect of each class of an independent variable on a dependent variable while all other independent variables in the data are held at a constant level. It should be pointed out that the program's convergence is not affected by interactions. Moreover, the program can not yield estimates of the interaction effects that are important in the prediction of the dependent variable (52, p. 4).

This program has advantages over multiple regression, since it does not have a limited set of available functions from which to draw. It accepts predictors in weak nomial scale form, such as an incident factor. It does not assume or require linearity and it does not need orthogonal data; i.e., it does not need equal numbers of observations in all cells of a cross classification of the independent variables (52, p. 1) (54, pp. 5-6). This program assumes additivity of the effects of the predictors. However, by conversion of the dependent variable to log N one finds that a multiplicative model can also be accommodated (55, p. HP 10). These models are respectively,

$$N_{ijk\ldots\alpha} = N + a_i + b_j + c_k + \ldots + e_{ijk\ldots\alpha}$$

where $N_{ijk\ldots\alpha}$ is the actual life value corresponding to the levels of the independent variables a, b, etc. a_i, b_j, etc. are the effects of variable a at the ith level, b at the jth level, etc. $e_{ijk\ldots\alpha}$ is the random error adjustment made for the portion of the life not predicted by the dependent variables (54, p. 3).

$$\log N_{ijk\ldots\alpha} = \log N + a_i + b_j + c_k + \ldots + e_{ijk\ldots\alpha}$$

where all terms have the same general meaning but life is handled in logarithmic form.

In order to provide these adjusted deviations, the MCA program minimizes the sum of squares of the errors, $e_{ijk\ldots\alpha}$, in the predicting equation while simultaneously examining the relationship of the several independent variables to the dependent variable. This is done by an iterative process developed by Yates (56) to solve the set of normal equations with the constraining equations; $\Sigma\, n_i\, a_i = 0$, $\Sigma\, n_j b_j = 0, \ldots$, etc., where n_i = number of observations in the a_ith classification (57, p. 28).

One now has the ability to examine the unadjusted class deviations and thus determine whether or not the predictor has any relationship to the dependent variable. This shows whether it is positive, negative, concave upward, or of another form. An examination of the adjusted deviations shows whether this effect is real or just caused by the other variables. It essentially provides a "purified" view of the real relationship between a single independent variable and the dependent variable.

One must realize that the program can generate a set of deviations that looks very convincing but an examination of the data will indicate that the fraction of the variance explained by the predictor is very small compared to the variance of the dependent variable. It, therefore, is not an effective predictor. To eliminate this problem the program prints out the square of the "partial beta coefficient", β^2 (53, pp. 6-8). This can be thought of as an approximate square of the partial correlation coefficient for that variable. Here, it will be termed the importance coefficient, since it is the proportion of the variance in the dependent variable that is explained by that particular independent variable while holding all other independent variables constant (53, p. 8). One can readily see why it is called an importance factor. The higher the factor the greater the amount of dependent variable variance that is explained by the independent variable. Thus one can order the predictor variables as to their importance in the prediction. Moreover, the square of the adjusted multiple correlation coefficient, R^2, is provided. This indicates the proportion of the variance in the dependent variable that is explained by all the predictors simultaneously (52, p.3). R^2 may be thought of as a multiple coefficient of determination.

4.1.1.2 MCA Implementation

In order to use the MCA program all the independent variables must be classified. The classification of each variable is shown in Appendix II adjacent to the actual value of the variable.

Note that the data are shown for the following variables: S, ΣE_L, ΣE_U, ΣE_{HR}, TIR, RMS, T, H, I, S_P, B, P, ΣE_T, and N. (See Appendix III for a list of symbols and terminology). All of these have been explained previously except the incident factor, I, which denotes special history associated with certain specimens. These various incident factors are defined in the legend of the data table in Appendix II.

4.1.1.3 Results of the MCA Program

Two groups of runs were completed in this program. The first group of runs, numbers 01 to 08, used the life data in numerical form. The second group of runs, numbers X1 to X13, use log life data.

Table 4.1 shows the run number, the order of the variable entry, the importance coefficient for each variable, and R^2 for each run. The order of variable entry will indicate, upon reversal of such order, large intercorrelation of the supposedly independent variables. This shows up as a large change in the importance coefficient, β^2, associated with the two or more intercorrelated variables when their order of entry is switched (53, p. 11).

Preliminary MCA runs, not shown in Table 4.1, indicated that S and S_p were highly intercorrelated. Subsequent runs showed that S_p was a better predictor than S. All the runs shown in Table 4.1 use S_p except 03 and X3. The improvement obtained through the use of S_p seems small when comparing runs X2 and X3 as well as 02 and 03. Since large intercorrelations such as those between S and S_p hamper convergence in the MCA program, one variable had to be excluded to complete the work. S was dropped, since it appeared less significant than S_p. Results shown later in the regression program indicate that S_p is actually a better predictor than the above comparisons would indicate. It is thought that the classification scheme may have obliterated some of the predictive value of S_p.

One immediately sees in runs 01 to 08 that R^2 is extremely low. This indicates one of two things. Either no variable is truly important in the prediction or that the wrong mathematical model has been used.

TABLE 4.1

MULTIPLE CLASSIFICATION ANALYSIS RESULTS
(all runs converged)

Run No.	Order	S	ΣE_L	ΣE_U	ΣE_{HR}	TIR	β^2 RMS	for T	H	I	S_P	B	P	ΣE_T	R^2	Iterations
01	S_P,T							.042			.196				.132	5
02	S_P,T,ΣE_U			.051				.048			.202				.114	6
03	S,T,ΣE_U	.199		.041				.015							.151	6
04	S_P,T,ΣE_T							.038			.194				.101	7
05	S_P,T,ΣE_U,P			.045				.121			.293			.036	.160	12
06	S_P,T,ΣE_U,I(with I_{MAX}= 0)			.057				.082			.197		.257		.013	7
07	S_P,T,ΣE_U,I			.054				.060		.029	.282				.012	51
08	P,ΣE_U,T,S_P			.046				.121			.293		.257		.160	13
X1	S_P,T							.036			.724				.706	4
X2	S_P,T,ΣE_U			.020				.036			.700				.703	4
X3	S,T,ΣE_U	.696		.036				.012							.695	4
X4	S_P,T,ΣE_T							.039			.687			.033	.718	5
X5	S_P,T,ΣE_U,P			.024				.068			.756		.091		.714	6
X6	S_P,T,ΣE_U,I(with I_{MAX}=0)			.024				.027		0.000	.680				.623	4
X7	S_P,T,ΣE_U,I			.008				.013		.180	.573				.808	26
X8	P,ΣE_U,T,S_P			.023				.067			.760		.089		.715	7
X9	S_P,T,ΣE_U,P,RMS			.025			.008	.067			.742		.102		.706	6
X10	S_P,P,T,ΣE_U,B,ΣE_L,ΣE_{HR}, H,TIR,RMS		.033	.038	.062	.049	.032	.110	.020		.860	.064	.190		.750	17
X11	RMS,TIR,H,ΣE_{HR},ΣE_L,B, ΣE_H,T,P,S_P		.032	.036	.060	.043	.029	.107	.021		.874	.046	.180		.751	18
X12	S_P,P,T,B,ΣE_{HR}							.064			.842		.048		.768	8
X13	ΣE_{HR},B,T,P,S_P							.062			.844		.047		.769	6

The X1 to X13 series shows a greatly increased R^2. Thus the multiplicative model appears to apply to the data. Concentrating now on runs X10 and X11, one sees little change in the β^2 with a change in order. The intercorrelation of independent variables is now low.

Comparison of X2 and X6 shows that the independent variable β^2 change is small. In X6 all the "contaminated" data, which resulted from specimens where some incident occurred, were removed from the analysis. In Table 4.1 this is indicated by $I_{max}= 0$. The insignificant change in the β^2 indicates the small effect of I, the incident factor. Note that R^2 went down in X6. This was expected since the sample size went down by approximately 33% and since R^2 is dependent upon sample size. It is concluded that the incidents recorded had little effect on the fatigue life.

Now, with S and I disregarded look at run X10. The order of variable importance is S_p, P, T, B, ΣE_{HR} , TIR, ΣE_U , ΣE_L, RMS, and H. Observe the difference between $\beta^2 = .860$ for S_P and the $\beta^2 = .19$ for P, the second best predictor. One can see that S_P is by far the best predictor and all other predictors are secondary.

Another observation concerns Table 4.1, run X7. It shows a large drop in S_P's β^2. Moreover, Figure 4.1 shows the same confounding effects on the estimates of the log life deviations at S_P = 31,500 psi. These effects were traced to a confounded data situation where two classes in S_P were almost directly associated with a single class in I. This will result in an occurrence such as seen in X7 and Figure 4.1 That is, some of the

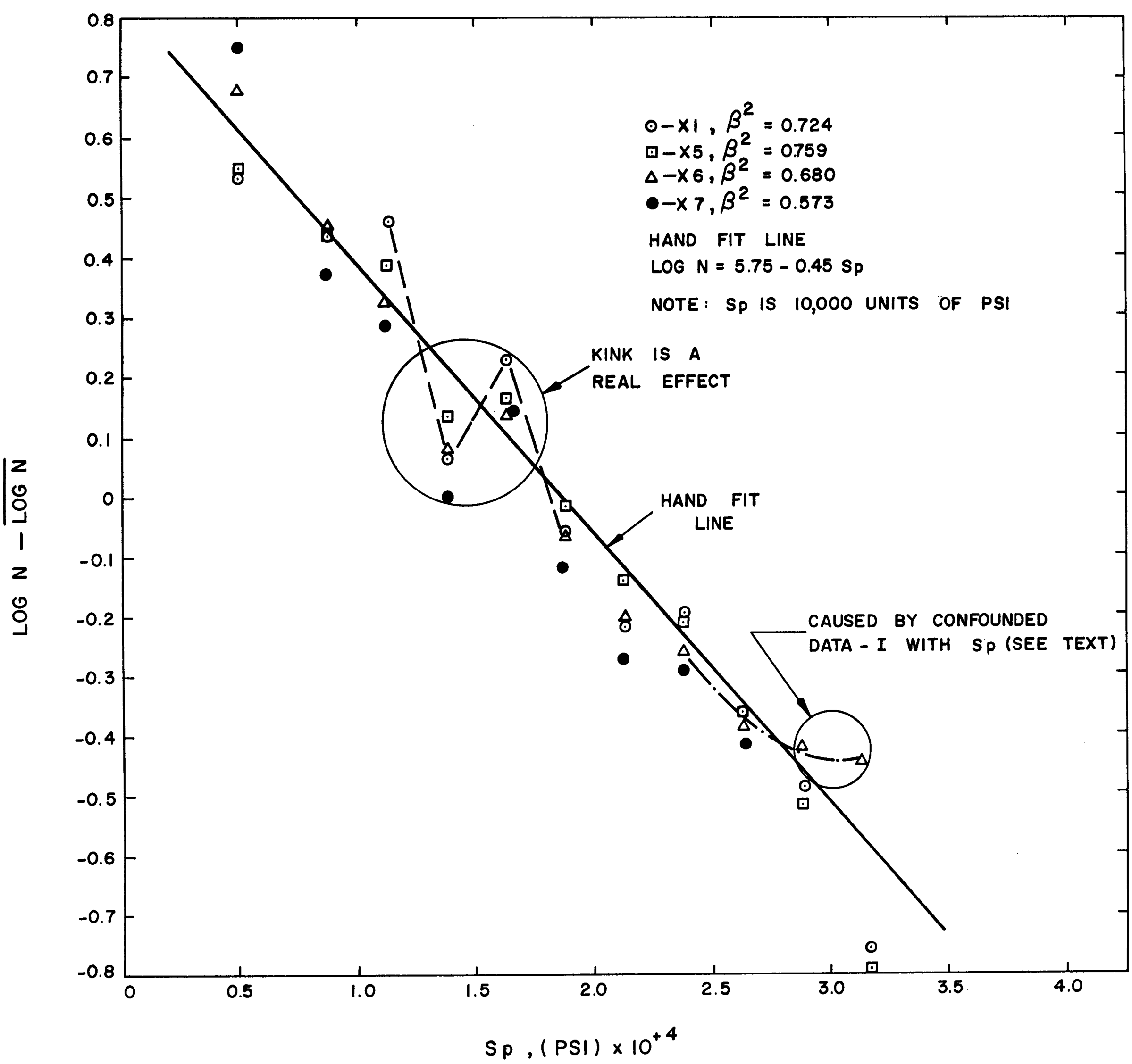

Figure 4.1. Multiple Classification Analysis Results of Log Life Deviations vs. Engineering Stress Beyond the Upper Yield Point, $\overline{\text{Log N}} = 4.95$.

variance in the dependent variable previously associated with one of the independent variables (namely, S_P) will, upon addition of a confounding variable, be associated with the predictor entered last (namely, I).

The predictor of primary interest is S_P. Figure 4.1 shows a plot of the adjusted deviation of log N associated with S_P. Note the negative nature of the curve. But the kink at about S_P = 15,000 psi is disturbing. Various adjustment techniques were used but they could not account for this kinking effect as being caused by the other variables. The kink appears to be a real phenomenon. No explanation is evident for the kinking of the curve, although others (3, p. 180) have reported data with similar phenomenon in AISI 4340 steel relative to their probability-stress-life diagrams.

In order to arrive at an estimate of the function necessary for the regression program, a straight line was hand fitted to the MCA output. This resulted in log N = 5.75 - .45S_P. This program does not provide the standard errors of the estimates used to develop this equation. However, certain standard errors are provided by the regression program. These standard errors will be presented in section 6.1. The regression program did not have such a function available. Moreover, the program had no means of making log N available. A change in one of the subroutines was necessary to accomplish the task. However, this pointed up a weakness in the program so recent revisions of the program now make any computer library function of the dependent variable available on request.

Figure 4.2 shows a similar plot of log N deviations relative to S. Again the trend is negative. In this case the class 7 (75,000 psi) data are non-representative since it is actually a collection of low life 75,000 psi specimens. Early in the experiment the 75,000 psi stress level was changed to 100,000 psi owing to non-failures at 75,000 psi. The recorded failures were of the early failure type, since the infinite life data could neither be recorded nor handled in the computer. The other low life specimens at 75,000 psi were from the dual stress level experiments that failed during the first set of stressings. Both cases represent the low life specimens in a population of about 35 specimens. Therefore, these are not representative data points. Thus the hand fit line in Figure 4.2 does not consider the 75,000 psi points. It is interesting to note that these low life specimens did not harm the linearity of the curve for Sp(Figure 4.1). Inspection of the Sp data corresponding to the low life 75,000 psi specimens show that their S_P value tends to be closer to the S_P values corresponding to the 80,000 psi stress level. Thus the engineering stress beyond the upper yield point can help detect the early failure whereas the gross stress value cannot detect it.

Many graphs similar to Figures 4.1 and 4.2 could be inspected but it is only appropriate to discuss the major predictors and the emission predictors. Thus Figures 4.3, 4.4, and 4.5 will show the effects of P, ΣE_{HR}, and ΣE_U, respectively, on log N.

Position, being the next best predictor, is presented in Figure 4.3.

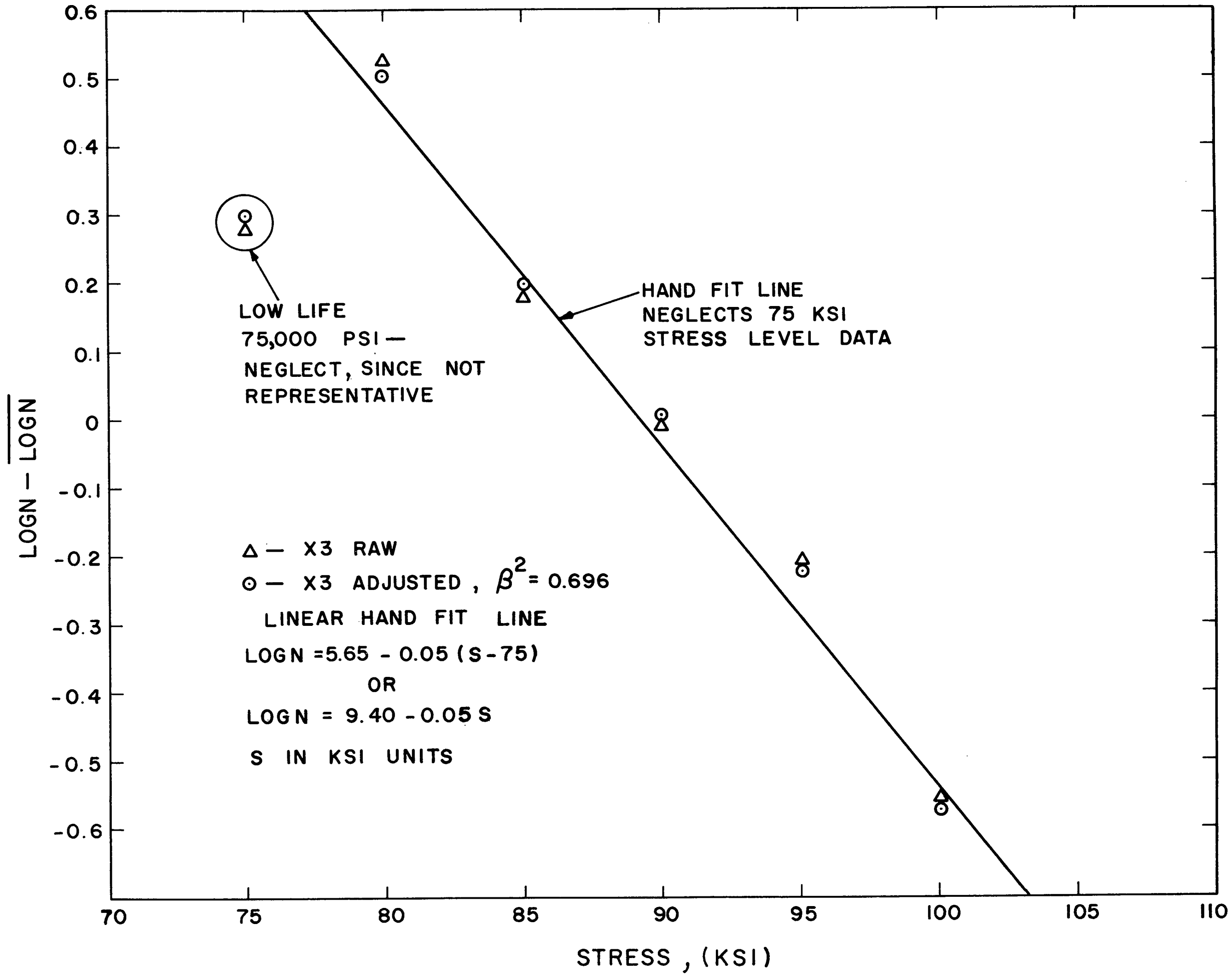

Figure 4.2. Multiple Classification Analysis Results of Log Life Deviations vs. Applied Fatigue Stress, $\overline{\text{Log N}}$ = 4.95.

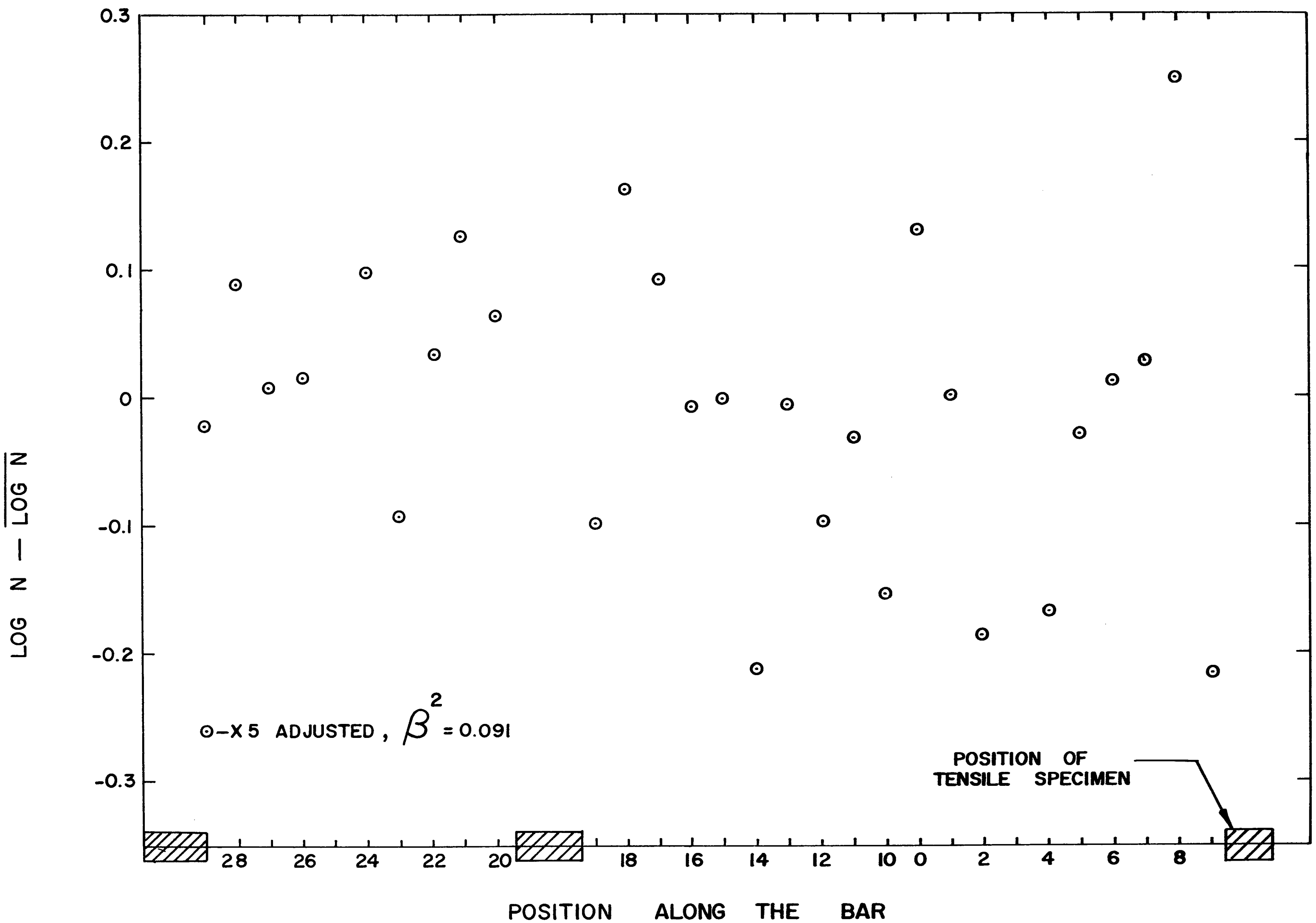

Figure 4.3. Multiple Classification Analysis Results for Log Life Deviations vs. Position, $\overline{\text{Log N}}$ = 4.95.

One must realize that the importance coefficient is below 10% for this variable. This means that the trend of the adjusted average deviations shown in this figure explains less than 10% of the unexplained variance in log N. A weak zigzag strength trend can be seen in Figure 4.3; however, it may not be a real effect, since the standard error of these adjusted deviations may be large relative to the deviations themselves. Thus the weak strength trends could be obliterated by the scatter in the individual observations. If it were important to determine the real position effect a separate determination of the standard error of these deviations would have to be made.

Figure 4.4 concerns the log N changes associated with ΣE_{HR}. Note the point to point scatter in the raw data values. But the adjusted points tend closer to zero effect. Again, it should be noted that a β^2 = .036 means that this variable can only explain 3.6% of the total variance in log N when all other variables are held constant. No conclusion can be drawn except that there appears to be no effect.

An even smaller value of β^2 is encountered for ΣE_U. Figure 4.5 shows the log N deviations versus ΣE_U. Since β^2 can be thought of as an approximate partial correlation coefficient squared, it is apparent that the approximate partial correlation coefficient, β, would be only about 4.5%. Thus little or no correlation exists since a correlation coefficient of this magnitude could probably result by chance.

4.1.2 Stepwise Regression

The purpose in using the stepwise regression was to investigate

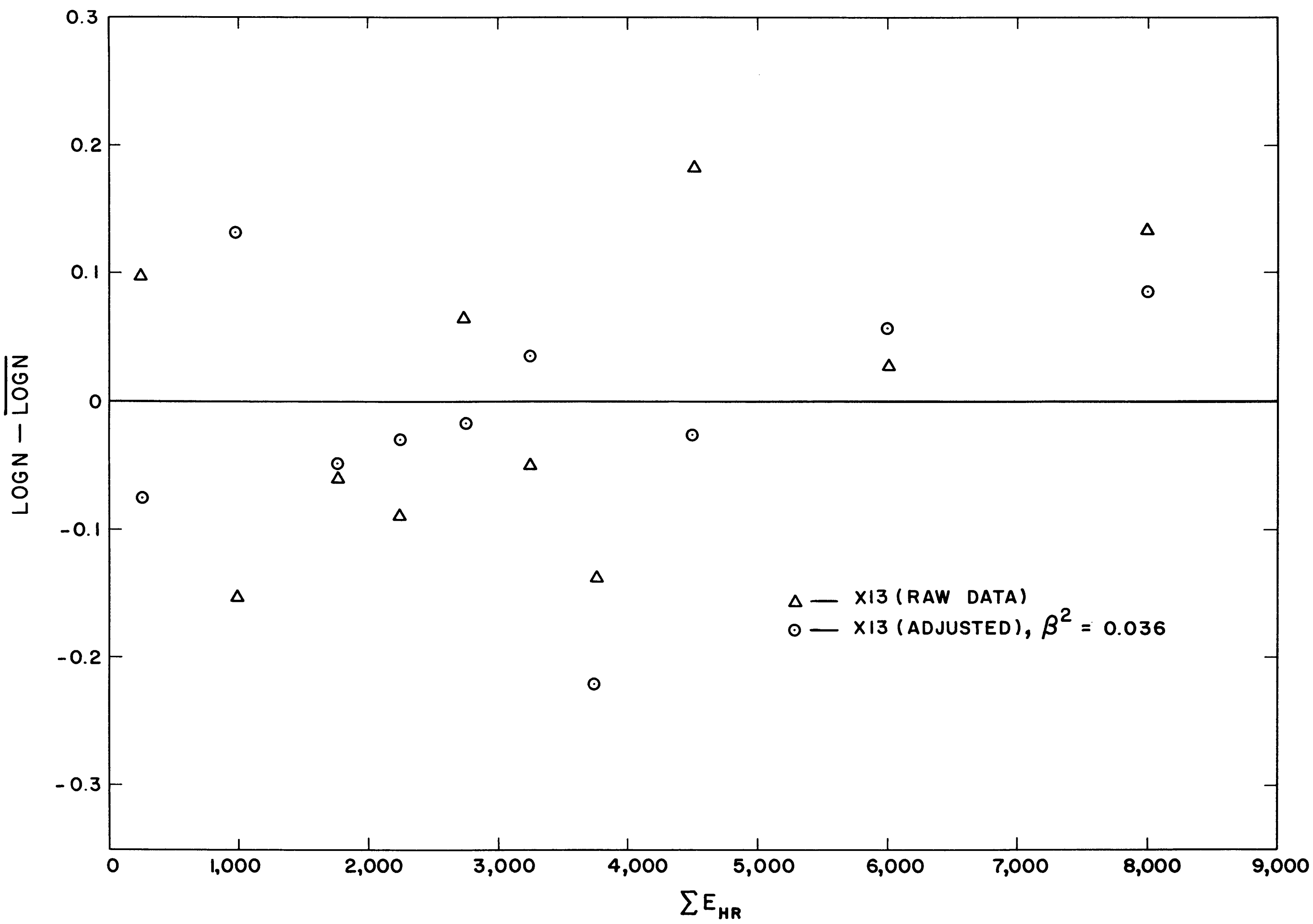

Figure 4.4. Multiple Classification Analysis Results for Log Life Deviations vs. Totalized High Rate Emission, $\overline{\text{Log N}} = 4.95$.

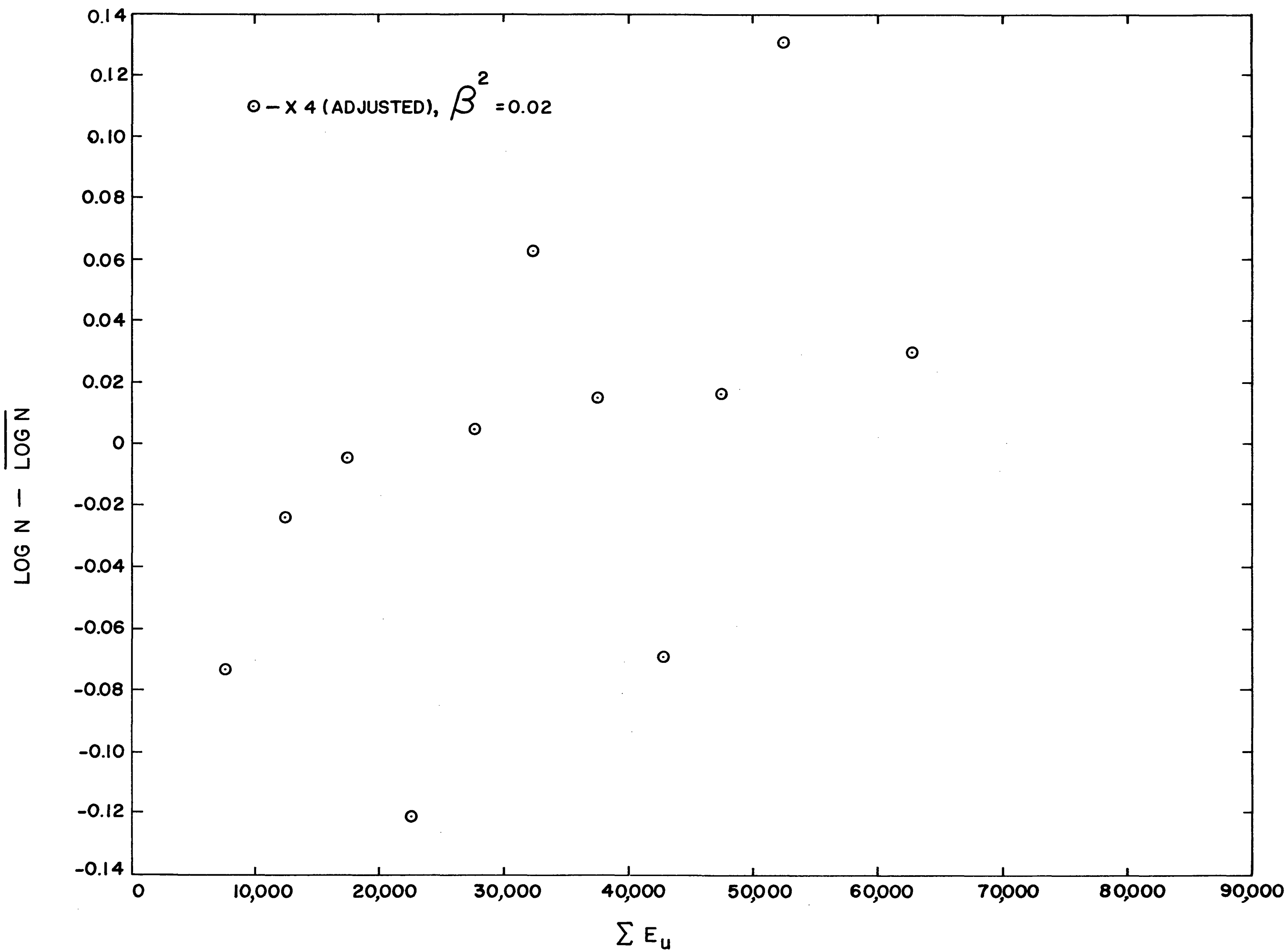

Figure 4.5. Multiple Classification Analysis Results for Log Life Deviations vs. Totalized Unload Emission, $\overline{\text{Log N}}$ = 4.95.

a number of possible functions that might be used to describe the dependent variable. The objective is to generate a predictive equation of the form

$$Y = b_o + b_1 X_1 + b_2 X_2 + \ldots + b_i X_i + \ldots + b_p X_p$$

where b_o is a constant and the b_i's for $i = 1, 2, \ldots, p$ are the coefficients of the individual predictor variables, X_i (58, p. 70) (59). In this case the X_i's can be any function or certain interactions of the following variables S, ΣE_L, ΣE_U, ΣE_{HR}, TIR, RMS, T, H, and S_P. The variables I, B, and P are eliminated because a regression cannot be done on such nominally scaled variables. ΣE_T is eliminated because the computer can form ΣE_T by $\Sigma E_L + \Sigma E_U$ if it is important to do so. In the average run of this program a set of possible X_i available for entry into the equation reached 100,000 to 300,000.

4.1.2.1 The Program

The program, based upon a set of parameter cards, established the set of possible terms for inclusion in the equation. These terms, in general, included functions of any one of the nine predictor variables, such as S, S^{-1}, S^2, S^{-2}, $S^{\frac{1}{2}}$, $S^{-\frac{1}{2}}$, S^3, S^{-3}, $S^{1/3}$, and log S, (58, pp. 71-72) where log S is entered as a special function. Moreover, it was requested in some cases to generate X_i's with interactions of order one, two, and three, which are respectively, for example, S^2, $S^{\frac{1}{2}} T^{1/3}$, and $S_P^{-\frac{1}{2}} T^{-3} \Sigma E_U^2$.

Once the program has determined the set of possible terms an equal probability of selection is associated with each term. Then a random selector is asked to pick, in this case, 55 X_i's as a subset on which to complete one pass and a specified number of random passes at the solution of the problem. Next the simple correlation coefficients of each function in the subset to the dependent variable is calculated. The X_i with the largest absolute value of this coefficient is selected for use in the equation. Here call it X_7. This is tested by means of an F test for an insertion error. If the term is significant enough to pass this test, the computer generates the first predicting equation.

$$N = b_0 + b_7 X_7$$

where b_0 and b_7 are the least squares estimates of the intercept and the slope.

The subset of X_i's is now divided into two sets $X_{i,1}$ and $X_{i,2}$ which are respectively, those functions in the predicting equation and those not in the equation. An importance factor (58, p. 80, footnote) is computed for each variable in $X_{i,1}$. The $X_{i,1}$ with the smallest of these factors is tested by an F test to determine whether it is less important than the program user requires for retention in the equation. This X_i is then removed or retained on the basis of the probability of making a deletion error. This probability was previously set by the user. In this use of the program the probabilities of both an insertion and a deletion error were set at .05. In the case where $X_{i,1}$ has more than one term the process of testing terms for deletion from the equation is continued until one of the terms being tested is significant enough not to be deleted from the set of terms $X_{i,1}$. Then the $X_{i,2}$ set is examined. A potential importance factor (58, p. 81) is computed for each function in this set. The term with the largest potential importance factor is isolated; call this term X_2 . Then X_2 is tested for its significance of insertion into the equation. If it passes, it is entered into the equation. Now, if X_7 was not removed, the equation becomes

$$N = b_0' + b_7' X_7 + b_2 X_2.$$

The primes indicate a modification of the coefficients upon generation of a least squares regression through the two variables. The functions are again sorted and checked as above. This process continues either until all the functions are entered into the equation or until there are no more terms of sufficient importance to insert into the equation (58, pp. 76-84).

In addition to generating the desired equation the computer prints out various statistics. The most interesting ones are the multiple correlation coefficient which is approximately the adjusted multiple correlation coefficient, R, of the MCA program and the coefficient of determination which is analogous to the multiple coefficient of determination, R^2 , in the MCA program.

4.1.2.2 The Results

Table 4.2 presents the best of the many equations generated by the regression program. The exception is equation 1.

TABLE 4.2

REGRESSION RESULTS
(See Appendix II for Units on Variables)

Eq. No.	Equation	Coef. of Det.	Mult. Corr. Coef.	Remarks
1	$N = 532{,}259 + .533\ S^{-2}$	.1620	.4020	Interaction = 1.
2	$\text{Log } N = 5.8488 - .4947\ S_P$	.7000	.8360	Interaction = 1.
3	$\text{Log } N = 5.453 - .131\ S_P^2$	.6995	.8360	Interaction = 1.
4	$\text{Log } N = 6.618 - .4977\ S_P - 4.377\times10^5\ T^{-3}$	.7096	.8424	Interaction = 1.
5	$\text{Log } N = -2.756 - 1.06\ S_P^{\frac{1}{2}} - 2.47\times10^7\ S^{-3} + 10{,}246\ S^{-1} + 1.7\times10^{-4}\ T^2$	.7105	.8430	Interaction = 1.
6	$\text{Log } N = 50.5 - 1.002\times10^6 S^{-3} - 1.739\times10^5 T^{-2} - 2.89\times10^{-5} T^3 - 2.80\times10^{-6} S^3 - 1.16 \log S_P$	.7215	.8494	Interaction = 1.
7	$\text{Log } N = 5.892 - .498\ S - 17.67\ \Sigma E_L \Sigma E_U{}^{-2}{}_{RMS}{}^{\frac{1}{2}}$	.7100	.8429	Interaction = 3.
8	$\text{Log } N = 5.745 - .353\ S_P - 19.89\ \Sigma E_L \Sigma E_U{}^{-2}{}_{RMS}{}^{\frac{1}{2}} - 8.9\times10^{-6}\ H^2\ S_P^3$	.7370	.8588	Interaction = 3.
9	$\text{Log } N = 9.21 - .0477\ S$	.6550	.8100	I = 1. S forced in.
10	$\text{Log } N = 9.53 - .0511\ S$	.6820	.8250	I = 1. S forced in. All 75ksi out.
11	$\text{Log } N = 5.91 - .5197\ S_P$	.7170	.8469	I = 1;S forced in then rejected. All 75ksi out.

Equation 1 is shown to indicate the ability of the program to predict using the numerical life data (additive model). Note the low value of the coefficient of determination in this equation.

Conversion to the multiplicative model resulted in equations 2 to 11. In equations 2 to 6 the computer was allowed to try to find the best regression line through the data with a maximum interaction of order one. Later, interactions of order one, two, or three were allowed. One sees that equation 2 gives a coefficient of determination of 70% while equations 3 through 8 indicate a futile attempt at increasing the predictive power of the equation. An increase of only 3.7% is attained by allowing interactions up to order three. Equation 8 was produced by a set of 124,600 possible functions for use in the equation. It is thought that the interaction terms, such as $\Sigma E_L \Sigma E_U^{-2} RMS$ in equation 8, are the result of strange data patterns and are valid only for this data set. If the insertion error probability is high enough and long enough time is allowed, this type of learning regression will try to fit functions through all the data points. However, this would only be valid for prediction in this particular set of data. For this reason, it is thought that either equation 2 or 11 is the best predictor.

Since the computer refused to pick up S as a predictor, it was forced into equation 9. Note that the coefficient of determination is about 4.5% lower than Sp. Recalling the curve deviation of S vs. $\log N - \overline{\log N}$ in Figure 4.2, the offending data points at 75,000 psi were removed from the regression data and S was again forced in the regression equation. An increase of 1.7% in the coefficient of determination results (Equation 10). Subsequently, the computer removed S and entered S_p resulting in equation 11.

5.1 DISCUSSION: ACOUSTIC EMISSION

As a result of the extensive testing carried out during this experiment, time and specimens were available in order to check several of the previously observed acoustic phenomena. During these investigations a number of new and different observations were made. The following sections recount these observations and show their place in the overall acoustic emission picture.

5.1.1 Repeatability: The Kaiser Effect

The previously explained Kaiser effect was checked during this research. Figure 5.1 shows the results of this work. The expanded scale for the emission provides better detail of the load and the Δ S character, but results in a suppression of the totalized emission to a zero level by the digital-to-analogue converter. This results in the sweeping effect in the plot. To obtain a real understanding of the emission occurring on unload, imagine each portion of the restarted curve shifted into position at the beginning of the sweep. This will give a curve similar in nature to that shown in Figure 3.3.

During the first load there is a type I emission curve for the loading bursts. Here, most of the burst emissions appear within the first

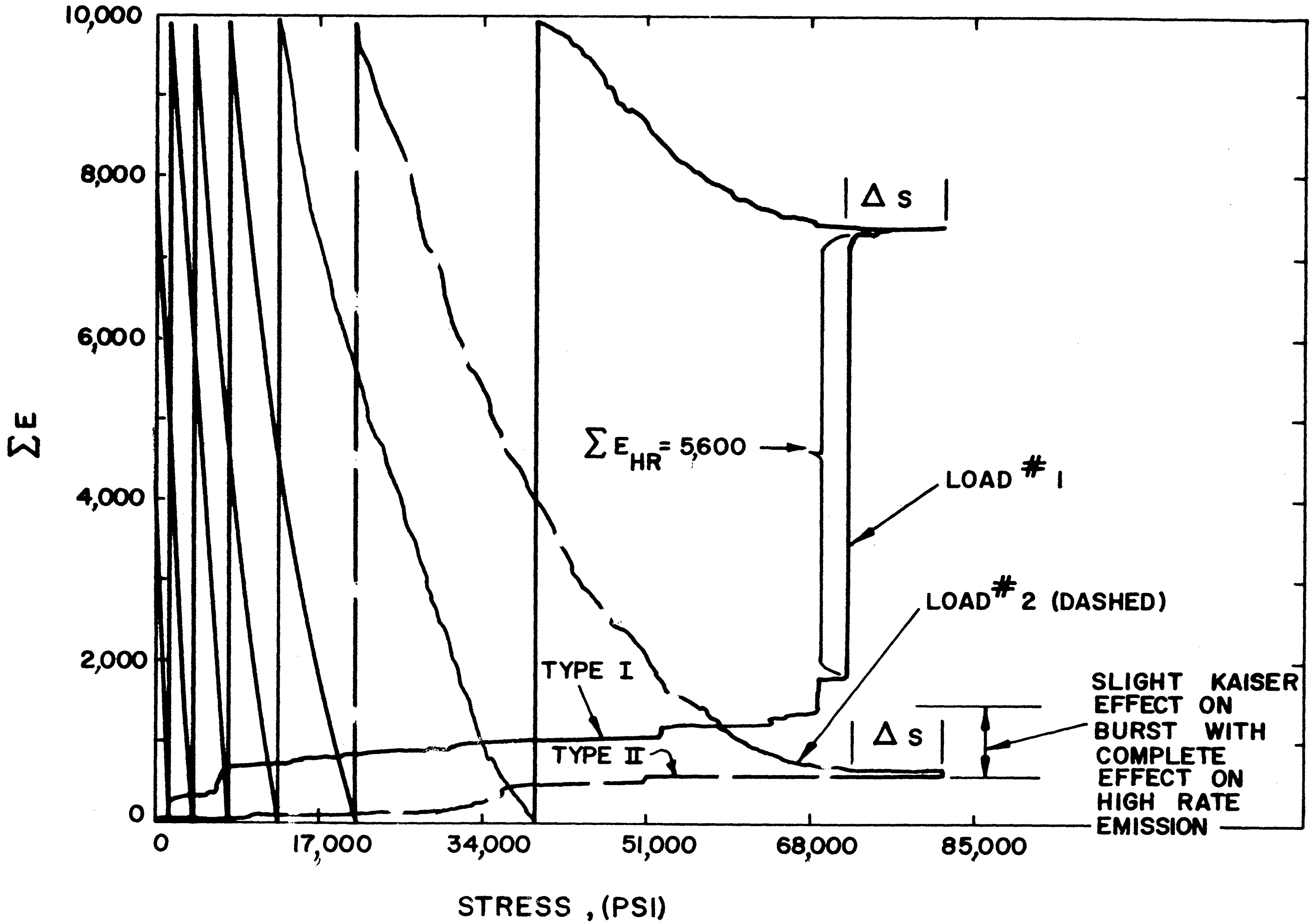

Figure 5.1. Expanded Emission Curve.
(Specimen 137-611-3-410)

17,000 psi. The remaining portion of the curve is standard in nature with $\Sigma E_L = 1,803$, $\Sigma E_{HR} = 5,600$, and $\Sigma E_U = 31,892$. It is of interest to note that the character of the burst type emission curve obtained during the observation of the increasing load changes when a second, immediately following, increasing load is applied.

The second type of curve is termed the type II emission curve for the load bursts. The type II curve has the highest emission rate near 34,000 psi. This shift in type was observed in all specimens that were checked. Other facts concerning the type change will be discussed later.

During the second load $\Sigma E_L = 589$, $\Sigma E_{HR} = 0$, and $\Sigma E_U = 34,880$. Note that a Kaiser effect is observed in the ΣE_{HR}. However, the ΣE_L did not experience a complete Kaiser effect. Tests on other specimens showed similar but variable reductions in ΣE_L. The ΣE_U in this case was shown to grow during the second stressing by about 10%. Therefore, no Kaiser effect is seen.

It is interesting to note that for this material with the limited yield point extension the technique of determining the stress level to which the material was previously stressed (see section 1.3.1) cannot be used effectively. This is true because the only emission affected markedly by the Kaiser effect is in the small stress range of the upper-lower yield point.

5.1.2 Unload Emission Response

Figures 5.2 and 5.3 show a method of analyzing unload emission data. This technique was suggested by Kerawalla (60). This method has been used to determine the fatigue limit on a number of materials. In this case it was used to obtain an insight into the ability of ΣE_U to predict fatigue life. An understanding of the reason for using this technique can be obtained from the following discussion of the procedure for obtaining and compiling the unload emission data.

A maximum stress to which the specimen is to be loaded, S^*_{max}, (see Figure 5.2) is first selected. This stress must be somewhere above the expected fatigue limit. Then a single load-unload cycle is completed The response to such a cycle is shown in Figure 5.2. The scales for the load and unload emissions are different. The specimen is reloaded to this same stress, S^*_{max}, several times. Notice, as shown in Figure 5.3, that the ΣE_U increases on each successive loading. The increase in ΣE_U diminished with each successive applied cycle. This process is termed saturation. It is thought that the mechanism which produces the unload emission is sensitive to stress and the sources of such emissions can be multiplied by high applied stress. Thus the unload emission grows after the application of a high stress. This also shows that only certain amounts of growth can be generated in this mechanism at a given S^*_{max}. The multiplication of the mechanism is said to have begun to saturate.

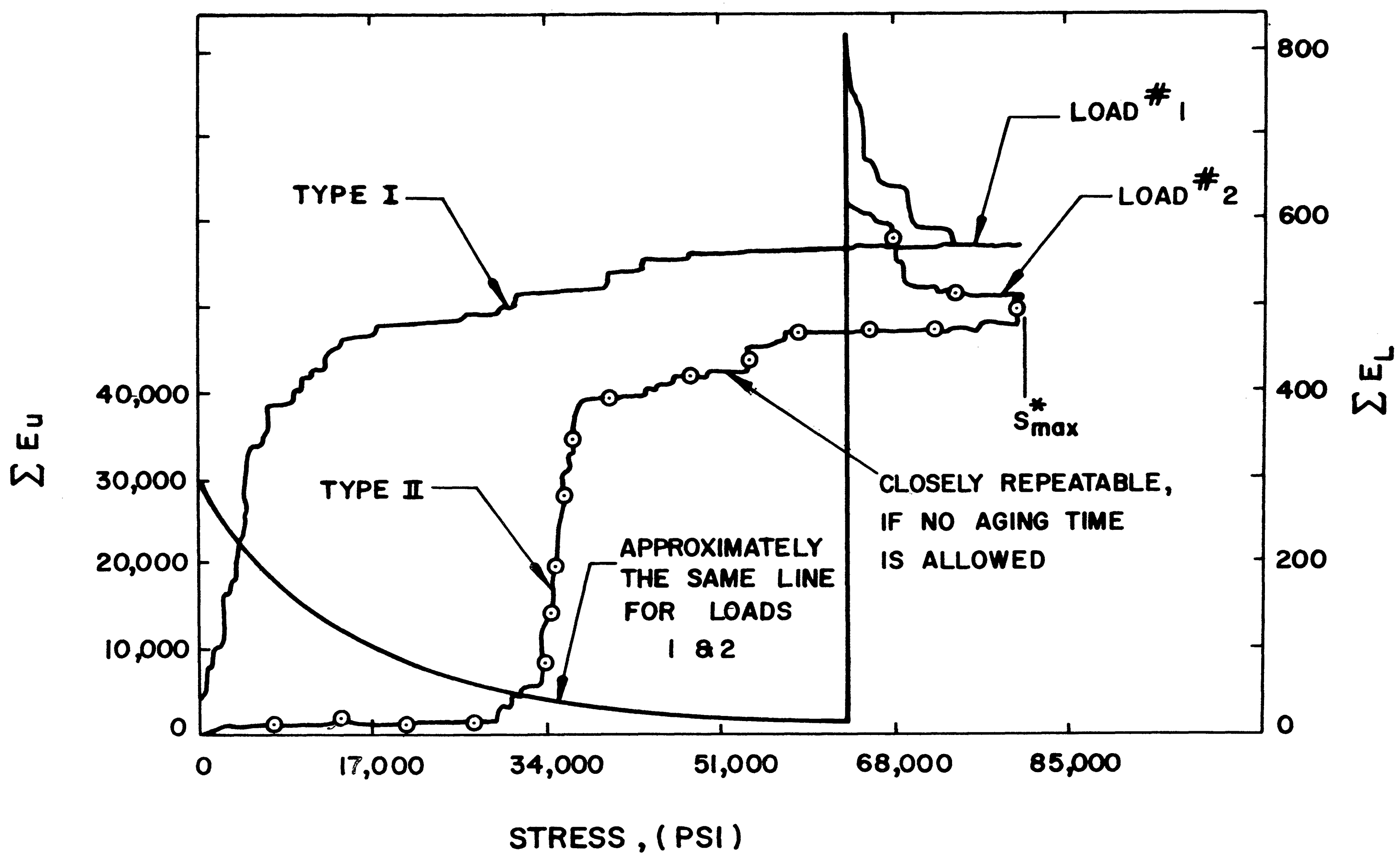

Figure 5.2. Unload Emission Response.
Note Scales--Load expanded one hundred times the unload scale.
(Specimen 62-019-3-014, previously loaded)

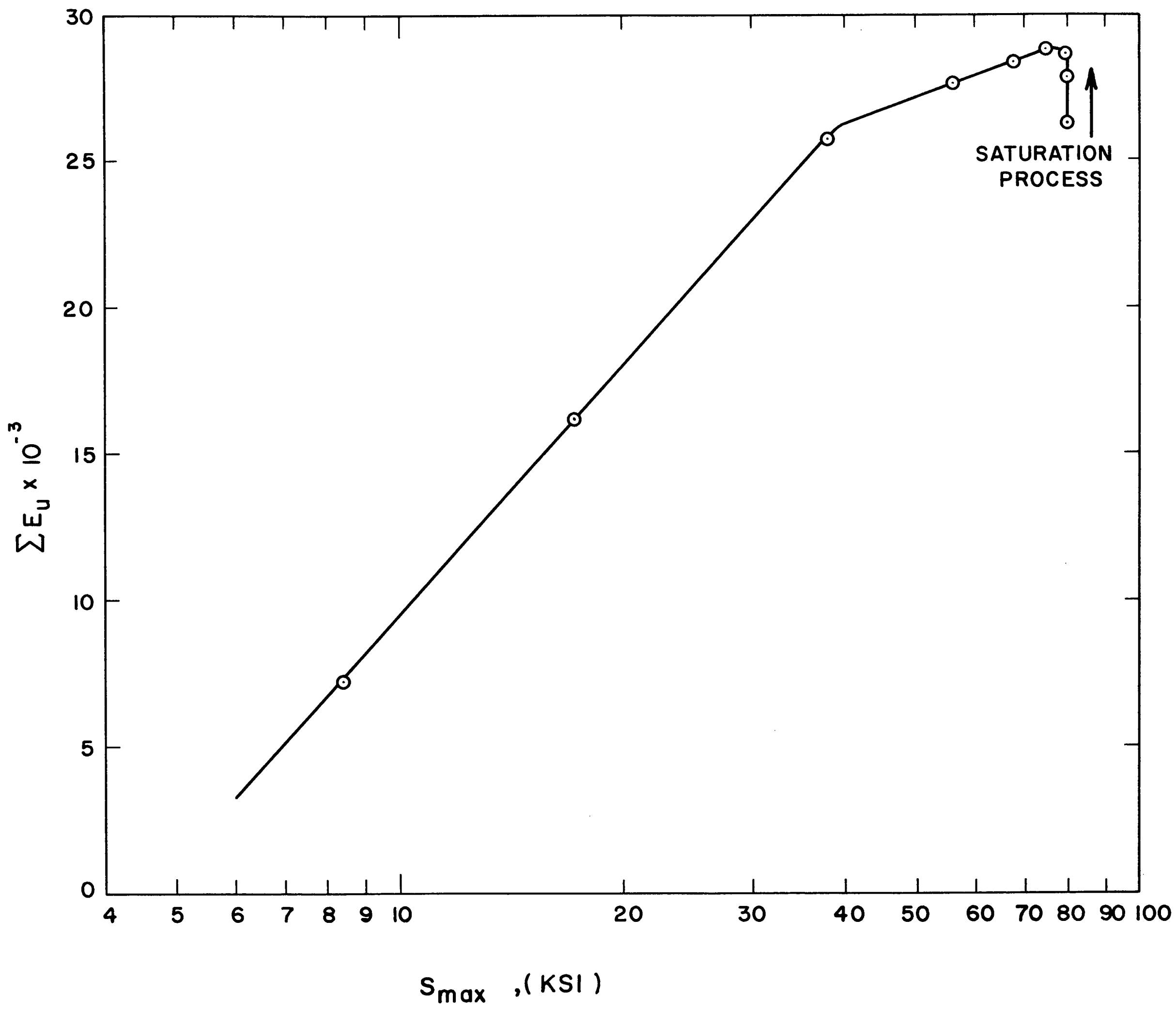

Figure 5.3. Unload Emission Curve.
(Specimen 62-019-3-014)
[Plotting Method Due to Kerawalla (60)]

Following the saturation process the maximum stress, S_{max}, in each successive cycle is lowered until the applied stress approaches zero. Then the results are plotted on a semi-logarithmic graph as ΣE_U vs. S_{max} in Figure 5.3. One notes that the curve is rather straight in the stress range below S_{yu} = 72,000 psi. The curve actually flattens out above 75,000 psi. After this point the emission has a slight downward trend. It appears that these emissions are intimately connected with the elastic behavior of the specimen and that when the upper elastic limit is exceeded the elastic effects are overcome and plastic effects, which are not heard, begin to dominate. It might also be noted that deviation from an actual straight line starts around 40,000 psi. Microstrain work might have indicated that this is the actual beginning of small plastic deformations in this particular specimen. Kerawalla (60) has found that the peaking or flattening of this curve is indicative of a fatigue limit. Figure 5.4 tends to support this view. This curve is the unload emission curve for a trial specimen which was subjected to a bending stress component which was 39.5% of the axial stress component. This was caused by an unnoticed machining burr in the nylon grip seat used on the acoustic test machine already mentioned in section 2.1.5.4. It can be seen that the unload mechanism peaked much sooner than in Figure 5.3. This indicated a lower fatigue limit than was expected. This was, in fact, another indicator of the bending problem discussed previously.

It is significant that, once again, the ΣE_U decreases slightly

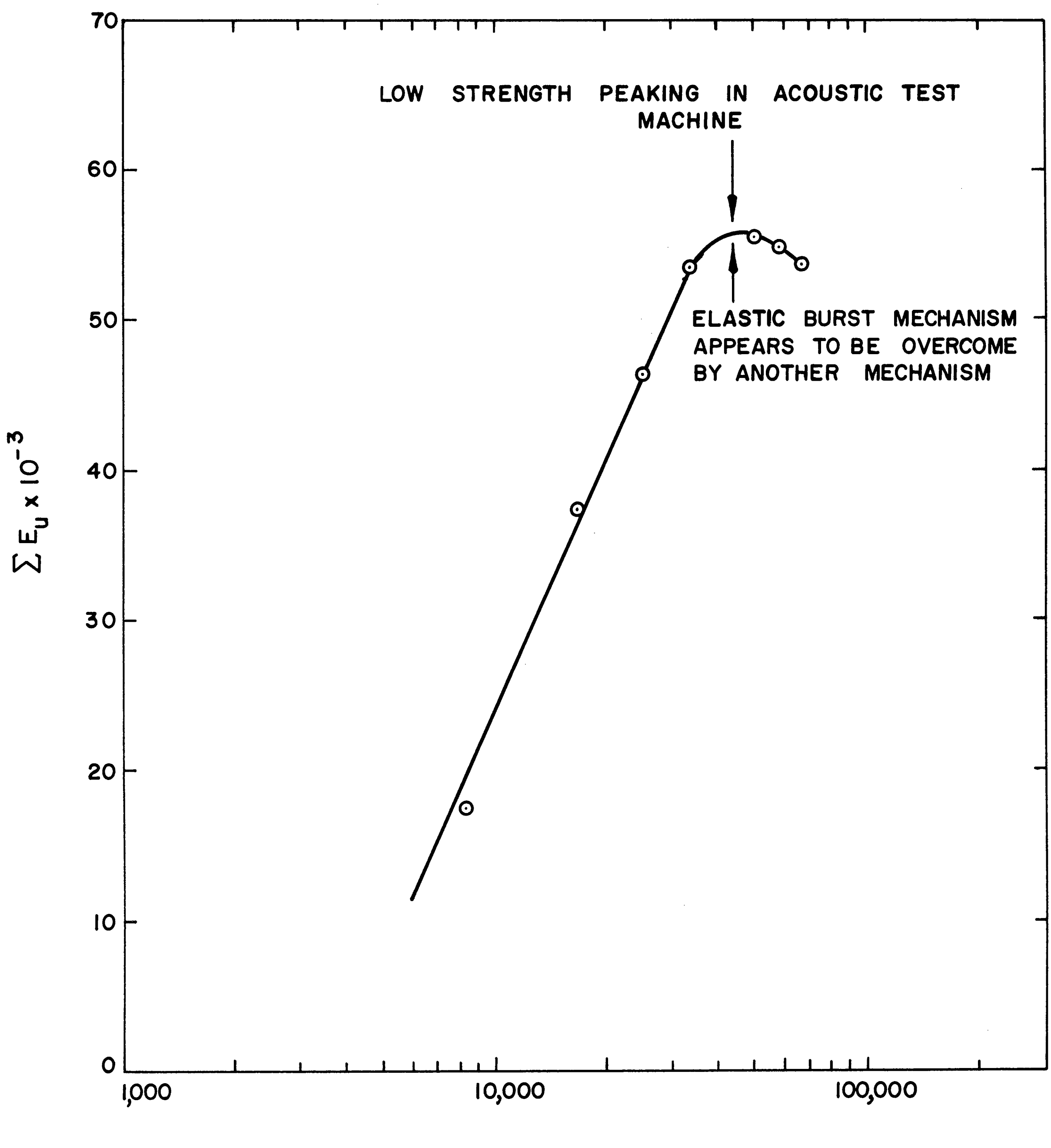

Figure 5.4. Unload Emission Curve with Specimen Bending. (Specimen TAE1-2 with 39.5% Bending)

after peaking. This would indicate that ΣE_U would not be a good predictor of life, since the emission appears to be measuring an elastic effect. The rolloff or decrease in emission seems to be due to the onset of a plastic mechanism which overcomes the elastic phenomenon present and becomes the dominant operative mechanism. It is desired to measure the magnitude of the activity of the plastic mechanisms within a specimen, if the fatigue life is to be predicted successfully. This is not being done.

It can be seen in Figure 5.2 that the unload and the load emissions have a high degree of repeatability. Repeatable behavior is not typical of a plastic deformation phenonenon. This repeatability in ΣE_U again suggests an elastic mechanism. The mechanism seems to form gradually with little or no noise on the load and seems to disappear during the unload with a release of energy. A analogous statement may be made with reference to the load emissions. However, not until the latter stages of the statistical analysis was there any reason to believe that the load and unload emissions were related. The details of the intercorrelation and the existence of same is discussed in section 7.1.4. At this time all that can be said is that after load emission type conversion the mechanisms causing the load and unload emissions are elastic in nature.

5.1.3 High Rate Emission

In the material used for this research the only high rate emission observable was that seen during the upper-lower yield point extension. The occurrence of this emission in only one stress region was not expected in view of the model proposed by Schofield, who suggested on the basis of his results that this type of emission was associated with repinning of dislocations and cross slip. If high rate emission is truly associated with such mechanisms, very large numbers of dislocations must be required to repin or cross slip in a unit time to generate sufficient noise to be detected. These types of mechanisms are surely operating during each cycle at the stresses used in this experiment. However, the second stressing of the specimen showed a disappearance of all the high rate emission. No small amounts of the high rate emission were seen on reloading. Therefore, the high rate emission reported here is an emission associated with a single plastic pheonomenon which is distinct from the plastic phenomena seen in fatigue.

5.2 CONCLUSIONS BASED UPON THE STATISTICALLY UNANALYZED ACOUSTIC EMISSION CHARACTER

In view of the discussion above the correlation previously expected is no longer promising.

First, the correlation of the load and unload emission characteristics with life is expected to be low and, if existent, to be weakly positive; i.e., increasing emission would bring an increasing life. This conclusion is based upon the fact that the following observations support the hypothesis that an elastic mechanism is generating the burst emission; the linearity of the maximum stress, S_{max}, versus unload emission plots in the elastic portion of the stress-strain curve, the non-linearity in the plastic stress region of the same curves, the repeatability of the load and unload emissions, the peaking of the unload emission curve at the fatigue limit above which plastic deformations ultimately cause failure, and the saturation process that occurs in the observed unload emissions at stresses above those which produce the peaking in the unload emission curve. Since this technique is apparently not measuring the localized irreversible plastic deformations and/or cross slip, one would then expect the correlation to be low. The slight positive correlation might be expected since a larger amount of burst emission seems to indicate a more extensive operation of an elastic mechanism. More elastic mechanisms may tend to raise the fatigue life.

The second type of emission, high rate, can be associated with the upper-lower yield extension. It, therefore, is associated with one type of plastic deformation. However, the plastic deformation at the yield extension does not necessarily bear any relationship to the plastic deformations that occur during each cycle of the fatigue process. Moreover, the Kaiser effect is seen in the high rate emission indicating that no sufficiently large plastic phenomena are operating so as to be heard during each load cycle beyond the first load cycle. The damage accumulated during each fatigue load cycle apparently cannot be heard by means of the high rate type emission. Therefore, it is expected that there will be little correlation of ΣE_{HR} to life, N.

6.1 DISCUSSION: STATISTICAL RESULTS

The results of the MCA program confirmed the conclusions made in section 5.2. The results of the program set the order of importance of the predictors as S_P, P, T, B, $\Sigma\ E_{HR}$, TIR, $\Sigma\ E_U$, $\Sigma\ E_L$, RMS, and H with S_P being the best predictor.

Reference to Figure 4.4 shows, in both the unadjusted and adjusted plots of $\Sigma\ E_{HR}$'s effect on log N, a scatter about zero with an importance coefficient of 3.6%. Additional confirmation of the ineffectiveness of the emission for prediction is reflected in the fact that the computer never during the running of the regression program picked up any emission term or function of such terms with interaction of order one.

Figure 4.5 shows a similar scatter around zero for the effect of $\Sigma\ E_U$ on log N but a much lower $\beta^2 = .02$ exists. No correlation is thought to exist between $\Sigma\ E_U$ and log N.

Also pointed out by the MCA statistical approach is the fact that surface finish has, within the range from 90 to 350 μ in. RMS for this material, little correlation to fatigue life. References to several textbooks (8, Figure 9.79) (4, Figure 57) (1, Figure 50) indicate that the so-called surface effect in fatigue is generally correlated in the form of finishes generated by different machining processes. The extremely low correlation found here would indicate that either large surface finish differences are necessary to affect the life or that it is not the surface shape that is important but mainly the amount and type of residual stresses produced in the surface by the machining process.

Also interesting is the fact that the humidity which was controlled by using a mineral oil coat has very little effect on the fatigue life in that it is the last in the ordered list of importance as generated by the MCA program.

Turning now to the regression program, the similarity of the hand fit equation in Figure 4.2 to equation 2 in Table 4.2 is good, being $\log N = 5.75 - .45\ S_P$ and $\log N = 5.8488 - .4947\ S_P$, respectively.

In order to obtain an idea of the scatter existing about this predictive regression equation, the regression program provides the standard error of the slope in the predictive equation and the standard error of log N about the fitted regression line. Using these statistics and others one can calculate the 95% confidence interval for the average value of log N, given S_P, and the 95% prediction interval for a future observation of log N, given S_P. A discussion of these intervals, their meaning, and their calculations is given in Appendix IV. These calculated intervals are shown in Figure 6.1. Here, the MCA results and the hand fit line from Figure 4.1 are included for reference. By checking the regression program's prediction sheet one finds that five of the one hundred and forty-five data values actually fell outside of the 95% prediction interval. The expected value of the number of data points outside of the predictive interval is 7.25 specimens.

The emission characteristics were completely disregarded in the regression program by the computer in its search for the best predictors in the life equation. Moreover, the multiple coefficient of determination, R^2, in the MCA program matches well the coefficient of determination generated by the regression program. This is a very good indication

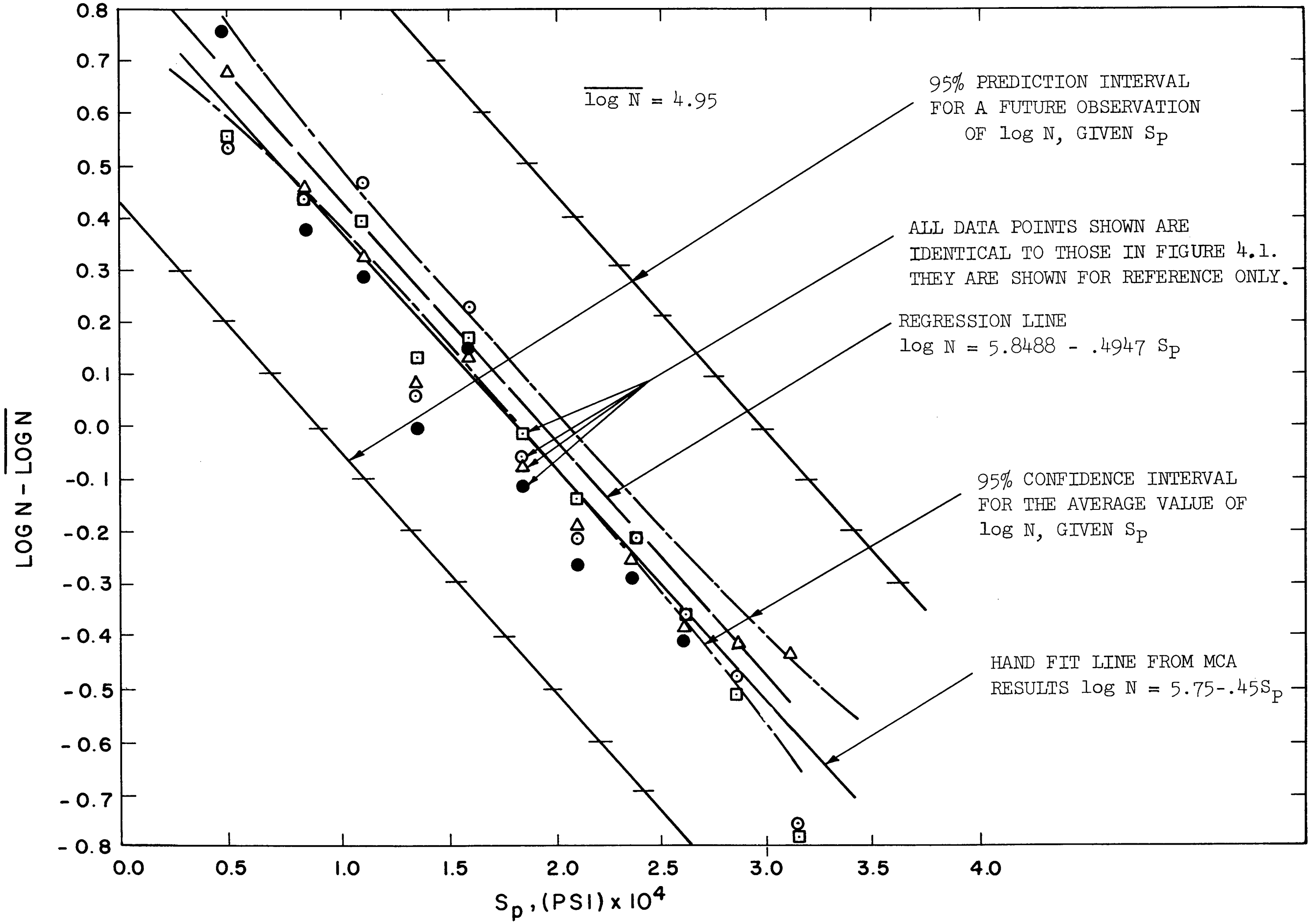

Figure 6.1. 95% Confidence Interval for the Average Value of Log N, Given S_p, and 95% Prediction Interval for a Future Observation of Log N, Given S_p.

that the best form of the equation has been found exclusive of interaction terms, which are not considered by the MCA program. It is enlightening to observe that predictive equation number 2 in Table 4.2 indicates a fatigue life close to 10^6 cycles when stressed at the upper-lower yield point. Published data on AISI 4340 indicate a fatigue limit at 10^6 cycles (4, pp. 304-305). Inspection of the data in Appendix II indicatesthe upper yield point rangesfrom about 69,000 to 75,000 psi. This correlates closely with the 75,000 psi seen at the peak in Figure 5.3 and other plots not presented here. Work done by Kerawalla (60) indicates this peak to be the fatigue limit. It appears that the upper-lower yield point is or is very close to the fatigue limit.

It seems significant that statistically the computer consistently chose to reject S and to use S_P . S_P is a very crude measure of the amount of plastic deformation caused by a given stressing cycle. This, of course, suggests that direct measurement of plastic deformation under typical applied fatigue stresses could provide better insight into the prediction of fatigue life. It may be that the variability in yield point and strain hardening coefficient from specimen to specimen could account for much of the variation in fatigue life.

6.2 CONCLUSIONS: STATISTICALLY BASED

The agreement of both the MCA and regression programs along with the agreement of the conclusions that were obtained from the acoustic character shows that no acoustic emission characteristic investigated here is highly correlated with the finite fatigue life of AISI E4340 cold drawn and annealed steel.

Moreover, it is concluded that the fatigue limit in tension-tension (zero to maximum load) fatigue is near the upper-lower yield point in the material.

7.1 ACOUSTIC EMISSION PHENOMENA THAT WERE NOT RELATED TO FATIGUE LIFE

During the execution of the planned experiment a number of points of interest appeared that may shed more light on the relationship between acoustic emission and fatigue, hysteresis, lattice friction, break-away stresses, and strain aging effects.

7.1.1 The Appearance of Low Frequency Emission

In the process of pulling the 220 specimens, four specimens emitted a continuous signal that had a frequency of about 250 cps. Figures 7.1 and 7.2 show two examples of the emission. Close examination of some of the RMS voltage output levels on the Visicorder traces indicates that about 20% of the specimens showed indications of such an emission, although the actual waveform was not observed. This type of emission appears symmetrically on both load and unload of these specimens and in the stress region extending from 4,000 to 20,000 psi. These emissions could be repeated upon restressing of the specimen. Specimens not showing this effect could be alternated in the test with those specimens that did show the effect. Consistently, this emission reappeared when specimens that had previously shown this phenomenon were retested. It is concluded

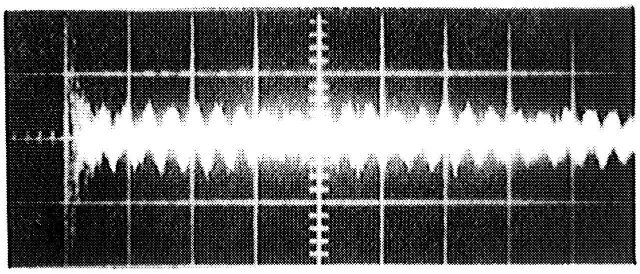

Figure 7.1. 250 Cycle Emission.
(Specimen 183-117-4-034 during unload)
Ordinate: 0.10 volts/cm
Abscissa: 10.0 msec/cm

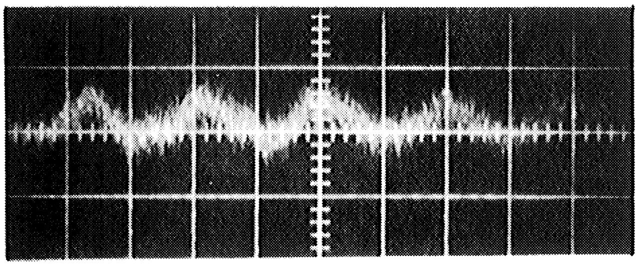

Figure 7.2. 265 Cycle Emission.
(Specimen 183-117-4-034 during unload)
Ordinate: 0.05 volts/cm
Abscissa: 2.0 msec/cm

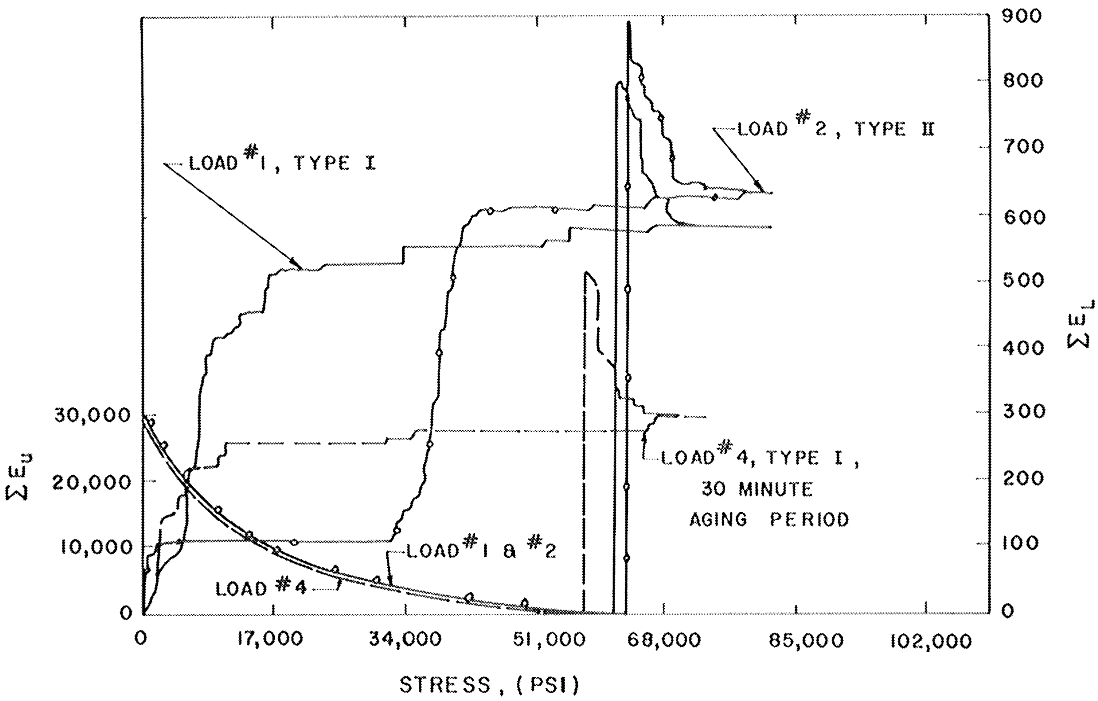

Figure 7.3. Type Conversion of Load Emission.
(Specimen 72-529-3-337)

that this is a real emission characteristic and is not related to any property of the testing machine. Lowering the Krohn-Hite high-pass filter action to its lower limit of 2 cps made this emission show up easily on the Visicorder trace of the RMS voltage output of the system.

In 1960 Fitzgerald (61, p. 1289) speculated during the reporting of his work regarding shear compliance in materials that it might be possible to generate self-excited sustained oscillations while loading a piece of material. It is possible that this is what is being heard in these 250 cycle emissions.

In order to investigate this emission one would have to obtain better acoustic and structural isolation at the low frequencies or to study the phenomenon with the aid of a lock-in type amplifier. The removal of the filter necessitates the suppression of the low cycle ambient noise.

7.1.2 The Effect of Strain Aging on Emission

Referring to Figures 5.1 and 5.2, one sees a conversion of the load emission curve from type I to type II (previously defined). In the process of running an acoustic test the first load curves are of type I, but the curves resulting from successive loadings are of type II character. However, if the specimen is allowed to age for a half of an hour and then is restressed, one finds a reversion to a type I pattern of load emission. This phenomenon is shown in Figure 7.3. This figure is the X-Y recorder output. This experiment shows that the acoustic emission technique could measure strain aging effects.

This discovery suggested further possible experiments concerning the aging effect on the unload emission. This will be reported by Kerawalla (60).

7.1.3 Stress Delay and Its Relation to the Maximum Stress

As more and more experience was gained with the various emission phenomena, it became more evident that the unload burst originated from some sort of elastic rather than plastic mechanism.

However, the activation of the mechanism seems to be inhibited by some sort of internal stress as indicated by the stress delay, ΔS, shown in Figure 3.3. It was thought that it would be of interest to observe what would happen to ΔS as the maximum stress, S_{max}, is changed. The results shown in Figure 7.4 are the results of multiple level stressing on twenty-five specimens. The positive correlation of these two variables indicates that the elastic mechanism encounters larger and larger internal friction stresses with increasing values of S_{max}. This is evident since more stress relaxation is necessary at the higher stress levels in order to allow the elastic mechanism to become abruptly unpinned and return to a near zero deformation state. Burst acoustic emissions result from energy dissipation during the collapse of the mechanism.

7.1.4 Correlation Among the Types of Emissions

In the process of running the regression program several tables of simple correlation coefficients were generated. In Table 7.1, entries

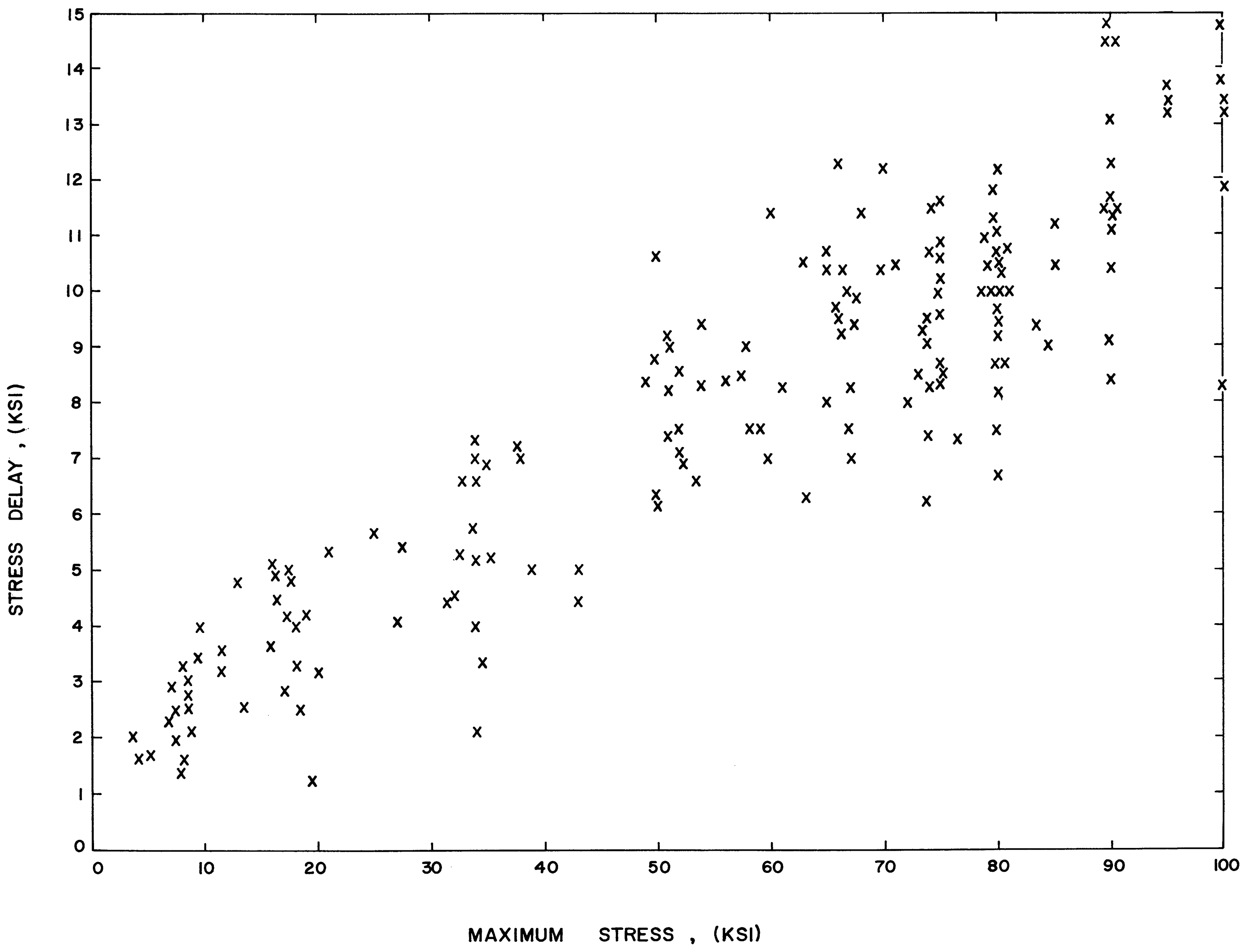

Figure 7.4. Stress Delay vs. Maximum Stress.

TABLE 7.1

SIMPLE CORRELATION COEFFICIENTS

Entry No.	Function One	VS. Function Two	Simple Corr. Coefficient	Remarks
1	$\Sigma E_U{}^{+3}$	$\Sigma E_{HR}{}^{+3}$	+ .499	---
2	$\Sigma E_U{}^{-1}$	$\Sigma E_L{}^{-\frac{1}{2}}$	+ .430	---
3	$\Sigma E_L{}^{-3}$	$\Sigma E_{HR}{}^{-1}$	+ .934	---
4	Log ΣE_{HR}	ΣE_L	+ .291	Forced in
5	Log ΣE_{HR}	ΣE_U	+ .474	" "
6	ΣE_L	ΣE_U	+ .345	" "
7	ΣE_L	ΣE_{HR}	+ .263	" "
8	ΣE_U	ΣE_{HR}	+ .512	" "
9	Log S	Log N	- .804	" "
10	S	Log N	- .809	" "
11	Log S_P	Log N	- .787	" "
12	S_P	Log N	- .837	" "

1, 2, and 3 give a summary of the coefficients which were unexpectedly large. Note that in trying to check the sign of such correlations one may find sign inconsistentencies. This is normal for simple correlation coefficients. If it is necessary to resolve any sign problem, one must obtain partial correlation coefficients and then make the necessary comparisons.

Since the simple correlation coefficients are high among the different types of emission and since numerically ΣE_L^{-3} can reach 10^{-9} , it appeared that the calculation of these coefficients could be grossly misleading. Subsequent, forced pickup instead of a random selection resulting in entries 4 - 12. The correlation is now moderate. These coefficients are high enough to have some reason to believe there might be some physical relationship between them, especially between ΣE_L and ΣE_{HR}.

As a result a special series of MCA programs was run. It must be kept in mind that these runs were made with classified variables as the dependent variables. This will probably affect the accuracy of the results to some extent. Referring to Figures 7.5 and 7.6, one sees that there appears to be a positive, linear relationship between ΣE_U and ΣE_{HR}. A less distinct and weaker correlation appears to exist between ΣE_U and ΣE_L. There is now some reason to believe that all these emission characteristics are interconnected. However, this interconnection may be via another phenomenon that tends to affect all the emissions.

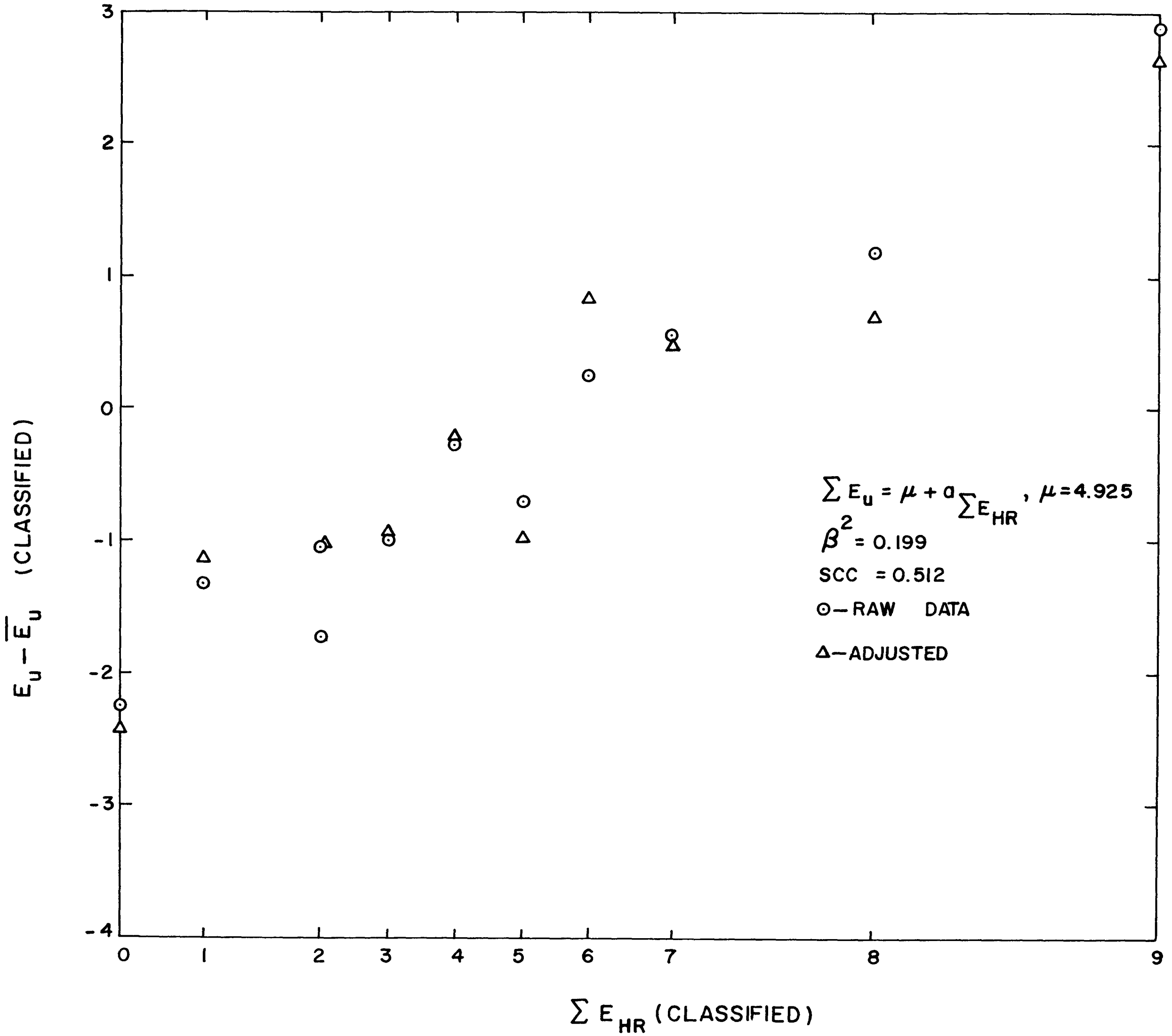

Figure 7.5. Totalized Unload Emission Correlated with Totalized High Rate Emission from Classified Multiple Classification Analysis Results.

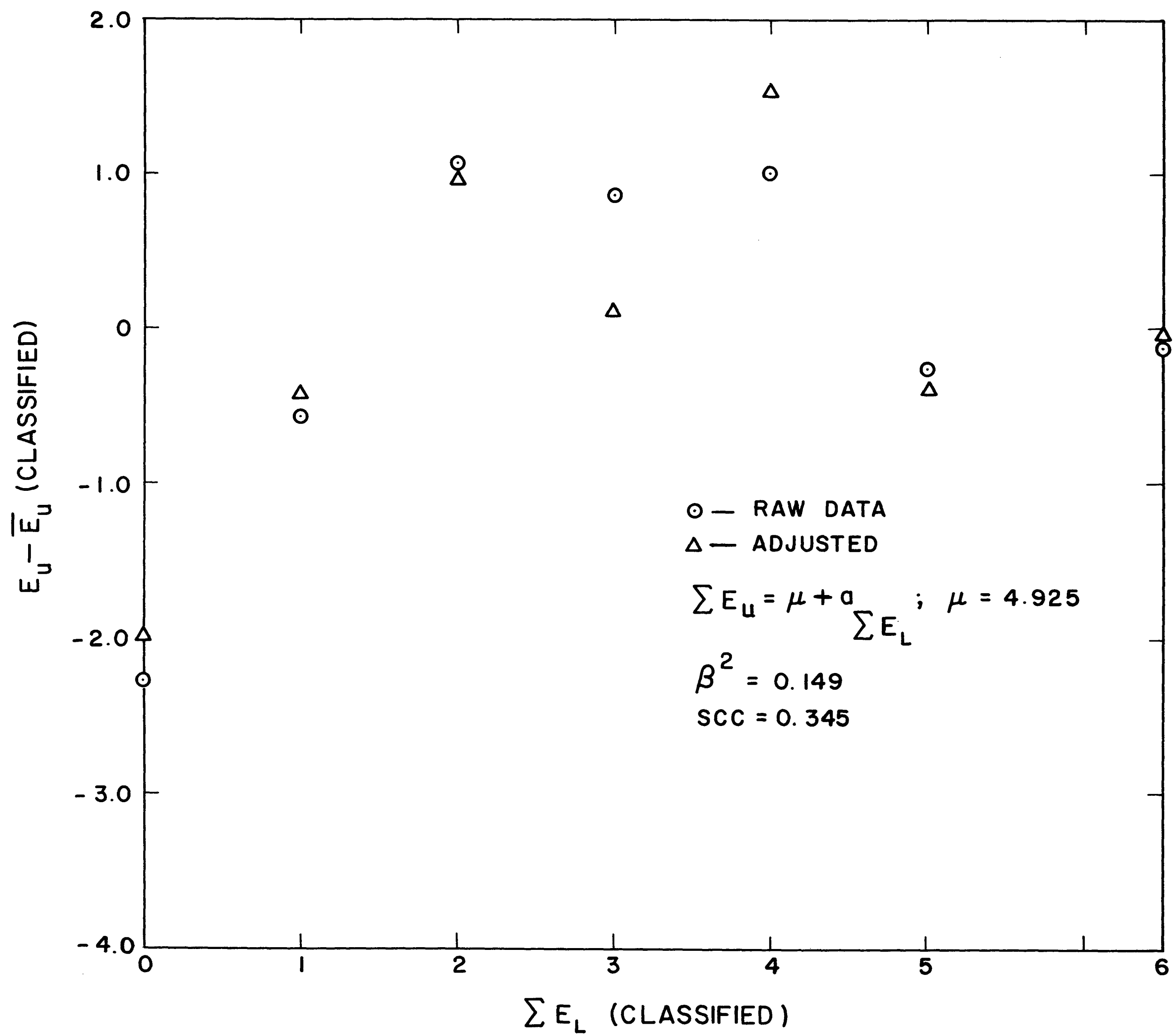

Figure 7.6. Totalized Unload Emission Correlated with Totalized Load Emission from Classified Multiple Classification Analysis Results.

7.1.5 Emissions from Nylon

During the debugging of the acoustic equipment it was decided to determine the emission generated by a specimen made from Zytel a molded nylon polymer. The emission was entirely burst type. Another way in which this polymer is different from AISI E4340 steel is that there is no stress delay, Δ S. The observed emission levels are lower in this plastic than in steel, both in intensity and in number. W. Statton of duPont (62) has indicated that emissions were not entirely unexpected in polymers since polymers, as well as metals, are thought to have dislocations within their structure (63) (64) (65) (66).

8.1 FUTURE RESEARCH

In the process of carrying out this research it was possible to see avenues of research that might lead to significant and worthwhile results.

Some projects that appear to be particularly worthy of more research effort are listed below.

1. Study the change in the burst emission character during loads below the yield point. In particular investigate the character change from type I to type II as shown in Figures 5.1 and 5.2 in order to learn more about the strain aging mechanisms and the magnitude of the breakaway stresses.

2. Study the stress delay phenomenon in metals and its relation to lattice friction. Also, investigate the lack of a stress delay in polymers. Determine if the stress delay will appear by the use of polymer alloying techniques.

3. Conduct a series of studies concerning the correlation between the microstrain hysteresis loop and the unload emissions. These tests should be performed simultaneously on the same specimen.

4. Conduct a study of the correlation between residual plastic microstrain and fatigue life.

5. Study the effect of grain size on the emission characteristic and try to utilize the Petch equation (6, p. 199) to determine what emission character can be associated with locking stresses and what can be associated with friction stresses.

6. Study more completely the effect of strain aging on the unload emission character. This could possibly be an important tool for sensitive determination of strain aging.

7. Study the yield point variation simultaneously with the strain hardening coefficient for each specimen as a predictor of fatigue life.

8. Investigate more thoroughly the low frequency emission phenomenon. Removing the filter from the instrumentation will allow ambient noise from the electrical lines and from the structure-borne vibrations to register on the electronic counter and, hence, render it useless. However, the low frequency emission at about 250 cps will appear in the Visicorder record of the total noise that is being measured. This might be examined as a possible indication of the stress induced, self-sustained oscillations proposed by Fitzgerald (61, p. 1289).

APPENDICES

APPENDIX I

MATERIAL PROCESSING HISTORY AND CERTIFICATION SHEETS (41) (42)

Detailed processing information on AISI E4340 grade, aircraft quality, cold finished, annealed, 1-1/8" round bars from Republic Steel's Heat 3321345.

Melting Process - 70 Ton Electric Arc Furnace, Ladle Vacuum Degassed.

Mold Size & Ingot Weight - 25" x 27" Big end up, hot topped, 12,000 lb. ingot.

Billet Size - 4" x 4".

Hot Rolled Bar Size - 1-5/32" rd. Bar Stock-

1. Pickle.
2. *Anneal in bundles in a surface combustion batch-type car furnace using W-shaped radiant heating tubes fired with natural gas. Atmosphere controlled under NX (dry nitrogen gas).

   Annealing Cycle:

   Heat to 1550° F. - Soak 4 hrs.

   Cool 50°/hr. to 1370° F.

   Cool 20°/hr. to 1200° F. - Soak 4 hrs. at 1200° F.

   Cool to 1000° F. and pull.

---

* Furnaces aligned along a North-South axis. Furnace temperature controlled with Chromel-alumel thermocouples and Leeds & Northrup Micromax control instruments.

3. Light pickle.
4. Lime coat
5. Cold draw to 1-1/8" rd. (1/32" draft).
6. Medart machine straighten.
7. Cracker cut to length.
8. *Subcritical anneal (1150° F.) through 30 ft., continous, open fired furnace in approximately three layers at travel rate of 15'/hr.
9. Light pickle.
10. Lime coat.
11. Restraighten (Medart straightener).

Aircraft Quality Steel Cleanliness - Average magnetic particle inspection ratings of all billet tests from this heat, in accordance with AMS 2301B, were 0.09 Frequency and 0.07 Severity.

---

* Furnaces aligned along a North-South axis. Furnace temperature controlled with Chromel-alumel thermocouples and Leeds & Northrup Micromax control instruments.

Certificate of Analysis and Hardenability

A GUIDE TO MORE UNIFORM HEAT TREATMENT RESULTS

Your Order No. ____________ Type Steel Aircraft Quality 4340 Ann.

Date ____________ Color Marking White & Yellow-Black Dot

Heat Treating Information, Only for Bars With this Symbol
3321345

	C.	Mn.	P.	S.	Si.	Ni.	Cr.	Mo.	Va.	Pb.	Grain Size
Heat Analysis:	.425	.80	.012	.010	.33	1.79	.78	.25			7

Working Temperatures: Oil Quench 1475-1575 °F. Anneal 1450-1550 °F. Forge 2000-2250 °F. Norm. 1600-1700 °F.

END-QUENCH HARDENABILITY TEST RESULTS TO ASTM A-255

INSTRUCTIONS: Draw a line vertically through the part diameter and the curve. The intersection with the curve indicates the asquenched core hardness of the alloy with the above certified symbol, when oil quenched.

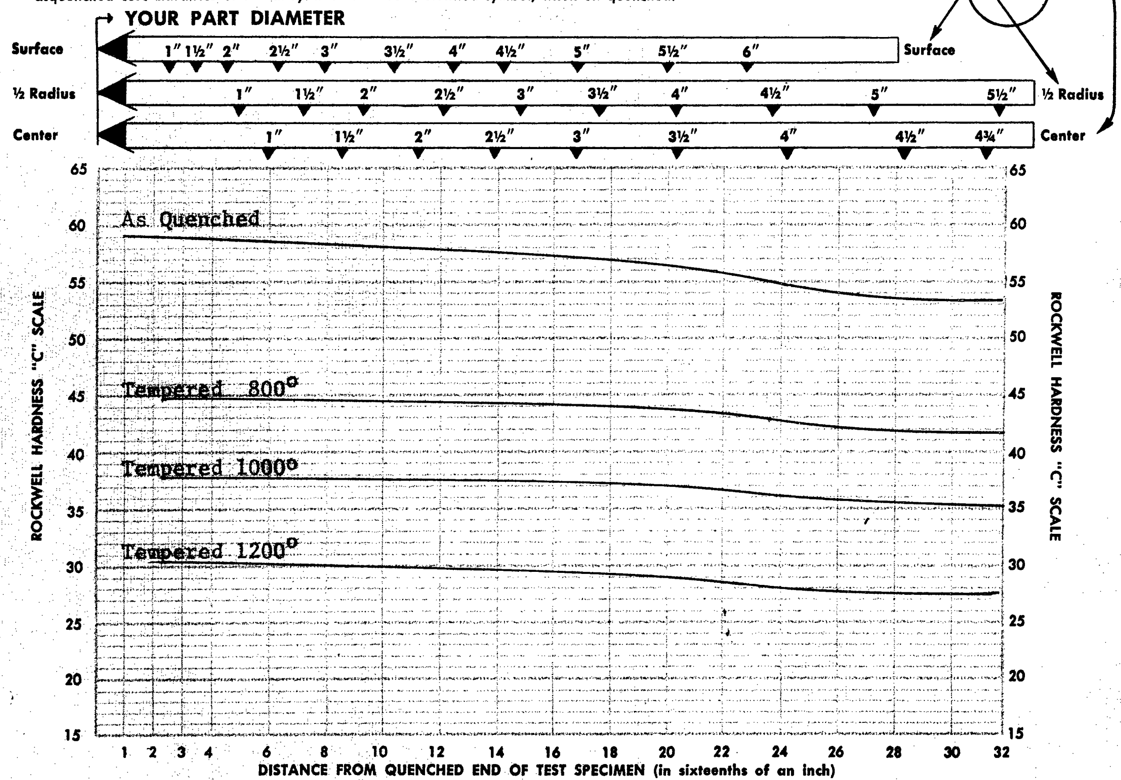

How Ryerson Tests:

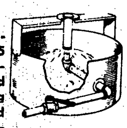

Each heat of alloy steel is tested in accordance with the Standard ASTM A-255 End-Quench Hardenability Test. Briefly—test samples after normalizing and machining, are heated to the quenching temperature. They are water quenched on one end only, until cold, in the fixture shown on the right. They are then ground to remove all decarburized surface. Rockwell "C" hardness readings are taken at regular intervals from the quenched end and are plotted into curves as shown. See other side for more data.

Mechanical Properties as Interpreted from End-Quench Tests

Quenched in Oil at 1550 °F., and tempered as shown.

Size of Round	Tempering Temperature	Tensile Strength P.S.I.	Yield Point P.S.I.	% Elong. (2 inches)	% Red. Area	Rock. "C" Hardness
1-inch, Center	800	208,000	200,000	11.5	43.7	45
	1000	174,000	163,000	15.5	51.5	38
	1200	142,000	128,000	19.1	59.0	30
4-inch, ½ Radius	800	204,000	194,000	12.0	45.2	44
	1000	170,000	159,000	16.0	52.3	37
	1200	136,000	119,000	20.0	60.6	28

NOTE: The chemical analysis reported was submitted by the mill. The ASTM A-255 end-quench results and mechanical interpretations were developed in the Ryerson laboratory. This data is believed accurate within normal testing limits, and is applicable only to material marked with the above symbol. Check your shipment to be sure it is stamped or tagged with the symbol on this certificate.

JOSEPH T. RYERSON & SON, INC. Plants: Chicago • Milwaukee • Indianapolis • St. Louis • Detroit • Cincinnati • Cleveland • Pittsburgh • Philadelphia Charlotte, N. C. • Buffalo • New York • Boston • Wallingford, Conn. • San Francisco • Los Angeles • Spokane • Seattle

Form 720 83-2 Feb. 58

RYERSON CERTIFIED TEST REPORT

UNIVERSITY OF MICHIGAN
PURCHASING OFFICE RESEARCH
ADMIN BLDG.
ANN ARBOR, MICH.
NORTH CAMPUS

DATE	RYERSON ORDER NUMBER	CUSTOMER'S ORDER NUMBER
9-15-64	1-865068	R51416

DESCRIPTION OF MATERIAL AND SPECIFICATIONS

8 BARS CF AQ E4340 ANNLD 1-1/8" RD x 11'11-3/4" to 12'

CHEMICAL ANALYSIS

HEAT NO.	CARBON	MANG.	PHOS.	SULPHUR	SILICON	NICKEL	CHROM.	MOLY.	COPPER	VA.	TI.	ALUM.	LEAD	OTHER
3321345	.425	.80	.012	.010	.33	1.79	.78	.25						

MECHANICAL PROPERTIES AND TESTS

TENSILE PSI	YIELD PSI	% ELONGATION	REDUCTION OF AREA %	HARDNESS	BEND	GRAIN	EMB.	HARDENABILITY	OTHER
				BHN 235-269		5-8		20/16 57 32/16 54	MACRO ETCHOK

MANUFACTURER

REPUBLIC

DECARB .020

DESCRIPTION OF MATERIAL AND SPECIFICATIONS

CHEMICAL ANALYSIS

HEAT NO.	CARBON	MANG.	PHOS.	SULPHUR	SILICON	NICKEL	CHROM.	MOLY.	COPPER	VA.	TI.	ALUM.	LEAD	OTHER

MECHANICAL PROPERTIES AND TESTS

TENSILE PSI	YIELD PSI	% ELONGATION	REDUCTION OF AREA %	HARDNESS	BEND	GRAIN	EMB.	HARDENABILITY	OTHER

MANUFACTURER

DESCRIPTION OF MATERIAL AND SPECIFICATIONS

CHEMICAL ANALYSIS

HEAT NO.	CARBON	MANG.	PHOS.	SULPHUR	SILICON	NICKEL	CHROM.	MOLY.	COPPER	VA.	TI.	ALUM.	LEAD	OTHER

MECHANICAL PROPERTIES AND TESTS

TENSILE PSI	YIELD PSI	% ELONGATION	REDUCTION OF AREA %	HARDNESS	BEND	GRAIN	EMB.	HARDENABILITY	OTHER

MANUFACTURER

THE ABOVE TESTS CONFORM TO THE REQUIREMENTS OF THE SPECIFICATIONS LISTED

THIS CERTIFICATE NOTARIZED ONLY WHEN REQUIRED

I,______________________________, a Notary Public do hereby certify that this affidavit was subscribed and sworn to before me by a duly authorized agent of Joseph T. Ryerson & Son, Inc., this_________day of_______________

MY COMMISSION EXPIRES

NOTARY PUBLIC

We hereby certify that the foregoing data is a true copy of the data furnished us by the producing mill or the data resulting from tests performed in the Ryerson Laboratory.

JOSEPH T. RYERSON & SON, INC.

BY [signature]
Authorized Agent

JOSEPH T. RYERSON & SON, INC

FORM 230-32-5 REV. 7-62 COPYRIGHT 1960
Joseph T. Ryerson & Son, Inc., Printed in U.S.A.

PLANTS AT: NEW YORK • WALLINGFORD, CONN. • BOSTON • BUFFALO • PHILADELPHIA • CHARLOTTE, N. C. • PITTSBURGH • CLEVELAND
CINCINNATI • DETROIT • MILWAUKEE • CHICAGO • ST. LOUIS • DALLAS • HOUSTON • INDIANAPOLIS • LOS ANGELES
SAN FRANCISCO • SEATTLE • SPOKANE

APPENDIX II

ACOUSTIC AND FATIGUE DATA

The tabulated data that follows is in two sections. The first is the single stress level data; the second, the dual stress level data. The first tabulation includes the actual data with the corresponding MCA classification. The second tabulation presents only the actual data and is presented here for a permanent record, but it is not used in the present investigation.

TABULATION LEGEND SECTION 1

Single Stress Level Fatigue Data

Units presented in the legend that follows will often be non-conventional. These were used because of scaling problems within the computer. All equations in the text use the same units to provide consistancy.

S = Stress; units: psi x 10^{+3}= ksi.

CS = Class of Stress: 102.5 - 97.5 = 0, 97.5 - 92.5 = 2 92.5 - 87.5 = 3, 87.5 - 82.5 = 4, 82.5 - 77.5 = 6, and 77.5 - 72.5 = 7.

ΣE_L = Totalized Load Emissions; units: counts x 10^{+3} = thousands of counts.

$C\Sigma E_L$= Class of ΣE_L; 0-0.500 = 0, 0.500-1.000-1.500 = 2, 1.500-2.000 = 3, 2.000-2.500 = 4, 2.500-3.000 = 5, 3.000 - 4.500 = 6.

ΣE_U = Totalized Unload Emissions; units: counts x 10^{+3}= Thousands of counts.

$C\Sigma E_U$ = Class of ΣE_U : 5-10 = 0, 10 - 15 = 1, 15-20 = 2, 20-25= 3, 25-30 = 4, 30-35 = 5, 35-40 = 6, 40-45 = 7, 45-50 = 8, 50-55 = 9, 55-80 = 10.

ΣE_{HR} = Totalized High Rate Emission; units: counts x 10^{+3} = Thousands of counts.

$C\Sigma E_{HR}$= Class of ΣE_{HR}: 0.0-0.5 = 0, 0.5-1.5 = 1, 1.5-2.0 = 2, 2.0 - 2.5 = 3, 2.5 - 3.0 = 4, 3.0 - 3.5 = 5, 3.5 - 4.0 = 6, 4.0 - 5.0 = 7, 5.0 - 7.0 = 8, 7.0 - 9.0 = 9.

TIR = Total indicator reading; units: 0.0001 in.

CTIR = Class of TIR: 0.0 - 1.5 = 0, 1.5 - 3.0 = 1, 3.0 - 5.0 = 2, 5.0 - 8.0 = 3, 8.0 - 11.0 = 4, 11.0 - 15.0 = 5, 15.0 - 30.0 = 6, 30.0 - 100.0 = 7.

RMS = Root Mean Square surface finish; units: μ inches x 10^2 = 10^{-4} inches RMS.

CRMS = Class of RMS: 0.8 - 1.1 = 0, 1.1 - 1.4 = 1, 1.4 - 1.7 = 2, 1.7 - 2.0 = 3, 2.0 - 2.5 = 4, 2.5 - 5.0 = 5.

T = Room Temperature; units: °F.

CT = Class of T: 78.0 - 80.5 = 0, 80.5 - 81.5 = 1, 81.5 - 82.5 = 2, 82.5 - 83.5 = 3, 83.5 - 84.5 = 4, 84.5 - 86.0 = 5, 86.0 - 87.5 = 6.

H = Room Humidity; units: grains of water per pound of dry air.

CH = Class of H: 10.0 - 20.0 = 0, 20.0 - 30.0 = 1, 30.0 - 40.0 = 2, 40.0 - 50.0 = 3, 50.0 - 60.0 = 4.

I = Incident factor: 0 = no happening,

1 = 1,200 RPM finish speed (normally 1,000 RPM),

2 = Tool chipped during facing cut,

3 = Misstressed,

4 = Hydraulic instability,

5 = Prestressed @ 75,000 psi before 100,000 psi,

6 = Radio interference,

7 = Dropped on floor,

8 = Preload lost,

9 = Stressing after original acoustic test,

10 = Gross yielding; acoustic machine does not reach stress,

11 = 5 and 7,

12 = 5 and 1,

13 = 4, 5, and 10,

14 = 1 and 9,

15 = 5 and 6,

16 = 4 and 5,

17 = 5 and 2,

18 = one cycle of overstress,

19 = Square wave generator inoperative,

20 = 39% bending stress.

S_P = Engineering stress above the upper-lower yield point; units: psi x 10^{+4} = tens of thousands of psi.

CS_P = Class of S_P : 0.00 - 0.25 = 0, 0.25 - 0.75 = 1, 0.75 - 1.00 = 3, 1.00 - 1.25 = 4, 1.25 - 1.50 = 5, 1.50 - 1.75 = 6, 1.75 - 2.00 = 7, 2.00 - 2.25 = 8, 2.25 - 2.50 = 9, 2.50 - 2.75 = 10, 2.75 - 3.00 = 11, 3.00 - 3.35 = 12.

B = Bar Number (see section 2.1.2.1): 0 - 6.

P = Position Number (see section 2.1.2.1): 0 - 29.

ΣE_T = Total totalized emission exclusive of the high rate emission; units: counts x 10^{+3} = thousands of counts.

$C\Sigma E_T$ = Class of ΣE_T : 5-10 = 0, 10 - 15 = 1, 15 - 20 = 2, 20 - 25 = 3, 25 - 30 = 4, 30 - 35 = 5, 35 - 40 = 6, 40 - 45 = 7, 45 - 50 = 8, 50 - 55 = 9, 55 - 80 = 10.

N = life; units: cycles.

ACOUSTIC AND FATIGUE DATA
SINGLE STRESS LEVEL

MCA Variable		x_1		x_2		x_3		x_4		x_5		x_6		x_7		x_8	x_9		x_{10}	x_{11}	x_{12}		x_{13}	Dependent
Regression Variable	x_1		x_2		x_3		x_4		x_5		x_6		x_7		x_8			x_9				x_{10}		Dependent
Sequence Number	S	CS	ΣE_L	C ΣE_L	ΣE_U	C ΣE_U	ΣE_{HR}	C ΣE_{HR}	TIR	C TIR	RMS	C RMS	T	C T	H	C H	I	S_P	C S_P	B	P	ΣE_T	C ΣE_T	Life
002	90.0	3	3.098	6	28.335	4	4.40	7	5.0	3	1.04	2	80.0	0	29.6	1	0	1.665	6	0	13	31.433	5	192,035
003	85.0	4	2.662	5	55.533	0	3.10	5	1.5	1	3.10	5	80.0	0	29.5	1	0	1.225	4	3	19	58.195	10	120,180
004	85.0	4	2.582	5	52.065	9	4.40	7	2.0	1	1.20	1	80.0	0	27.4	1	1	1.462	5	2	24	54.647	9	197,702
005	90.0	3	1.347	2	43.318	7	3.00	5	3.0	2	2.25	4	79.0	0	24.3	1	0	1.900	7	6	18	44.665	7	96,069
006	95.0	2	2.308	4	48.460	8	2.30	3	7.0	3	1.45	2	79.5	0	25.5	1	2	2.000	8	2	03	50.768	9	135,071
009	95.0	2	.406	0	11.740	1	2.10	3	7.0	3	1.65	2	80.0	0	24.8	1	0	2.310	9	4	24	12.146	1	46,326
010	85.0	4	1.110	2	54.863	9	4.00	7	5.5	3	1.30	1	80.0	0	24.8	1	0	1.160	4	2	01	55.973	10	180,676
012	85.0	4	.056	0	15.668	2	.15	0	9.5	4	1.75	3	80.0	0	28.9	1	0	1.660	6	5	24	15.724	2	125,292
014	75.0	7	.546	1	54.161	9	4.00	7	4.0	2	2.20	4	80.0	0	29.3	1	5	.260	2	2	16	54.707	9	348,502
016	90.0	3	3.806	6	24.039	3	3.00	5	7.0	3	2.30	4	80.0	0	29.5	1	0	2.000	8	6	13	27.845	4	44,805
020	95.0	2	1.500	3	35.225	6	4.10	7	5.5	3	2.40	4	80.0	0	32.3	2	0	2.430	9	5	00	36.725	6	58,453
025	90.0	3	1.729	3	46.838	8	5.60	8	2.0	1	.90	0	80.0	0	24.5	1	9	1.635	6	1	06	48.567	8	68,363
026	90.0	3	1.228	2	41.220	7	3.40	5	9.0	4	1.20	1	80.0	0	20.4	1	9	1.660	6	1	12	42.448	7	63,367
027	85.0	4	.470	0	21.259	3	2.70	4	1.5	1	2.65	5	82.0	2	17.5	0	9	1.580	6	4	05	21.729	3	99,604
031	80.0	6	.600	1	34.881	5	2.50	4	1.0	0	1.80	3	83.0	3	17.7	0	9	.677	2	6	17	35.481	6	510,882
033	90.0	3	.893	1	44.168	7	3.90	6	8.0	4	1.20	1	84.0	4	14.8	0	9	1.635	6	2	04	45.061	8	94,822
034	95.0	2	1.223	2	51.319	9	6.30	8	1.5	1	1.55	2	83.0	3	16.5	0	3	2.140	8	1	01	52,542	9	94,752
035	80.0	6	.700	1	28.815	4	4.50	7	5.0	3	1.85	3	82.0	2	18.5	0	9	.980	3	5	19	29.515	4	188,178
041	81.5	6	.759	1	21.296	3	2.00	3	6.0	3	1.10	1	83.0	3	17.0	0	3	1.040	4	2	22	22.055	3	349,786
044	100.0	0	.751	1	21.303	3	3.50	6	2.0	1	1.55	2	79.0	0	45.8	3	13	3.170	12	3	14	22.054	3	480
045	85.0	4	2.658	5	12.241	1	2.20	3	3.0	2	1.20	1	79.0	0	45.8	3	0	1.160	4	4	23	14.899	1	53,820
051	95.0	2	1.224	2	51.451	9	6.10	8	2.0	1	1.35	1	83.0	3	54.3	4	1	2.150	8	2	12	52.675	9	70,979
053	90.0	3	1.815	3	77.274	10	7.40	9	8.0	4	1.15	1	83.0	3	43.1	3	0	1.970	7	3	09	79.089	10	81,764
054	85.0	4	1.256	2	71.797	10	6.40	8	4.0	2	1.60	2	82.0	2	38.4	2	0	1.530	6	2	26	73.053	10	159,297
055	80.0	6	1.140	2	65.249	10	8.70	9	15.0	5	1.20	1	82.0	2	37.9	2	14	1.010	4	1	28	66.389	10	338,320
057	80.0	6	1.140	2	38.330	6	7.00	9	8.0	4	2.00	4	84.0	4	39.1	2	9	1.050	4	3	01	39.470	6	151,896
058	85.0	4	.912	1	30.554	5	2.70	4	1.0	0	1.60	2	84.0	4	38.9	2	0	1.500	6	3	16	31.466	5	131,834

ACOUSTIC AND FATIGUE DATA
SINGLE STRESS LEVEL (CONT'D)

MCA Variable		x_1		x_2		x_3		x_4		x_5		x_6		x_7		x_8	x_9		x_{10}	x_{11}	x_{12}		x_{13}	Dependent
Regression Variable	x_1		x_2		x_3		x_4		x_5		x_6		x_7		x_8			x_9				x_{10}		Dependent
Sequence Number	S	CS	ΣE_L	C ΣE_L	ΣE_U	C ΣE_U	ΣE_{HR}	C ΣE_{HR}	TIR	C TIR	RMS	C RMS	T	C T	H	C H	I	S_P	C S_P	B	P	ΣE_T	C ΣE_T	Life
059	100.0	0	1.657	3	29.859	4	1.30	1	6.0	3	1.20	1	84.0	4	38.8	2	5	2.910	11	2	21	31.516	5	41,554
060	100.0	0	.956	1	40.640	7	8.50	9	2.0	1	2.05	4	83.0	3	40.2	3	5	2.960	11	3	23	41.596	7	29,713
061	90.0	3	1.141	2	43.767	7	4.90	7	2.5	1	1.80	3	83.0	3	38.0	2	0	2.080	8	6	15	44.908	7	65,558
062	80.0	6	.509	1	20.343	3	3.00	5	13.0	5	1.50	2	83.0	3	36.0	2	9	.780	3	0	19	20.852	3	251,160
063	85.0	4	1.004	2	54.265	9	5.00	8	3.5	2	1.50	2	82.0	2	31.8	2	0	1.220	4	0	02	55.269	10	220,007
064	98.5	0	1.875	3	40.015	7	7.20	9	5.0	3	1.00	0	82.0	2	33.8	2	3	2.575	10	1	24	41.890	7	38,006
065	80.0	6	.532	1	11.728	1	.70	1	13.0	5	2.10	4	83.0	3	36.3	2	9	.760	3	0	06	12.260	1	387,665
067	100.0	0	.451	0	28.150	4	6.20	8	8.0	4	1.75	3	83.0	3	41.4	3	5	3.240	12	5	23	28.601	4	19,566
072	80.0	6	.606	1	15.661	2	1.80	2	10.0	4	1.15	1	83.0	3	33.8	2	9	.922	3	5	29	16.267	2	246,804
073	80.0	6	1.429	2	50.992	9	8.60	9	7.0	3	1.55	2	83.0	3	31.0	2	0	.827	3	2	14	52.421	9	378,481
076	100.0	0	1.151	2	29.120	4	2.40	3	3.0	2	1.20	1	83.0	3	33.6	2	5	2.780	11	2	09	30.271	5	28,462
078	100.0	0	.598	1	11.200	1	1.40	1	3.0	2	1.75	3	83.0	3	31.5	2	15	3.045	12	5	05	11.798	1	32,684
079	90.0	3	1.605	3	15.668	2	4.10	7	8.0	4	2.20	4	83.0	3	31.9	2	0	2.020	8	5	18	17.273	2	69,867
080	100.0	0	.858	1	34.060	5	2.20	3	8.0	4	1.60	2	83.0	3	31.5	2	5	3.030	12	6	24	34.918	5	22,227
083	90.0	3	.773	1	20.252	3	5.00	8	5.0	3	1.65	2	82.0	2	29.9	1	0	2.100	8	5	06	21.025	3	90,283
084	90.0	3	.706	1	19.532	2	3.30	5	2.0	1	1.30	1	82.0	2	29.7	1	0	1.635	6	4	19	20.238	3	114,112
085	80.0	6	.407	0	39.911	6	5.10	8	3.5	2	1.50	2	82.0	2	29.6	1	0	.780	3	4	17	40.318	7	248,356
086	90.0	3	.363	0	8.003	0	1.50	2	5.5	3	1.75	3	83.0	3	27.3	1	0	1.820	7	4	13	8.363	0	97,451
088	95.0	2	1.180	2	43.035	7	7.00	9	7.5	3	1.10	1	84.0	4	25.5	1	0	2.130	8	1	18	44.215	7	49,806
091	90.0	3	.917	1	24.252	3	3.70	6	4.0	2	1.15	1	83.0	3	23.0	1	0	1.750	7	2	13	25.169	4	85,099
092	95.0	2	.520	1	11.974	1	2.90	4	3.5	2	1.55	2	83.0	3	22.8	1	0	2.560	10	4	24	12.494	1	47,274
095	95.0	2	.713	1	25.062	4	3.00	5	2.0	1	2.25	4	82.0	2	23.9	1	0	2.210	8	4	06	25.775	4	48,708
096	80.0	6	.379	0	31.556	5	1.00	1	3.5	2	1.25	1	83.0	3	22.4	1	7	.825	3	2	02	31.935	5	640,118
097	80.0	6	1.000	2	38.810	6	3.20	5	12.0	5	1.25	1	84.0	4	20.9	1	0	1.010	4	0	09	39.810	6	200,497
098	90.0	3	.862	1	55.388	10	7.65	9	3.0	2	1.75	3	84.0	4	24.7	1	0	2.030	8	5	17	56.250	10	122,541
099	100.0	0	.690	1	28.481	4	3.40	5	7.0	3	3.50	5	82.0	2	26.7	1	15	3.070	12	4	27	29.171	4	21,739
101	90.0	3	.823	1	43.155	7	5.20	8	3.0	2	2.80	5	83.0	3	36.2	2	0	2.040	8	3	24	43.978	7	85,375
102	85.0	4	.975	1	16.788	2	3.00	5	2.0	1	1.20	1	83.0	3	36.4	2	0	1.415	5	2	27	17.763	2	139,119
104	90.0	3	1.166	2	32.570	5	6.20	8	5.0	3	1.85	3	82.0	2	51.4	4	0	2.040	8	3	12	33.736	5	81,618
106	95.0	2	2.317	4	51.801	9	5.00	8	4.0	2	1.70	3	82.0	2	49.1	3	0	2.200	8	2	15	54.118	9	96,064
107	95.0	2	1.713	3	37.527	6	5.40	8	5.0	3	1.40	2	82.0	2	44.8	3	0	2.245	8	0	17	39.240	6	105,679
111	85.0	4	1.034	2	24.802	3	5.10	8	12.0	5	1.35	1	84.0	4	26.4	1	0	1.415	5	4	22	25.836	4	115,538
112	100.0	0	.908	1	30.738	5	2.10	3	17.0	6	1.30	1	83.0	3	28.1	1	16	2.900	11	0	28	31.646	5	35,995
113	95.0	2	1.363	2	18.938	2	5.00	8	7.0	3	1.85	3	82.0	2	27.5	1	0	2.180	8	1	15	20.301	3	44,708
114	85.0	4	.557	1	36.952	6	1.70	2	6.5	3	1.05	0	83.0	3	26.0	1	0	1.393	5	0	03	37.509	6	283,573

ACOUSTIC AND FATIGUE DATA
SINGLE STRESS LEVEL (CONT'D)

MCA Variable		x_1		x_2		x_3		x_4		x_5		x_6		x_7		x_8	x_9		x_{10}	x_{11}	x_{12}		x_{13}	Dependent
Regression Variable	x_1		x_2		x_3		x_4		x_5		x_6		x_7		x_8			x_9				x_{10}		Dependent
Sequence Number	S	CS	ΣE_L	C ΣE_L	ΣE_U	C ΣE_U	ΣE_{HR}	C ΣE_{HR}	TIR	C TIR	RMS	C RMS	T	C T	H	C H	I	S_P	C S_P	B	P	ΣE_T	C ΣE_T	Life
117	80.0	6	.415	0	10.554	1	3.80	6	4.0	2	1.90	3	84.0	4	40.4	3	0	1.220	4	5	15	10.969	1	269,221
118	100.0	0	1.054	2	43.860	7	5.10	8	6.0	3	1.85	3	84.0	4	47.0	3	5	2.810	11	4	16	44.914	7	30,236
120	95.0	2	.658	1	48.327	8	3.60	6	4.0	2	1.15	1	84.0	4	34.9	2	0	2.400	9	0	00	48.985	8	80,575
121	95.0	2	.502	1	23.440	3	1.20	1	1.5	1	1.70	3	84.0	4	34.6	2	0	2.670	10	6	29	23.942	3	52,719
123	100.0	0	.717	1	14.304	1	1.80	2	5.0	3	1.20	1	84.0	4	29.7	1	5	2.900	11	0	20	15.021	2	24,309
124	85.0	4	.417	0	10.063	1	2.70	4	2.0	1	1.70	3	84.5	5	29.1	1	0	1.200	4	1	10	10.480	1	120,860
125	95.0	2	2.863	5	39.785	6	5.20	8	1.0	0	1.10	1	84.5	5	29.1	1	0	2.005	8	1	03	42.648	7	48,000
126	80.0	6	1.411	2	34.265	5	4.40	7	5.0	3	1.50	2	85.0	5	28.2	1	0	1.180	4	5	21	35.676	6	278,577
129	90.0	3	2.836	5	47.393	8	7.50	9	14.0	5	2.50	5	84.0	4	30.4	2	0	2.090	8	3	11	50.229	9	42,456
131	80.0	6	.511	1	20.471	3	1.40	1	2.0	1	1.75	3	84.0	4	34.3	2	0	1.270	5	6	06	20.982	3	92,806
135	90.0	3	2.121	4	27.725	4	0.00	0	100.0	7	2.40	4	84.0	4	33.7	2	0	1.800	7	0	23	29.846	4	49,072
136	85.0	4	1.395	2	16.781	2	0.00	0	90.0	7	1.95	3	85.0	5	30.1	2	0	1.570	6	5	28	18.176	2	229,204
137	80.0	6	1.803	3	31.892	5	5.60	8	9.0	4	1.70	3	86.0	6	29.0	1	0	1.000	4	6	11	33.695	5	294,145
138	80.0	6	.863	1	32.646	5	2.50	4	5.0	3	1.95	3	85.0	5	32.8	2	0	.980	3	6	22	33.509	5	183,960
140	85.0	4	1.046	2	28.882	4	5.00	8	12.0	5	2.00	4	84.0	4	34.4	2	0	1.480	5	5	26	29.928	4	130,178
142	90.0	3	1.346	2	33.683	5	3.90	6	9.0	4	1.60	2	84.0	4	34.4	2	0	1.970	7	6	08	35.029	6	94,055
143	90.0	3	1.168	2	32.786	5	2.70	4	3.5	2	2.20	4	84.0	4	33.6	2	0	1.650	6	4	01	33.954	5	141,862
145	90.0	3	1.023	2	27.730	4	5.20	8	6.0	3	1.55	2	87.0	6	41.6	3	0	1.670	6	1	08	28.753	4	88,644
146	100.0	0	1.024	2	27.121	4	5.00	8	3.0	2	1.45	2	84.0	4	33.5	2	5	2.960	11	5	16	28.145	4	25,266
147	95.0	2	1.578	3	29.707	4	2.50	4	8.0	4	1.80	3	84.0	4	33.4	2	0	2.300	9	0	29	31.285	5	55,904
148	90.0	3	.881	1	38.686	6	3.00	5	3.0	2	1.25	1	84.0	4	33.4	2	0	1.890	7	0	18	39.567	6	114,086
149	100.0	0	.645	1	29.564	4	1.00	1	5.0	3	1.40	2	84.0	4	33.3	2	5	3.050	12	0	01	30.209	5	46,751
150	95.0	2	.735	1	37.986	6	4.90	7	2.0	1	1.05	0	84.0	4	35.7	2	0	2.140	8	2	00	38.721	6	51,030
151	95.0	2	1.133	2	34.992	5	2.20	3	2.0	1	1.85	3	84.0	4	37.5	2	0	2.300	9	1	26	36.125	6	49,718
152	95.0	2	1.054	2	34.008	5	3.20	5	5.0	3	1.15	1	83.5	4	43.5	3	0	2.060	8	2	08	35.062	6	76,808
153	95.0	2	1.290	2	19.125	2	2.00	3	3.0	2	1.75	3	84.0	4	42.9	3	0	2.210	8	0	10	20.415	3	51,455
154	100.0	0	.953	1	23.665	3	3.20	5	19.0	6	2.30	4	84.0	4	45.3	3	5	2.880	11	5	10	24.618	3	17,005
155	95.0	2	1.016	2	45.725	8	3.00	5	2.5	1	2.10	4	84.0	4	45.3	3	0	2.120	8	3	22	46.741	8	44,476
156	90.0	3	2.440	4	53.832	9	2.20	3	9.0	4	1.75	3	85.0	5	53.0	4	0	2.040	8	6	28	55.272	10	72,283
157	100.0	0	2.511	5	28.060	4	2.00	3	8.0	4	1.60	2	85.0	5	55.1	4	5	2.560	10	1	05	30.571	5	31,014
158	95.0	2	1.046	2	43.436	7	3.80	6	4.0	2	1.60	2	85.0	5	55.1	4	0	2.370	9	6	21	44.482	7	46,704
159	85.0	4	.468	0	15.473	2	2.10	3	11.0	5	2.25	4	85.0	5	55.1	4	0	1.485	5	5	08	15.941	2	118,934

ACOUSTIC AND FATIGUE DATA
SINGLE STRESS LEVEL (CONT'D)

MCA Variable		x_1		x_2		x_3		x_4		x_5		x_6		x_7		x_8	x_9		x_{10}	x_{11}	x_{12}		x_{13}	Dependent
Regression Variable	x_1		x_2		x_3		x_4		x_5		x_6		x_7		x_8			x_9				x_{10}		Dependent
Sequence Number	S	CS	ΣE_L	C ΣE_L	ΣE_U	C ΣE_U	ΣE_{HR}	C ΣE_{HR}	TIR	C TIR	RMS	C RMS	T	C T	H	C H	I	S_P	C S_P	B	P	ΣE_T	C ΣE_T	Life
160	85.0	4	1.417	2	41.237	7	2.00	3	.5	0	1.85	3	85.0	5	52.8	4	0	1.520	6	6	23	42.654	7	123,528
161	80.0	6	1.091	2	48.313	8	2.50	4	3.5	2	1.75	3	84.0	4	46.7	3	0	.840	3	4	26	49.404	8	303,846
162	85.0	4	1.193	2	30.988	5	4.00	7	8.0	4	2.40	4	84.0	4	46.3	3	0	1.370	5	2	19	32.181	5	74,862
163	100.0	0	.877	1	35.094	6	1.59	2	5.0	3	1.10	1	84.0	4	44.4	3	5	2.480	9	1	00	35.971	6	46,515
164	85.0	4	1.373	2	44.767	7	2.40	3	36.0	7	1.25	1	83.5	4	44.3	3	0	1.580	6	2	29	46.140	8	139,572
165	95.0	2	1.916	3	47.975	8	5.50	8	8.0	4	1.05	0	84.0	4	43.9	3	0	2.320	9	3	05	49.891	8	31,747
166	95.0	2	1.448	2	33.760	5	3.00	5	3.0	2	2.55	5	84.5	5	42.1	3	0	2.350	9	6	04	35.208	6	39,121
167	95.0	2	1.597	3	28.657	4	2.80	4	7.0	3	1.40	2	85.0	5	41.1	3	0	2.140	8	3	24	30.254	5	37,660
168	100.0	0	.977	1	34.797	5	2.80	4	8.0	4	1.60	2	84.0	4	41.2	3	5	2.830	11	5	22	35.774	6	37,650
169	100.0	0	1.091	2	26.286	4	1.20	1	4.5	2	1.10	1	84.0	4	41.2	3	17	2.880	11	2	23	27.377	4	39,626
170	100.0	0	1.640	3	40.975	7	1.30	1	6.0	3	1.10	1	83.5	4	42.3	3	10	2.840	11	3	02	42.615	7	7,666
171	95.0	2	.265	0	13.246	1	1.90	2	7.0	3	2.10	4	84.0	4	41.3	3	0	2.250	9	6	20	13.511	1	77,039
172	90.0	3	.592	1	25.199	4	1.70	2	12.5	5	1.25	1	84.0	4	41.3	3	0	1.730	6	2	02	25.791	4	127,029
173	85.0	4	.441	0	30.900	5	3.80	6	5.0	3	1.90	3	83.0	3	43.1	3	0	1.400	5	3	13	31.341	5	55,133
174	100.0	0	1.208	2	39.900	6	2.00	3	21.0	6	3.50	5	83.0	3	43.8	3	5	2.850	11	4	07	41.108	7	18,244
175	95.0	2	.785	1	27.569	4	2.50	4	5.5	3	2.00	4	83.0	3	43.9	3	7	2.200	8	2	06	28.354	4	62,102
176	95.0	2	1.309	2	26.561	4	1.20	1	4.0	2	1.80	3	83.0	3	43.9	3	0	2.320	9	0	04	27.870	4	40,053
177	80.0	6	1.034	2	38.929	6	4.20	7	10.0	4	1.05	0	84.0	4	42.2	3	0	.900	3	3	03	39.963	6	507,755
178	80.0	6	.493	0	10.574	1	2.10	3	12.0	5	1.50	2	84.0	4	42.1	3	0	.950	3	6	19	11.067	1	219,222
179	100.0	0	.553	1	14.525	1	2.30	3	4.5	2	.95	0	83.5	4	42.2	3	5	2.800	11	0	21	15.078	2	41,411
180	85.0	4	2.034	4	42.644	7	5.80	8	6.5	3	1.50	2	83.0	3	34.1	2	9	1.220	4	4	11	44.678	7	192,163
181	90.0	3	.662	1	22.844	3	4.00	7	19.0	6	2.20	4	83.5	4	32.7	2	0	1.950	7	3	20	23.506	3	92,591
182	85.0	4	1.216	2	45.555	8	3.10	5	2.0	1	1.75	3	83.5	4	32.7	2	0	.850	3	1	20	46.771	8	254,545
183	100.0	0	2.131	4	15.705	2	3.30	5	4.5	2	.95	0	84.0	4	32.8	2	0	2.500	10	1	17	17.836	2	38,294
184	80.0	6	1.293	2	15.660	2	2.00	3	18.0	6	2.30	4	83.0	3	32.8	2	0	.920	3	5	20	16.953	2	279,960
185	100.0	0	1.341	2	35.483	6	2.00	3	5.5	3	.95	0	84.0	4	32.8	2	5	2.950	11	0	26	36.824	6	48,881
186	100.0	0	.966	1	27.798	4	3.00	5	7.0	3	1.50	2	83.0	3	28.6	1	12	2.880	11	0	14	28.764	4	37,380
187	95.0	2	.608	1	12.318	1	1.80	2	7.0	3	1.40	2	83.0	3	27.1	1	0	2.570	10	6	01	12.926	1	43,988
188	85.0	4	1.308	2	45.889	8	5.20	8	5.0	3	1.80	3	83.0	3	26.3	1	0	1.530	6	5	27	47.197	8	125,952
189	90.0	3	.936	1	46.922	8	2.80	4	5.5	3	1.05	0	83.5	4	34.0	2	9	2.040	8	3	07	47.858	8	79,640
190	100.0	0	.743	1	29.955	4	1.80	2	3.5	2	1.00	0	83.5	4	38.4	2	11	3.330	12	3	10	30.698	5	7,663

ACOUSTIC AND FATIGUE DATA
SINGLE STRESS LEVEL (CONT'D)

MCA Variable		x_1		x_2		x_3		x_4		x_5		x_6		x_7		x_8	x_9		x_{10}	x_{11}	x_{12}		x_{13}	Dependent
Regression Variable	x_1		x_2		x_3		x_4		x_5		x_6		x_7		x_8			x_9				x_{10}		Dependent
Sequence Number	S	CS	ΣE_L	C ΣE_L	ΣE_U	C ΣE_U	ΣE_{HR}	C ΣE_{HR}	TIR	C TIR	RMS	C RMS	T	C T	H	C H	I	S_P	C S_P	B	P	ΣE_T	C ΣE_T	Life
191	90.0	3	.804	1	28.914	4	3.60	6	2.0	1	1.40	2	83.0	3	39.1	2	0	1.690	6	1	09	29.718	4	126,568
192	95.0	2	1.192	2	42.230	7	5.10	8	13.0	5	1.50	2	83.0	3	40.3	3	0	2.650	10	6	16	43.422	7	40,766
193	100.0	0	1.934	3	35.218	6	5.20	8	1.0	0	2.25	4	83.0	3	40.4	3	5	3.000	12	6	14	37.152	6	35,643
194	80.0	6	.360	0	38.674	6	3.60	6	5.0	3	1.50	2	83.0	3	45.4	3	0	.930	3	0	11	39.034	6	226,188
195	80.0	6	.720	1	46.188	8	7.00	9	5.5	3	1.10	1	83.0	3	50.7	4	0	.750	3	1	13	46.908	8	298,328
196	85.0	4	4.489	6	48.825	8	3.70	6	16.0	6	2.20	4	83.0	3	50.9	4	0	1.400	5	3	21	53.314	9	148,410
197	85.0	4	2.115	4	21.981	3	6.00	8	7.0	3	1.50	2	83.0	3	50.9	4	0	1.320	5	5	14	24.096	3	150,981
198	80.0	6	1.771	3	29.381	4	7.30	9	16.0	6	2.15	4	83.0	3	55.8	4	0	.380	2	1	07	31.152	5	620,697
199	80.0	6	.421	0	9.424	0	2.00	3	4.0	2	1.50	2	83.0	3	41.3	3	0	.780	3	4	14	9.845	1	242,804
200	90.0	3	.921	1	30.486	5	2.70	4	6.0	3	1.10	1	83.0	3	41.2	3	0	2.040	8	1	29	31.407	5	46,797
201	85.0	4	.868	1	35.508	6	4.00	7	5.5	3	1.55	2	83.0	3	41.1	3	7	1.670	6	6	02	36.376	6	94,256
202	90.0	6	.582	1	32.758	5	2.90	4	3.0	2	1.05	0	83.0	3	40.9	3	0	.925	3	3	26	33.340	5	209,775
203	80.0	6	1.022	2	25.164	4	3.30	5	12.0	5	1.45	2	83.0	3	45.1	3	0	.750	3	1	19	26.186	4	304,015
204	80.0	6	1.350	2	33.721	5	5.40	8	13.0	5	1.55	2	83.0	3	40.4	3	0	1.200	4	3	08	35.071	6	3,249,328
205	80.0	6	.462	0	37.560	6	2.80	4	4.5	2	1.80	3	83.0	3	31.0	2	0	1.100	4	4	09	38.022	6	122,692
206	85.0	4	.751	1	27.676	4	1.80	2	5.0	3	1.90	3	85.0	5	33.9	2	0	1.630	6	6	27	28.427	4	157,158
207	85.0	4	.580	1	31.262	5	2.50	4	1.0	0	2.30	4	86.0	6	37.1	2	0	1.150	4	4	10	31.842	5	136,719
208	85.0	4	.762	1	35.007	6	1.80	2	5.0	3	1.50	2	85.0	5	36.2	2	0	1.120	4	4	15	35.769	6	149,346
209	85.0	4	1.170	2	29.368	4	6.20	8	4.5	2	2.30	4	84.0	4	38.1	2	0	1.200	4	1	14	30.538	5	132,631
008	75.0	7	1.363	2	60.558	10	5.70	8	7.0	3	1.50	2	80.0	0	25.0	1	18	.550	2	6	09	61.921	10	115,928
090	75.0	7	.898	1	12.114	1	3.00	5	7.5	3	2.60	5	84.0	4	25.5	1	18	.795	3	3	17	13.012	1	139,966
141	75.0	7	.484	0	12.408	1	4.00	7	18.0	6	1.65	2	84.0	4	34.4	2	18	.530	2	5	12	12.892	1	160,665

TABULATION LEGEND SECTION 2

Dual Stress Level Fatigue Data

S_1 = First stress level in cumulative damage; units: ksi.

N_1 = Cycles at S; units: cycles.

S_2 = Second stress-run to failure; units: ksi.

ΣE_{L1} = Totalized burst load emission when stressed to S_1; units: counts.

ΣE_{L2} = Totalized burst load emission when stressed to S_2; units: counts.

ΣE_{U1} = Totalized unload emission when stressed to S_1; units: counts.

ΣE_{U2} = Totalized unload emission when stressed to S_2 ; units: counts.

ΣE_{HR} = Totalized high rate emission; units: counts.

ΣE_{T1} = Totalized emission exclusive of the high rate emission when stressed to S_1; units: counts.

ΣE_{T2} = Totalized emission exclusive of the high rate emission when stressed to S_2; units: counts.

N_2 = life cycles at second stress level; units: cycles.

TIR = Total indicator reading in 0.00001 in.

RMS = Root means square surface finish; units: μ inches RMS.

T = Room temperature; units: °F.

H = Room humidity; units: grains of water per pound of dry air.

I = Incident factor defined in legend of section one.

B = Bar number (see section 2.1.2.1): 0 - 6.

P = Position number (see section 2.1.2.1): 0 - 29.

ACOUSTIC AND FATIGUE DATA
DUAL STRESS LEVEL DATA

Sequence Number	S_1	N_1	S_2	ΣE_{L1}	ΣE_{L2}	ΣE_{U1}	ΣE_{U2}	ΣE_{HR1}	ΣE_{T1}	ΣE_{T2}	TIR	RMS	T	H	I	B	P	N_1
000	75	$2x10^5$	90	Lost	1,549	42,846	45,781	Lost	Lost	47,330	60	175	83.0	24.3	19	2	10	12,308
001	90	10^4	75	3,504	537	44,737	48,186	3,200	48,241	48,723	110	220	80.0	30.4	0	6	12	169,900
007	75	$2x10^5$	90	403	749	8,749	9,542	2,000	9,152	10,271	35	245	80.0	25.0	0	5	01	63,847
008	Early 90ksi Failure See Data Table Above																	
011	90	10^4	75	1,870	1,202	67,269	23,117	7,200	69,139	24,319	20	325	80.0	24.8	0	3	29	207,143
013	90	10^4	75	688	379	65,357	68,882	2,500	43,545	69,261	35	135	79.0	30.5	0	4	03	269,665
015	75	$2x10^5$	90	899	596	27,270	29,263	Lost	28,169	29,859	40	180	80.0	27.3	0	0	05	70,364
017	90	10^4	75	3,371	564	39,470	43,336	3,200	42,841	43,890	30	115	79.5	26.5	2	2	17	273,700
018	75	$2x10^5$	90	866	360	11,281	12,691	2,000	12,147	11,051	20	250	78.0	33.2	0	4	29	22,501
019	90	10^4	75	2,098	818	42,806	46,318	5,200	44,904	47,136	30	120	79.5	30.3	0	4	18	255,736
021	90	10^4	75	1,305	591	22,995	24,879	2,900	24,200	25,370	60	175	80.0	29.7	0	5	07	160,271
022	90	10^4	75	959	561	23,648	26,398	1,000	24,607	26,959	15	150	80.0	29.7	0	6	10	88,050
023	90	10^4	75	1,143	582	30,823	32,015	300	31,966	32,597	12	115	80.0	29.7	0	6	25	188,701
028	75	$2x10^5$	90	383	542	48,887	52,289	6,000	49,270	52,831	80	90	83.0	16.0	0	1	25	14,277
029	75	$2x10^5$	90	1,099	510	46,374	52,983	7,300	47,473	53,493	75	235	82.0	18.2	0	5	11	28,387
030	75	$2x10^5$	90	928	870	20,252	22,677	2,500	21,180	23,347	120	210	82.0	16.9	0	4	20	3,195
036	75	$2x10^5$	90	268	232	35,108	38,644	3,300	35,376	38,876	125	150	82.0	18.6	0	0	15	123,318
037	90	10^4	75	885	440	21,921	23,325	2,500	22,806	23,765	10	130	82.0	23.2	0	1	02	469,204
038	90	10^4	75	591	244	33,125	35,220	5,000	33,716	35,464	70	325	80.0	26.8	0	5	13	244,264
040	75	$2x10^5$	90	792	724	20,329	21,975	700	21,121	22,699	100	110	82.0	18.5	3	2	11	60,034
043	75	$2x10^5$	90	436	995	39,718	40,594	3,900	40,154	41,589	20	125	81.0	25.8	10	2	18	137,336
046	90	10^4	75	526	255	31,532	34,902	4,500	36,958	35,457	40	140	80.0	39.9	0	5	04	263,454
047	90	10^4	75	1,256	671	24,240	25,410	7,700	25,496	26,081	90	120	82.0	50.1	0	4	28	158,455
048	90	10^4	75	668	225	31,512	34,557	2,100	32,180	34,782	90	120	84.0	66.2	0	2	07	429,792
049	90	10^4	75	371	240	26,024	28,346	3,000	26,395	30,586	40	170	84.0	62.0	0	6	07	118,189
050	90	10^4	75	1,141	250	28,496	35,226	4,400	29,637	35,476	100	140	83.0	58.7	9	5	03	149,771
052	90	10^4	75	1,523	299	25,658	27,654	7,500	27,181	27,953	120	160	83.0	49.5	0	3	28	160,230
056	90	10^4	75	1,010	331	44,819	48,165	5,000	45,829	48,496	50	95	77.0	33.8	0	2	28	248,339
066	75	$2x10^5$	90	562	596	15,332	20,333	4,800	15,894	20,929	65	135	83.0	37.1	0	3	15	22,948
068	75	$2x10^5$	90	421	464	8,921	10,488	3,000	9,342	10,952	100	210	83.0	37.1	0	5	02	34,577
069	90	10^4	75	797	227	34,114	37,556	4,600	34,911	37,783	150	175	83.0	36.9	0	6	00	148,286
070	90	10^4	75	699	303	15,650	16,256	4,200	16,349	16,559	20	220	83.0	29.6	3	3	18	80,198
071	90	10^4	75	1,090	409	31,611	33,649	7,400	32,701	34,058	45	110	84.0	33.9	3	3	04	369,243
074	90	10^4	75	1,474	458	45,042	47,468	9,900	46,516	47,926	55	130	83.0	33.5	0	1	23	417,133
075	90	10^4	75	1,703	331	25,087	25,897	3,000	26,790	26,228	30	170	83.0	31.0	0	3	06	212,232
077	75	$2x10^5$	90	498	499	28,885	31,212	2,800	29,383	31,711	10	135	83.0	35.2	0	0	16	182,250
081	75	$2x10^5$	90	817	590	31,310	35,526	6,300	32,127	36,116	100	170	79.0	37.7	0	3	27	11,802
082	90	10^4	75	889	389	11,631	11,811	1,200	12,510	12,200	60	135	75.0	34.0	0	3	40	359,775
087	75	$2x10^5$	90	692	889	25,979	28,336	8,500	26,671	29,225	75	130	84.0	25.6	0	2	56	142,957
089	90	10^4	75	584	394	13,277	12,266	1,800	13,861	12,660	45	175	84.0	25.5	0	2	25	229,385
090	Early 90ksi Failure See Data Table Above																	
093	75	$2x10^5$	90	454	358	19,843	24,317	3,600	20,297	24,675	35	130	83.0	22.6	0	1	22	61,878
094	90	10^4	75	320	261	16,821	22,691	2,600	17,141	22,952	15	375	83.0	24.5	0	4	00	44,271
100	75	$2x10^5$	90	1,190	487	30,764	33,482	3,000	31,954	33,969	55	200	82.5	26.3	18	0	24	108,129
103	75	$2x10^5$	90	730	772	61,851	65,375	7,300	62,581	56,147	90	160	82.0	44.5	0	3	24	4,802
105	90	10^4	75	944	410	11,008	11,802	3,600	11,952	12,212	70	135	82.0	49.1	6	1	04	170,437
108	90	10^4	75	1,179	579	61,341	63,286	7,500	62,520	63,865	65	135	82.0	40.3	0	4	02	260,674
109	75	$2x10^5$	90	512	461	20,923	22,708	1,000	21,435	23,169	140	135	82.0	35.7	0	0	07	62,839
110	75	$2x10^5$	90	1,325	681	40,139	42,696	4,000	41,464	43,380	70	175	82.0	33.3	0	6	05	9,963
115	75	$2x10^5$	90	460	516	8,870	11,058	2,200	9,330	11,564	45	170	82.0	27.1	0	1	21	87,235
116	90	10^4	75	1,111	282	17,313	20,199	2,800	18,424	20,481	160	160	82.0	27.2	0	3	00	103,471
119	90	10^4	75	2,050	513	27,556	30,984	4,600	29,606	31,497	30	225	84.0	44.3	0	1	11	192,860
122	90	10^4	75	1,535	512	42,897	44,273	4,700	44,432	44,785	60	155	84.0	34.5	0	5	25	250,408
127	90	10^4	75	1,851	602	41,701	42,722	4,900	43,552	43,324	60	165	85.0	28.3	0	4	04	187,797
128	90	10^4	75	1,472	623	23,524	25,028	4,000	24,996	25,651	60	220	85.0	33.0	0	4	21	329,474
130	75	$2x10^5$	90	582	877	37,291	39,352	1,400	37,873	40,229	110	180	84.0	30.3	0	6	26	6,078
132	90	10^4	75	1,704	516	33,158	34,101	1,600	34,862	34,617	95	160	84.0	33.9	1	2	20	121,869
139	75	$2x10^5$	90	1,125	635	36,201	41,180	5,000	37,326	41,815	75	150	84.0	30.0	0	0	12	121,753
141	Early 90ksi Failure See Data Table Above																	
144	75	$2x10^5$	90	2,074	1,380	61,338	67,527	5,400	63,412	68,907	90	105	85.0	36.0	0	0	25	130,963

APPENDIX III

LIST OF SYMBOLS AND TERMINOLOGY

The terminology is presented in subject groups.

Symbol	Term
	Acoustic Emission Terms
ΣE	Totalized acoustic emission above the counter threshold of 24.8 μ volts peak voltage.
ΣE_L	Totalized load emission above the counter threshold excluding ΣE_{HR}.
ΣE_{HR}	Totalized high rate emission above counter threshold.
ΣE_U	Totalized unload emission above the counter threshold.
ΣE_T	Totalized total emission above the counter threshold excluding ΣE_{HR}.
ΔS	Stress delay associated with acoustic silence during the start of the unload process.
RMS Volts	RMS output amplitude of the detection system in volts.
Type I	Load emission characteristic where most of the bursts are accumulated before 17,000 psi.
Type II	Load emission characteristic where most of the bursts are accumulated at about 34,000 psi.
	Stress and Fatigue Terms
N	Fatigue life
log N	Logarithm to the base 10 of the fatigue life.
S	Applied stress. When associated with fatigue experiments this is the zero to maximum fatigue stress.
S_{max}	The maximum stress to which a specimen is loaded during a single acoustic test cycle.

S^*_{max}	The largest S_{max} to which a specimen is taken during an acoustic test series.
S_{yu}	The stress at the upper yield point of the specimen.
S_P	$S_{max} - S_{yu}$.
	<u>Inspection Terms</u>
TIR	Total Indicator Reading in 0.0001 inches.
RMS	Root mean square surface finish in units of μ in. RMS.
	<u>Acoustic Detection System Terms</u>
dB	Decibels; $dB = 20 \log \frac{P}{P_o}$.
re	"Referenced to" used to denote the P_o to which the decibel calculation is referenced.
g_{33}	Piezoelectric stress constant.
PZT-5	Lead zirconate titanate piezoelectric ceramic.
	<u>Data Terms</u>
B	The number of the bar from which the specimen was taken.
P	The number of the position of the specimen within the bar.
H	Room humidity measured in grains of water per pound of dry air.
T	Room temperature in °F.
I	Incident factor, see Appendix II for detailed listing.
	<u>Statistical Terms</u>
MCA	Multiple Classification Analysis.
SRWSL	Stepwise Regression with Simple Learning.
β^2	MCA'S importance coefficient, see section 4.1.1.1.
R^2	MCA'S adjusted multiple correlation coefficient squared, see section 4.1.1.1.

$\log N - \overline{\log N}$	Logarithmic life deviations.
$\hat{a}$	Unbiased estimator of the intercept, a, in y = a + bx.
$\hat{b}$	Unbiased estimator of the slope, b, in y = a + bx.
$\widehat{Var}(\hat{a})$	The estimator of the variance of $\hat{a}$.
$\widehat{Var}(\hat{b})$	The estimator of the variance of $\hat{b}$.
$\widehat{Cov}(\hat{a}, \hat{b})$	The estimator of the covariance of $\hat{a}$, $\hat{b}$.
$y_{\mid x}$	The value of the dependent variance, y, given x.
$\widehat{Var}(y_{\mid x})$	The estimate of the variance of y, given x.
$S_{y\mid x}$	Sample standard error of the dependent variable about the regression line given x, $S^2_{y\mid x} = \widehat{Var}(y_{\mid x})$.
$\hat{y}$	The estimated value of y from $\hat{y} = \hat{a} + \hat{b}x$.
$Var(\hat{y})$	The variance of the estimated value of y.
α	The probability of a random variable falling outside a stated interval defined by an upper and a lower cutoff point.
ν	The degrees of freedom associated with the calculated statistic.
$t_{\alpha;\nu}$	The cutoff point in a one sided t statistic interval.
$t_{\alpha/2;\nu}$	The cutoff point in a two sided t statistic interval.

APPENDIX IV

THE MEANING AND MATHEMATICS OF CONFIDENCE INTERVALS AND PREDICTION INTERVALS IN SECTION 6.1

In order to obtain an idea of the scatter of the data around the predictive regression equation, one usually calculates a confidence and/or a predictive interval around the regression result. In order to do this, one needs the estimated variance of $\hat{b}$, $\widehat{\text{Var}}(\hat{b})$, where $\hat{b}$ is an unbiased estimator of b, the slope, in the model, y = a + b x. But the $\sqrt{\widehat{\text{var}}(\hat{b})}$, which is the sample standard error of the slope, is provided by the regression program. Also, it can be shown that

$$\widehat{\text{Var}}(\hat{b}) = \frac{S_{y|x}^2}{\sum_{i=1}^{n} (x_i - \bar{x})^2} \qquad (67,\ p.\ 247)$$

where $S_{y|x}^2$ is the square of the sample standard error of the dependent variable, given the independent variable. This also is printed out by the regression program. Now $\sum_{i=1}^{n} (x_i - \bar{x})^2$ may be calculated. Bowker and Lieberman (67, p. 248) give

$$S_{y|x} = \sqrt{\frac{\sum_{i=1}^{n} (y_i - \hat{y}_i)^2}{n - 2}} \qquad \text{where } \hat{y}_i = \hat{a} + \hat{b}\, x_i.$$

It is evident that $\sum_{i=1}^{n} (y_i - \hat{y}_i)^2$ is the sum of squares of the deviations about the regression line.

The confidence interval estimate of the average value of the dependent variable for a given x can be developed by using $S_{y|x}^2$, $\widehat{Var(\hat{b})}$, $\bar{x}$, and $\sum_{i=1}^{n} x_i^2$. This means that the interval developed by the equation given below will surround the population value of the expected value of the dependent variable, given the independent variable, $(1 - \alpha)\%$ of the time. That is to say, there is an $\alpha\%$ chance that the interval so constructed will not include the population expected value of y. The interval is given by

$$\hat{a} + \hat{b}\, x_i \pm t_{\alpha/2;\, n-2} \sqrt{\widehat{Var(\hat{y})}}. \qquad (67, \text{ section } 9.5.2)$$

In the application in this thesis α was chosen as .05 so that a 95% confidence interval was generated. However, the $\widehat{Var(\hat{y})}$ is unknown.

But $$\widehat{Var(\hat{y})} = \widehat{Var(\hat{a})} + x_i^2\, \widehat{Var(\hat{b})} + 2x_i\, \widehat{cov(\hat{a}, \hat{b})}$$

where $$\widehat{Var(\hat{a})} = \frac{S_{y|x}^2 \sum_{i=1}^{n} x_i^2}{n \sum_{i=1}^{n} (x_i - \bar{x})^2} \qquad (67, \text{ p. } 247)$$

and

$$\widehat{Cov(\hat{a}, \hat{b})} = - \widehat{Var(\hat{b})}\, \bar{x}.$$

Calculation gives $\sum_{i=1}^{n} x_i^2 = 557.06001$ and $\bar{x} = 1.817697$. The above equations with $S_P = x_i = 0.5, 1.0, 1.5, 2.0, 2.5,$ and 3.0 give the 95% confidence interval on the average value of log N given S_P . This interval is shown in Figure 6.1.

Next, it is of interest to form a prediction interval around the regression line. One is usually interested in how high or how low a future observation of log N will be, given a value of S_P. The prediction interval with probability of $(1 - \alpha)$ is given by

$$\hat{a} + \hat{b}\, x_i \pm t_{\alpha/2;\ n-2} \sqrt{\widehat{Var}(\hat{y}) + \widehat{Var}\ y|x}\ .$$

The prediction interval in Figure 6.1 is a 95% interval, so $\alpha = .05$. The meaning of this prediction interval is that there is $(1 - \alpha)$ probability that a future observation of log N, given S_P, will fall within this established interval.

LIST OF REFERENCES

1. Faires, V. M., Design of Machine Elements, The Macmillan Company, New York, 1955.

2. Dieter, G. E., and Mehl, R. F., "Investigation of the Statistical Nature of the Fatigue of Metals," NACA TN 3019, Sept., 1953.

3. Epremian, E., and Mehl, R. F., "Investigation of the Statistical Nature of Fatigue Properties," NACA TN 2719, Jan., 1952.

4. Grover, H. J., Gordon, S. A., and Jackson, L. R., Fatigue of Metals and Structures, U.S. Department of the Navy, Revised 1960, NAV-WEPS-00-25-534.

5. Despres, T. A., A Study of the Dislocation Distributions in Annealed 304 Stainless Steel Produced by Fatigue Loading at Various Levels of Strain and Number of Cycles, University of Michigan Industry Program, IP 631, Sept., 1963.

6. McLean, D., Mechanical Properties of Metals, John Wiley and Sons, Inc., New York, 1962.

7. Wood, W. A., "Some Basic Studies of Fatigue in Metals," Fracture, Auerbach, B. L., Felbeck, D. K., Hahn, G. T., and Thomas, D. A. (eds.), Technology Press of MIT, John Wiley & Sons, New York, and Chapman & Hill Ltd., London, 1959.

8. Faupel, J. H., Engineering Design, John Wiley & Sons, Inc., New York, 1964.

9. Lipson, C., and Juvinall, R. C., Handbook of Stress and Strength, The Macmillan Company, New York, 1963.

10. Lipson, C., Kerawalla, J., and Mitchell, L., Engineering Applications of Reliability, University of Michigan Engineering Summer Conference, Summer, 1963.

11. Kusenberge, F. N., Barton, J. R., and Donaldson, W. L., Nondestructive Evaluation of Metal Fatigue, U.S. Dept. of Commerce, ACCESS #AD600277.

12. Metals Research Laboratory, Brown University, Ultrasonic Methods in the Study of Fatigue and Deformation in Single Crystals, U.S. Dept. of Commerce, ACCESS # AD408704.

13. Kaiser, J., Untersuchungen über das Auftreten von Geräuschen biem Zugversuch, A doctoral dissertation presented to Fahultät für Waschinenwesen und Elektrotechnik Der Technischen Hochschule München, München, Germany, 1950.

14. Schofield, B. H., personal commumication.

15. Kaiser, J., "Erkenntnisse und Folgerungen aus der Messung Von Geräuschen bei Zugbeanspruchung von metallischen Werkstaff", Archiv für das Eisenhüttenwesen, 24, No.$\frac{1}{2}$, Jan.-Feb., 1953, pp. 43-45.

16. Späth, W., "Zur Entstehung von Gleitlinien auf plastisch verformten Metalloberflachen," Metalloberfläche, 7, No. 12, Dec.,1953, pp. 177-180.

17. Schofield, B. H., and Bareiss, R. A., Acoustic Emission Under Applied Stress, Progress Report 1, Contract No. AF 33 (616) - 5640, Wright-Patterson Air Force Base, Ohio.

18. Schofield, B. H., Acoustic Emission Under Applied Stress, Progress Report 2, Contract No. AF 33 (616) - 5640, Wright-Patterson Air Force Base, Ohio.

19. Schofield, B. H., Acoustic Emission Under Applied Stress, Progress Report 3, Contract No. AF 33 (616) - 5640, Wright-Patterson Air Force Base, Ohio.

20. Schofield, B. H., Acoustic Emission Under Applied Stress, Progress Report 6, Contract No. AF 33 (616) - 5640, Wright-Patterson Air Force Base, Ohio.

21. Schofield, B. H., Acoustic Emission Under Applied Stress, Progress Report 7, Contract No. AF 33 (616) - 5640, Wright-Patterson Air Force Base, Ohio.

22. Schofield, B. H., Acoustic Emission Under Applied Stress, Progress Report 8, Contract No. AF 33 (616) - 5640, Wright-Patterson Air Force Base, Ohio.

23. Schofield, B. H., Acoustic Emission Under Applied Stress, Progress Report 9, Contract No. AF 33 (616) - 5640, Wright-Patterson Air Force Base, Ohio.

24. Schofield, B. H., Acoustic Emission Under Applied Stress, Progress Report 10, Contract No. AF 33 (616) - 5640, Wright-Patterson Air Force Base, Ohio.

25. Schofield, B. H., Acoustic Emission Under Applied Stress, Progress Report 11, Contract No. AF 33 (616) - 5640, Wright-Patterson Air Force Base, Ohio.

26. Schofield, B. H., Bareiss, R. A., and Kyrala, A. A., Acoustic Emission Under Applied Stress, Lessells and Associates, Inc., WADC Technical Report 58-194, 1958, Wright-Patterson Air Force Base, Ohio.

27. Schofield, B. H., Acoustic Emission Under Applied Stress, Technical Documentary Report No. ADS-TDR-63-509, Part I, Office of Technical Services, U.S. Dept. of Commerce, April, 1963.

28. Schofield, B. H., Acoustic Emission Under Applied Stress, Technical Documentary Report No. ASD-TDR-63-509, Part II, Office of Technical Service, U.S. Dept. of Commerce, May, 1964.

29. Kaiser, J., "Über das Auftreten von Geräuschen beim Schmelzen und Erstarren von Metallen," Forschuung auf dem Gebiete des Ingeneuenwesens, 23, No. 1-2, 1957, pp. 38-42.

30. Borchers, H., and Kaiser, J., "Akustische Effekte bei Phaenübergängen im System Blei-Zinn," Zeit. für Metallkunde, 49, No. 2, 1958, pp. 95-101.

31. Plateu, J., Buchet, C., and Crussard, C., "Sur la formation d'ondes sonores, au cours d'essais de traction, das des eprovettes metalliques," Computes Rendus, 246, No. 20, May 19, 1958, pp. 2845-2848.

32. Borchers, H., and Tensi, H. M., "Eine verbesserte piezoelektrische Methode zur Untersuchung von Vorgängen in Metallen bei mechanischer Beanspruchung und bei Phasenanderung," Zeit. für Metallkunde, 51, No. 4, 1960 pp. 212-218.

33. Borchers, H., and Tensi, H. M., "Piezoelecktrische Impulsmessungen während der mechanischen Beanspruchung von Al Mg 3 und Al 99, "Zeit. für Metallkunde, 53, No. 10, 1962, pp. 692-695.

34. Tatro, C. A., Sonic Techniques in the Detection of Crystal Slip in Metal, Division of Engineering Research, College of Engineering, Michigan State University, East Lansing, Mich., Jan., 1959.

35. Tatro, C. A., Sonic Techniques in the Detection of Crystal Slip in Metals, undated report not the same as above, Engineering Experimental Station, East Lansing, Michigan.

36. Tatro, C. A., and Liptai, R. G., "Acoustic Emission from Crystalline Substances," Symposium on Physics and Nondestructive Testing, Southwest Research Institute, Texas, 1962.

37. Liptai, R. G., and Tatro, C. A., "Acoustic Emission - A Surface Phenomenon," Symposium on Nondestructive Testing of Aircraft and Missile Conponents, Southwest Research Institute, Texas, 1963.

38. Hall, A. A., Holowenko, A. R., and Laughin, H. G., Theory and Problems of Mechanical Design, Schaum Publishing Co., New York, 1961.

39. Cummings, H. N., Stulen, F. B., and Schulte, W. C., "Relation of Inclusions to the Fatigue Properties of SAE 4340 Steel," Trans. of ASM, 49, 1957, pp. 482-516.

40. Hicks, C. R., Fundamental Concepts in the Design of Experiments, Holt, Rinehart and Winston, New York, 1964.

41. Bower, E. S., letter dated 1/6/65, Republic Steel Corp., Canton, Ohio.

42. Prendergast, M., Certification dated 9/15/65, J. T. Ryerson Steel Co., Detroit, Michigan.

43. Ryerson Certified Steel Book, Edition 117, Ryerson Steel, Detroit, Michigan, p. 239.

44. Rand Corp., A million random digits with 100,000 normal deviates, Free Press, Glencoe, Ill., 1955.

45. Committee E-9 on fatigue, Manual on Fatigue Testing, American Society For Testing Materials, Spec. Tech. Pub. No. 91, 1949.

46. Little, Robert E., Analysis of the Effect of Mean Stress on the Fatigue Strengths of Notched Steel Specimens, University of Michigan Industry Program IP 630, Ann Arbor, Michigan, August, 1963.

47. Extension of Materials Testing Capabilities by use of Electo Hydraulic Closed-Loop Systems, MTS Division, Research Incorp., Minneapolis, Minn., undated.

48. Garlock Designers' Handbook, Garlock Bearing Products, England, undated.

49. "Glacier Dry Bearings," Automobile Engineer, 50, No. 5, pp. 177-181.

50. Kerwin, Jr., E. M., "Decibels and Levels," Noise Reduction, Beranek, L. L. (ed.), McGraw-Hill, New York, 1960, pp. 43-63.

51. Modern Piezoelectric Ceramics, Clevite Electronics Corp., Bulletin No. 9244-1, March, 1961.

52. Andrews, F. M., The Revised Multiple Classification Analysis Program, a report of the Institute for Social Research, University of Michigan, Aug., 1963.

53. Pelz, D. C., and Andrews, F. M., The SRC Computer Program for Multivariate Analysis: Some Uses and Limitations, a report of the Institute for Social Research, University of Michigan, undated but 1961 or later.

54. Morgan, J., Barbara, B., and Sonquist, J., Interim Write-up The Multiple Classification Analysis Program, a report of the Survey Research Center, Institute of Social Research, University of Michigan, Nov., 1962.

55. Hess, I., and Pillai, R. K., Multiple Classification Analysis, a report of the Survey Research Center, University of Michigan, Nov., 1960.

56. Yates, F., "The Analysis of Multiple Classifications with Unequal Numbers in the Different Classes," Amer. Stat. Assoc., 29, 1934, pp. 51-65.

57. Squire, D. D., Product Profit Optimization Considering the Managerial Decisions of Price, Marketing, and Inventory, University of Michigan Industry Program report IP 702, April, 1965.

58. Westervelt, F. H., A Study of Automatic System Simulation Programming and the Analysis of the Behavior of Physical Systems Using an Internally Stored Program Computer, Part II Stepwise Regression Program with Simple Learning, University of Michigan Industry Program report IP 470, Oct., 1960.

59. Bottenberg, P. A., and Ward, Jr., H. H., Applied Multiple Linear Regression, U.S. Dept. of Commerce, ACCESS # AD 413128, Washington, D. C., 1963.

60. Kerawalla, J. N., personal communication, 1963-1965. To be published as University of Michigan Industry Program report.

61. Fitzgerald, E. R., "Mechanical Resonance Dispersion and Plastic Flow in Crystalline Solids," The J. of the Acous. Soc. of Amer., 32, No. 10, pp. 1270-1289.

62. Statton, W., personal communication, 1965.

63. Keith, H. D., and Passagila, E. P., "Dislocations in Poylmer Crystals", J. of Res. of the NBS, 68A, 1964, p. 513.

64. Holland, V. F., "Dislocations in Polyethylene Single Crystals", J. Appl. Phys., 35, 1964, p. 3235.

65. Geil, P. H., "Nylon Single Crystals", J. Polymer Sci., 44, 1960, p. 449.

66. Reneker, D. H., "Point Dislocations in Crystals of High Polymer Molecules", J. Polymer Sci., 59, 1963, p. 539.

67. Bowker, A. H., and Lieberman, G. J., Engineering Statistics, Prentice-Hall, Inc., Englewood Cliffs, N. J., 1960